UNIVERSITY OF INDONESIA

DEVELOPMENT OF HIGH PERFORMANCE PtCo/C ELECTROCATALYST FOR CATHODE PROTON EXCHANGE MEMBRANE FUEL CELL: STUDY OF ACTIVITY AND STABILITY ENHANCEMENT BY NITROGEN AND CARBON MONOXIDE TREATMENT

DISSERTATION

ABDUL HAMID BUDIMAN
0706221054

FACULTY OF ENGINEERING
CHEMICAL ENGINEERING DEPARTMENT
DEPOK
JULY 2011

UNIVERSITY OF INDONESIA

DEVELOPMENT OF HIGH PERFORMANCE PtCo/C ELECTROCATALYST FOR CATHODE PROTON EXCHANGE MEMBRANE FUEL CELL: STUDY OF ACTIVITY AND STABILITY ENHANCEMENT BY NITROGEN AND CARBON MONOXIDE TREATMENT

DISSERTATION

Submitted to the Chemical Engineering Department,
Faculty of Engineering, University of Indonesia in Partial Fulfillment of
the Requirements for the Degree of DOCTOR
in Chemical Engineering

ABDUL HAMID BUDIMAN
0706221054

FACULTY OF ENGINEERING
CHEMICAL ENGINEERING DEPARTMENT
DEPOK
JULY 2011

ii

PROMOTER:

Prof. Dr. Ir. Widodo Wahyu Purwanto, DEA
Professor of Chemical Engineering, Faculty of Engineering
University of Indonesia

CO-PROMOTERS:

Prof. Ir. Rinaldy Dalimi, M.Sc., Ph.D
Professor of Electrical Engineering, Faculty of Engineering
University of Indonesia

Dr. Eng. Eniya Listiani Dewi, B.Eng., M.Eng
Senior Researcher
Center for Material Technology
Agency for the Assessment and Application of Technology

EXAMINER BOARD

1. Prof. Dr. Ir. Widodo Wahyu Purwanto, DEA
   Department of Chemical Engineering, Faculty of Engineering, University of Indonesia

2. Prof. Ir. Rinaldy Dalimi, M.Sc., Ph.D
   Department of Electrical Engineering, Faculty of Engineering, University of Indonesia

3. Dr. Eng. Eniya Listiani Dewi, B.Eng., M.Eng
   Center for Material Technology, Agency for the Assessment and Application of Technology

4. Prof. Dr. Ir. Martin Djamin, M.Sc
   Center for Energy Conversion and Conservation Technology, Agency for the Assessment and Application of Technology

5. Prof. Ir. Sutrasno Kartohardjono, M.Sc., Ph.D
   Department of Chemical Engineering, Faculty of Engineering, University of Indonesia

6. Prof. Dr. Ir. Slamet, MT
   Department of Chemical Engineering, Faculty of Engineering, University of Indonesia

7. Prof. Bing Joe Hwang
   Department of Chemical Engineering, National Taiwan University of Science and Technology

STATEMENT OF ORIGINALITY

I herewith declare that the dissertation entitled:

DEVELOPMENT OF HIGH PERFORMANCE PtCo/C ELECTROCATALYST FOR CATHODE PROTON EXCHANGE MEMBRANE FUEL CELL: STUDY OF ACTIVITY AND STABILITY ENHANCEMENT BY NITROGEN AND CARBON MONOXIDE TREATMENT

which is submitted to the Chemical Engineering Department,

Faculty of Engineering, University of Indonesia in partial fulfillment of

the requirements for the Degree of DOCTOR in Chemical Engineering, as I know is

not as a duplication or copy of dissertation which had published at University of

Indonesia or in other Universities/Institutions, and that all the sources I have used or

quoted have been indicated and acknowledged by means of complete refer references

Name	:	Abdul Hamid Budiman
Student Register Number	:	0706221054
Signature	:	
Date	:	July 8th, 2011

v

PAGE OF APPROVAL

This dissertation is submitted by

Name	:	Abdul Hamid Budiman
SRN	:	0706221054
Study Program	:	Chemical Engineering
Title	:	Development of High Performance PtCo/C Electrocatalyst for Cathode Proton Exchange Membrane Fuel Cell: Study of Activity and Stability Enhancement by Nitrogen and Carbon Monoxide Treatment

Has been successfully defended in front of the board of examiners and accepted as part of the requirements for the degree of DOCTOR in Chemical Engineering in the Chemical Engineering Department, Faculty of Engineering, University of Indonesia

BOARD OF EXAMINERS

Promoter : Prof. Dr. Ir. Widodo Wahyu Purwanto, DEA --------------------------

Co-Promoter I : Prof. Ir. Rinaldy Dalimi, M.Sc., Ph.D --------------------------

Co-Promoter II : Dr. Eng. Eniya Listiani Dewi, B.Eng., M.Eng --------------------------

Examiners : Prof. Dr. Ir. Martin Djamin, M.Sc --------------------------

Prof. Ir. Sutrasno Kartohardjono, M.Sc., Ph.D --------------------------

Prof. Dr. Ir. Slamet, MT --------------------------

Prof. Bing Joe Hwang --------------------------

Approved in	:	Depok
Date	:	July 8th, 2011

vi

ACKNOWLEDGEMENT

Finally, and surely the most, I wish to express my deepest thank to all my families for their love, their patience and their motivation. I thank my wife Virleidya Lusinta Hutagalung and my lovely children Rafi Aditya Haviantama and Safira Naulida Havianda for sharing with me all the good and the bad times. You are my inspiration and motivation. I thank also to my parents Drs. MB. Hutagalung., MBA and Dra. Zuraida Bustami for their support and pray. I dedicate this book to them. Hopefully, this dissertation would be useful for all.

Depok, July 8th, 2011

Abdul Hamid Budiman
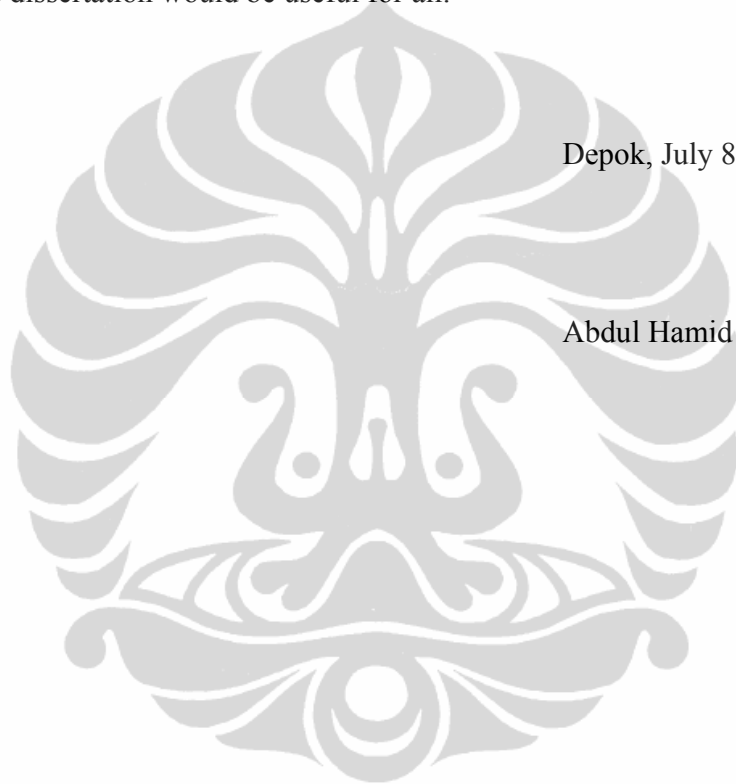
APPROVAL STATEMENT OF DISSERTATION PUBLICATION
FOR ACADEMIC INTEREST

As an Academic of University of Indonesia, I the undersigned this:

Name   :   Abdul Hamid Budiman

SRN   :   0706221054

Study Program :   Chemical Engineering

Faculty   :   Engineering

For the development of science, I agree to give to the University of Indonesia Non-exclusive Royalty-Free Right on my scientific work entitled: "Development of High Performance PtCo/C Electrocatalyst for Cathode Proton Exchange Membrane Fuel Cell: Study of Activity and Stability Enhancement by Nitrogen and Carbon Monoxide Treatment" along with existing devices. With this right, University of Indonesia is entitled to store, convert in other media, manage in the form of a database, maintain and publish my dissertation as along put my name as author and owner of copyright.

Depok, July 8$^{\text{th}}$, 2011

Abdul Hamid Budiman

ABSTRACT

Name   : Abdul Hamid Budiman
Study Program : Chemical Engineering
Title   : Development of High Performance PtCo/C Electrocatalyst for Cathode Proton Exchange Membrane Fuel Cell: Study of Activity and Stability Enhancement by Nitrogen and Carbon Monoxide Treatment

The synthesis procedure on a commercial catalyst still needs to be improved in order to get a better catalyst performance for application on fuel cell. There is no guarantee that the commercial catalyst has a good property. The commonly used method to prepare PtCo/C electrocatalyst is through impregnation of the second metal on platinum supported carbon (Pt/C) followed by alloying at high temperature in an inert gas. This high temperature heat treatment facilitates the growing of the alloy nanoparticles (NPs) due to sintering, which is undesirable because it may result in reduction of the Pt mass activity for the oxygen reduction reaction (ORR).

Core shell NPs consist of a shell of one type of atom surrounding a core of another type of atom. This structure can be achieved by high temperature annealing, chemical leaching of the non noble material or electrochemical deposition technique. Nevertheless, all of these methods exhibit significant disadvantages such as losses in active surface area and material, formation of an incomplete noble metal shell, and necessity for potential control during preparation.

It is important to understand the atomic distribution and alloying extent of participating elements in individual bimetallic NPs, as these factors also influence the intrinsic catalytic activity. In recent years, x-ray absorption spectroscopy (XAS) studies have been well explored on bimetallic NPs. However, XAS studies focusing on estimation of atomic distributions or alloying extent in the NPs are limited. Therefore, we propose a methodology to estimate the structural characteristics such as alloying extent or atomic distribution in bimetallic NPs, by deriving the structural parameters from XAS analysis and to demonstrate the results on commercially available carbon supported PtCo NPs.

The overall objective of this study is to enhance the activity and stability of commercial PtCo/C electrocatalyst through treatment with nitrogen (N_2) and carbon monoxide (CO). In this work, a commercial PtCo/C catalyst was treated using two different strategies to study the effect of particle size and structure on its activity and stability.

The research methodology consists of PtCo/C catalyst treatment, physical characterization, electrochemical characterization and single cell proton exchange membrane (PEM) fuel cell performance test. The catalysts were treated with nitrogen at various temperatures in order to study the effect of the particle size on its activity and stability, and also treated with carbon monoxide at various times in order to study the effect of the structure on its activity and stability. Physical characterizations were done through x-ray diffraction (XRD), transmission electron microscopy (TEM) and XAS. The electrochemical characterizations were done using cyclic voltammetry (CV) and linier sweep voltammetry (LSV).

For the PtCo/C that is subjected to N_2 treatment, XRD result shows the particle size is increased with increasing temperature of treatment. TEM result shows that all the PtCo NPs are well dispersed on the surface of carbon and it is in accordance with the XRD result. The electrochemical characterization shows that the base voltamogram becomes more Pt-like, which is indicative of leaching Co from the surface. While for PtCo/C that is subjected to CO treatment, the XRD result shows that treatmnet for 5, 7, 10 and 15 hours leads to surface segregation, at which the peak of Co-related species is clearly observed. The alloying extent and coordination number of the catalysts were investigated with XAS, show that treatments for 1, 3 and 5 hours resulted in Pt rich in core Co rich in shell. On the contrary, treatments for 7, 10 and 15 hours resulted in Pt rich in shell Co rich in core.

It is clearly demonstrated that the PtCo/C subjected to CO treatment for 1-5 hours shows the enhanced ORR activity, but the catalyst is unstable due to the dissolution of Co, while samples treated for 7-15 hours display poor activities. However, the catalyst is stable, which is likely due to the fact that Pt in the surface protects Co from dissolution.

The single cell PEM fuel cell performance test shows that PtCo/C subjected to CO treatment for 3 hours shows the best performance. This result is in accordance with the specific surface area and mass activity of PtCo/C that is subjected to CO treatment for 3 hours, which has a better activity toward ORR. Catalyst treatment would increase the fuel cell performance by 20.49 % (Power density of commercial PtCo/C electrocatalyst: 88.33 mW/cm^2, PtCo/C electrocatalyst subjected to CO treatment for 3 hours: 108.82 mW/cm^2)

Keywords :   catalyst treatment, core shell, atomic distribution, alloying extent, surface segregation, activity, stability

ABSTRAK

Nama   :   Abdul Hamid Budiman
Program Studi   :   Teknik Kimia
Judul   :   Pengembangan Katalis PtCo/C Kinerja Tinggi untuk Katoda Proton Exchange Membrane Fuel Cell: Studi Peningkatan Aktifitas dan Stabilitas dengan Perlakuan Nitrogen dan Karbon Monoksida

Katalis komersial tidak selalu mempunyai properti yang baik. Katalis ini masih memerlukan perlakuan sehingga dapat memberikan kinerja yang tinggi ketika diaplikasikan pada fuel cell. Metode yang sering digunakan untuk sintesa katalis PtCo/C adalah impregnasi logam pada Platina yang disangga Karbon diikuti proses paduan/*alloying* pada suhu tinggi. Perlakuan pada suhu tinggi akan menyebabkan aglomerasi sehingga katalis menjadi lebih besar ukurannya, akibatnya terjadi penurunan aktifitas.

Struktur *core shell* terdiri atas kulit/shell dari suatu atom yang mengelilingi inti/core dari jenis atom yang lain. Struktur ini dapat dicapai melalui proses aneling suhu tinggi, *chemical leaching* ataupun teknik deposisi elektrokimia. Namun demikian, semua metode tersebut mempunyai kelemahan antara lain berkurangnya luas aktif area, pembentukan shell logam nobel yang tidak lengkap dan memerlukan kontrol potensial selama preparasinya.

Distribusi atom dan *alloying extent* dari bimetal nanopartikel dapat mempengaruhi aktifitas katalis. Akhir-akhir ini aplikasi *x-ray absorption spectroscopy (XAS)* banyak digunakan pada bimetal nanopartikel. Namun demikian studi tentang distribusi atom ataupun *alloying extent* masih terbatas. Pemahaman teori tentang distribusi atom dan *alloying extent* masih sangat diperlukan.

Tujuan dari studi ini adalah untuk mempelajari peningkatan aktifitas dan stabilitas katalis komersial PtCo/C dengan perlakuan Nitrogen dan Karbon Monoksida untuk mempelajari efek ukuran partikel dan struktur katalis terhadap aktifitas dan stabilitasnya.

Metodologi yang digunakan meliputi perlakuan katalis komersial PtCo/C, karakterisasi fisik, karakterisasi kimia serta pengujian kinerja sel tunggal. Katalis dilakukan perlakuan dengan Nitrogen pada berbagai macam suhu untuk mengetahui efek ukuran partikel terhadap aktifitas dan stabilitasnya, serta perlakuan dengan Karbon Monoksida pada berbagai macam waktu untuk mengetahui efek struktur katalis terhadap aktifitas dan stabilitasnya. Karakterisasi fisik yang dilakukan adalah *x-ray diffraction (XRD), transmission electron microscopy (TEM)* dan *XAS.*

Sedangkan karakterisiasi kimia yang dilakukan adalah *cyclic voltammetry (CV)* dan *linear sweep voltammetry (LSV)*.

Analisa XRD yang dilakukan pada katalis PtCo/C dengan perlakuan Nitrogen menunjukkan bahwa ukuran partikel menjadi lebih besar dengan bertambahnya suhu perlakuan. Analisa TEM menggambarkan distribusi partikel yang merata dan sesuai dengan hasil XRD. Sedangkan, analisa elektrokimia menunjukkan kurva voltammogram yang bentuknya seperti kurva voltammogram Pt.

Untuk katalis PtCo/C dengan perlakuan Karbon Monoksida, analisa XRD menunjukkan bahwa adanya puncak Kobal untuk katalis dengan perlakuan selama 5, 7, 10 dan 15 jam. Hal ini mengindikasikan adanya segregasi ke permukaan katalis. Analisa XAS memberikan hasil struktur *Pt rich in core Co rich in shell* untuk katalis dengan perlakuan selama 1, 3 dan 5 jam. Sebaliknya perlakuan selama 7, 10 dan 15 jam menghasilkan struktur *Pt rich in shell Co rich in core*. Dari analisa elektrokimia yang dilakukan, dihasilkan tidak adanya perubahan CV untuk katalis dengan perlakuan selama 1-5 jam, mengindikasikan adanya peningkatan aktifitas. Sebaliknya perlakuan selama 7-15 jam menunjukkan katalis bersifat kurang aktif.

Pengujian stabilitas menunjukkan katalis dengan perlakuan 1-5 jam bersifat tidak stabil. Hal ini dikarenakan Pt yang terletak di core tidak mampu untuk melindungi Co yang berada di shell dari disolusi. Sebaliknya katalis dengan perlakuan selama 7-15 jam bersifat stabil, karena Pt yang terletak di shell mampu melindungi Co yang berada di core dari proses disolusi.

Pengujian kinerja sel tunggal menunjukkan bahwa katalis dengan perlakuan Karbon Monoksida selama 3 jam merupakan katalis yang mempunyai kinerja terbaik. Hal ini sesuai dengan aktifitas masa dan luas permukaan spesifik dari katalis dengan perlakuan Karbon Monoksida selama 3 jam, di mana katalis ini mempunyai aktifitas paling baik terhadap reaksi reduksi oksigen. Terlihat bahwa terjadi peningkatan power densitas sebesar 20,49 %, di mana katalis PtCo/C komersial mempunyai power density 88,33 mW/cm^2 dan katalis PtCo/C dengan perlakuan Karbon Monoksida selama 3 jam mempunyai power density 108,82 mW/cm^2.

Kata kunci : perlakuan katalis, *core shell*, distribusi atom, *alloying extent*, segregasi permukaan, aktifitas, stabilitas

LIST OF PUBLICATIONS

The following papers were published during the period of study:

1. Budiman, A.H., Purwanto, W.W., Dewi, E.L., Dalimi, R., Hwang, B.J, *Understanding Adsorbate-Induced Surface Segregation in PtCo/C Electrocatalyst, Asia Pacific Journal of Chemical Engineering,* **2011** (in press)

2. Budiman, A.H., Purwanto, W.W., Dewi, E.L., Dalimi, R., Hwang, B.J, *Activity Enhancement of Carbon-Supported PtCo Electrocatalyst through Controlled Heat-Treatment for Proton Exchange Membrane Fuel Cell Applications, International Journal of Chemical Engineering Research,* ISSN 0975-6442, Volume 3, No. 2, **2011,** 125-133

3. Budiman, A.H., Purwanto, W.W., Dewi, E.L., Dalimi, R., Hwang, B.J., Pan, C.J., Taufany, F., *An Investigation of Surface Segregation in PtCo Nanoparticles* (in preparation)

4. Budiman, A.H., Dewi, E.L., Purwanto, W.W., Dalimi, R., Hwang, B.J, *Atomic Distribution of PtCo/C Nanoparticles as Investigated by X-ray Absorption Spectroscopy, Indonesian Journal of Materials Science, Special Edition on Materials for Energy and Device,* **2010**, 35-39

5. Budiman, A.H., Dewi, E.L., Purwanto, W.W., Dalimi, R., Hwang, B.J, *Effect of PtCo/C Treatment on Performance of Single Cell PEM Fuel Cell, Indonesian Journal of Materials Science,* Volume 11, No. 3, **2010**, 145-149

6. Budiman, A.H., Purwanto, W.W., Dewi, E.L., *Effect of Heat Treatment of Pt-Co/C Electrocatalyst on their Activity and Stability, Proceedings International Conference on Fuel Cell and Hydrogen Technology,* ISBN 978-602-95555-1-6, **2009**, 132-137

7. Budiman, A.H., Purwanto, W.W., Dalimi, R., Dewi, E.L, *Material Combination for Cathode PEMFC Electrocatalyst Development : A Review, International Conference on Advanced and Sustainable Polymer,* **2008**

TABLE OF CONTENT

LIST OF FIGURES

xviii

LIST OF TABLES

ABBREVIATIONS

AES	:	Auger Electron Spectroscopy
AFC	:	Alkaline Fuel Cell
CE	:	Counter Electrode
CV	:	Cyclic Voltammetry
DFT	:	Density Functional Theory
EASA	:	Electrochemical Active Surface Area
EXAFS	:	Extended X-ray Absorption Fine Structure
FT	:	Fourier Transform
GCE	:	Glassy Carbon Electrode
GDL	:	Gas Diffusion Layer
HOR	:	Hydrogen Oxidation Reaction
ISS	:	Ion Scattering Spectroscopy
LEED	:	Low Energy Electron Diffraction
MCFC	:	Molten Carbonate Fuel Cell
MEA	:	Membrane Electrode Assembly
NHE	:	Normal Hydrogen Electrode
NPs	:	Nanoparticles
OCP	:	Open Circuit Potential
ORR	;	Oxygen Reduction Reaction
PAFC	:	Phosphoric Acid Fuel Cell
PEMFC	:	Proton Exchange Membrane Fuel Cell
RDE	:	Rotating Disk Electrode
RE	:	Reference Electrode
RHE	:	Reversible Hydrogen Electrode
SCLS	:	Surface Core Level Shift
SHE	:	Standard Hydrogen Electrode
TEM	:	Transmission Electron Microscopy
WE	:	Working Electrode
XANES	:	X-ray Absorption Near Edge Structure
XAS	:	X-ray Absorption Spectroscopy
XPS	:	X-ray Photoemission Spectroscopy
XRD	:	X-ray Diffraction

SYMBOLS

Ar	:	Argon
C	:	Carbon
Co	:	Cobalt
CO	:	Carbon Monoxide
Fe	:	Iron
He	:	Helium
H_2O_2	:	Hydrogen Peroxide
H_2SO_4	:	Sulfide Acid
H_2	:	Hydrogen
Ni	:	Nickel
N_2	:	Nitrogen
Pt	:	Platinum
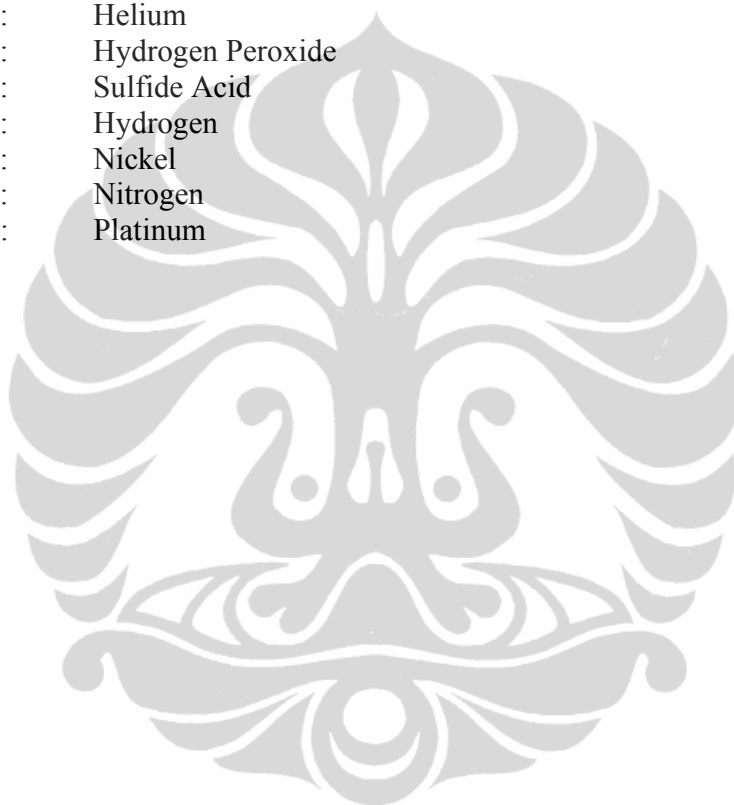
CHAPTER 1
INTRODUCTION

1.1. Background

Proton exchange membrane (PEM) fuel cell have been recognized as the most promising energy converting devices in term of low or zero emission and high efficiency [1-5]. It has been demonstrated that PEM fuel cells are able to meet transportation and stationary power requirements due to their high power density, relatively quick start-up, rapid response to varying loading, and relatively low operating temperature. However, commercialization of PEM fuel cell technology has been challenged due to two major technical gaps: high cost and low reliability and durability [1-9].

The fuel cell catalyst is the major contributor to these difficulties. In recent years, although a great deal of effort has been put into the synthesis of cost-effective, active and stable fuel cell catalyst, there is no real breakthrough can be seen yet. Therefore, exploring breakthrough catalyst, improving catalyst activity, stability and durability and also reducing catalyst cost are the major task in fuel cell commercialization.

Platinum is known to present the best catalytic activity for the oxygen reduction reaction (ORR) among all pure metals and when supported on a conductive carbon serves as state of the art electrocatalyst in low temperature fuel cell air cathode [10]. However, due to kinetic limitations of the oxygen reduction reaction the cathodic overpotential losses amount to 0.3-0.4 V under typical PEM fuel cell operating conditions [10]. In addition, Pt is expensive and the world's supply is limited. Therefore, the development of more active and less expensive oxygen reduction electrocatalysts than pure Pt has been the subject of extensive research for a number of decades and has favored the use of suitable Pt alloys [11].

Alternatively, it has been shown that the activity and stability of the catalyst can be improved by alloying Pt with some transition metals. Among these Pt alloys,

PtCo nanomaterials have been widely studied as promising alternative catalyst for proton exchange membrane fuel cell applications. It was reported that Pt alloyed with Co on the carbon support yields better catalytic activity than pure Pt, where Pt:Co ratios of 1:1 to 3:1 are most studied [12-15]. Among these Pt catalysts, the intermetallic Pt_3Co solid solution was extensively studied. Few reasons for the high catalytic activity for these alloys are ascribed to the modification of the electronic structure of Pt on alloying with Co and the structural effect on Pt eventhough the exact cause is still unclear [16,17].

One of the major approaches to improve the activity and stability of Pt based catalysts is to optimize the catalyst synthesis procedure. It is well known that the electrocatalyst performance is strongly dependent on the preparation procedures, including the addition of metal and its precursor, the support type, and heat treatment methods [18]. Heat treatment has a significant impact on the metal particle size and size distribution, particle size morphology, and metal dispersion on the support. It has a benefit to remove any undesirable impurities resulting from early preparation stages, allow a uniform dispersion and stable distribution of the metal on the support.

Regarding ORR catalyst synthesis, heat treatment has been recognized as an important and sometimes necessary step for catalytic activity improvement [19-24]. Many heat treatment techniques have been applied to prepare PEM fuel cell electrocatalyst. Among the heat treatment techniques, the traditional furnace heating technique is the most widely used. In general it involves heating the catalyst under an inert atmosphere (N_2, Ar or He) or reducing atmosphere (H_2) in the temperature range of 80-900 ^{o}C for 1-4 h [21,24].

Core shell nanoparticles consist of a shell of one type of atom surrounding a core of another type of atom. This structure can be achieved by high temperature annealing, chemical leaching of the non noble material or electrochemical deposition technique. Nevertheless, all these methods exhibit significant disadvantages such as the loss in active surface area and material, the formation of an incomplete noble metal shell, and the necessity for potential control during preparation.

University of Indonesia

Recently, Mayrhofer [25] has presented novel preparation procedure of such core shell nanoparticles using an adsorbate-induced surface segregation effect. Depending on the heat of segregation and the surface mixing energy, the composition of the surface of a bimetallic system can be very different from the bulk. This effect is additionally dependent upon the chemical potential of the gas phase since the strong bonding of adsorbates will result in a gain in energy of the system. Consequently, for bimetallic systems, enrichment at the surface of the component that binds a certain adsorbate more strongly may occur.

It is important to understand the atomic distribution and alloying extent of participating elements in individual bimetallic nanoparticles, as these factors also influence the intrinsic catalytic activity. Therefore, a fundamental understanding of ORR activity enhancement and nanoparticle structure is essential. X-ray diffraction (XRD) technique is capable to predict the atoms arrangement preferably in single crystals or polycrystals with sufficient long range order. However, it lacks to provide the structural parameters required to understand the atomic distribution in bimetallic nanoparticles. Hence, we can't conclude the structural evolution of nano-sized particles from XRD [26].

X-ray absorption spectroscopy (XAS) has become a widely used technique to determine the local atomic structure of materials since last two decades. The increasing use of XAS may be attributed to its unique potential to provide information regarding the oxidation state and local coordination numbers as well as the identity of neighbors, and absorbing atom. The advantage of XAS over other characterization methods lies in the ability to conduct the measurement in situ. XAS technique can provide information on the morphology of the considered species, as well as the distribution of the two metals insides the species [27,28]. XAS consists of X-ray absorption near edge structure (XANES) which provide critical information about the oxidation state and fractional d-electron density, and also electronic environment of the absorbing atoms and extended X-ray absorption fine structure (EXAFS) which can provide details about the number, type and distance of the

backscattering atom surrounding the central absorbing atom, investigation on the short range ordering and geometric information.

In recent year, XAS studies have been well explored on bimetallic nanoparticles. However, XAS studies focusing on estimation of atomic distributions or alloying extent in the NPs are limited. In this regard, we attempt to propose a general methodology to estimate the structural characteristics such as alloying extent or atomic distribution in bimetallic nanopaticles, by deriving the structural parameters from XAS analysis and to demonstrate the results on commercially available carbon supported Pt-Co nanoparticles.

1.2. Motivation

Fuel cell is one of the existing researches of major efforts to develop clean and renewable energy. Among the types of fuel cell, PEM fuel cell probably has the widest present and research due to its many advantages and various applications. However, there still exist some problems that need to be solved in the present fuel cell technologies, catalyst dispersion, degradation, manufacturing process etc.

In this study, we developed a controlled treatment strategy to alter the surface population of Pt and Co without varying the particle size of the initial PtCo nanoparticles. The adsorbate-induced strategy allowed us to induce changes in the surface Pt and Co population. X-ray diffraction (XRD) can provide information on the atomic composition of Pt and Co in the bulk but not at the surface of NPs. X-ray absorption fine structure (XAFS) spectroscopy has proven to be an appropriate and suitable technique for estimating alloy formation and surface composition in the bimetallic nanoparticles.

1.3. Problem Statement

The synthesis procedure on a commercial catalyst still needs to be improved in order to get a better catalyst performance for application on fuel cell. There is no

guarantee that the commercial catalyst has a good property. The commonly used method to prepare PtCo/C electrocatalyst is through impregnation of the second metal on platinum supported carbon (Pt/C) followed by alloying at high temperature in an inert gas. This high temperature heat treatment facilitates the growing of the alloy nanoparticles due to sintering, which is undesirable because it may result in reduction of the Pt mass activity for the ORR.

1.4. Hypothesis

- Adsorbate-induced by CO is able to alter the surface population, so that the structure of the catalyst changes from alloy to core shell structure, which has a significant influence on nanoparticles activity and stability. This hypothesis is taken based on the following :
    1. The energy binding of CO on Pt is higher than on Co, so that Pt segregates to the surface of the nanoparticles and correspondingly displaces Co to the core
    2. Higher alloying extent would result on the active catalyst
    3. Dissolution of Co could be inhibited, if Pt located in the shell and Co located in the core, so that Pt could protect Co therefore the catalyst would be stable.
- Catalyst treatment would improve the fuel cell performance, hence the energy output of the fuel cell will increase and the power density of fuel cell would increase as well

1.5. Research Objectives

The overall objective of this study is to enhance the activity and stability of PtCo/C commercial electrocatalyst using adsorbate-induced strategy. In this work, a commercial PtCo/C catalyst was treated using two different adsorbate (nitrogen and carbon monoxide) to study:

University of Indonesia

1. effect of particle size on its activity and stability
2. effect of structure on its activity and stability

1.6. Outlines of the Dissertation

This dissertation consists of five main parts. It begins with Chapter 1 as an introduction, which is the background, motivation, problem statement, hypothesis as well as objective of the work are given. A literature review is presented in Chapter 2. An overview of fuel cell and its essential characteristics, a fundamental of electrocatalyst and its structural characterization are explained. In chapter 3, the experimental part of the work is described. The chemicals, instrumentation and preparation, as well as its characterization procedure are explained.

The results of the work are summarized in Chapter 4. In this chapter, discussion about the effect of particle size of PtCo/C on its activity and stability, adsorbate-induced surface segregation in Pt-Co/C electrocatalyst were briefly explained. The characteristics were done by X-ray diffraction, transmission electron microscopy, electrochemical measurement, and X-ray absorption spectroscopy. The electrocatalyst, then was applied on single cell PEM fuel cell to determine its performance as well. The dissertation is closed by the conclusion and described in Chapter 5.

University of Indonesia

CHAPTER 2
LITERATURE REVIEW

In this chapter, literature review was composed from an overview of fuel cell, thermodynamic and kinetics consideration of fuel cell, general feature of electrocatalyst and its structural characterization, surface segregation, heat treatment of electrocatalyst till structural model and atomic distribution of bimetal nanoparticles.

2.1. An Overview of Fuel Cell

Over the past 20 years, one of the most important challenges facing industry has been the search for a solution to the energy crisis. It is necessary to find an environmentally friendly and cost effective alternative to the traditional power production methods since natural resources become scarcer and the environmental constraints on industry grow tighter.

In recent years, there is an enormous demand for energy. Environmental concerns necessitate that new energy sources must be highly efficient and has very low emission. As a result, many industries have invested considerable resources in finding and implementing new methods of power production. One of the new technologies under considerations is fuel cell that can meet these demands.

A fuel cell is conventionally defined as an electrochemical cell which can continuously convert the chemical energy of a fuel and an oxidation to electrical energy by a process involving an essentially invariant electrode-electrolyte system [29]. Fuel cells directly convert chemical energy stored in the fuel into electricity without taking the loop of heat production [30].

The use of fuel cells in both stationary and mobile power applications can offer significant advantages for the sustainable conversion of energy [31]. Fuel cells are clean enough for power to be generated at the point of use utilizing a variety of fuels. Benefit arising from the use of fuel cells includes efficiency and reliability, as

well as economy, unique operating characteristics, planning flexibility and future development potential [31].

Every fuel cell has two electrodes, one positive and one negative, called the anode and cathode respectively. A fuel cell also has an electrolyte which allows electrically charged particles to migrate from one electrode to the other, and sometimes a catalyst which accelerates the reactions at the electrodes. Hydrogen is the basic fuel for the fuel cell, but oxygen is also required. One great appeal of fuel cell is that they generate electricity with very little pollution much of the hydrogen and oxygen used in generating electricity ultimately combines to form a harmless by product namely water [32].

In a typical fuel cell, gaseous fuels are fed continuously to the anode compartment and an oxidant is fed continuously to the cathode compartment, the electrochemical reactions take place at the electrodes to produce an electric current [33]. A fuel cell, much like a typical battery, produces electrical energy. However, unlike a battery, the reactants are continuously supplied and products are continuously removed in a fuel cell. Hence, a fuel cell does not store energy. A fuel cell will be able to continually generate energy as long as fuel and the oxidant are provided to the cell [34]. Their operating principal is schematically illustrated in Figure 2.1. It is analogical to that of a conventional battery.
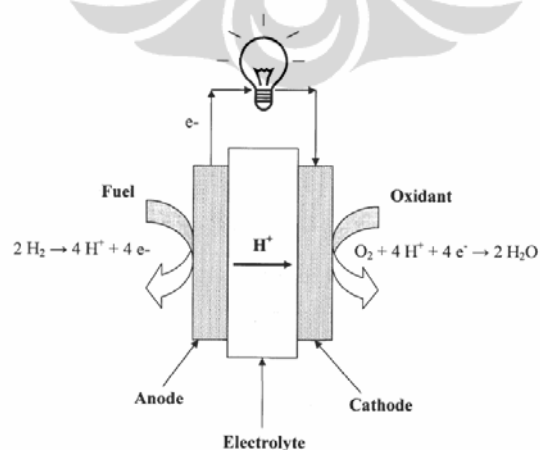
Figure 2.1. Operating Principle of Fuel Cell [34]

University of Indonesia

Fuel cell technology has been around for a long time. Initiated at 1839, Sir William Grove discovered the operating principle of fuel cells by reversing water electrolysis to generate electricity with hydrogen and oxygen [35]. However, the so-called "Gaseous Voltaic battery" set up by Grove was a fragile apparatus filled with diluted sulfuric acid into which a platinum electrode was dipped, as shown in Figure 2.2.
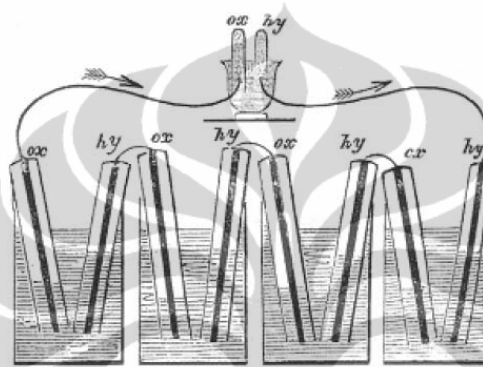
Figure 2.2. The Schematic of "Gaseous Voltaic Battery" Invented by Sir William Grove [35]

One also must mention Francis T Bacon, who constructed a fuel cell to repeat the experiment of Grove in 1939 [36]. Bacon developed the "double layer" electrode and solved the liquid flooding and gas bubbling problem by forming an oxide coating on the nickel electrode. Bacon built a 6 kW fuel cell stack in 1959. One of his patents was used in the alkaline fuel cell (AFC's) fabricated for the Apollo space program.

Various different fuel cell types are known, the main difference being the electrolyte material. Due to material properties like temperature stability and/or conductivity, the operation temperature of the fuel cell depends strongly on the applied electrolyte. Both the utilized fuel and the area of application are a consequence of the operation temperature and therefore of the fuel cell type. The major types of fuel cells, classified by the type of electrolyte, are outlined in Table 2.1

Table 2.1. Types of Fuel Cell [37]

Fuel Cell Type	Electrolyte	Operating Temperature (^oC)	Electrochemical Reactions	Field of Applications
Polymer Electrolyte Membrane (PEMFC)	Solid organic polymer	30-80	Anode : $H_2 \rightarrow 2H^+ + 2e$ Cathode : $\frac{1}{2} O_2 + 2H^+ + 2e \rightarrow H_2O$ ------------------------------ Cell : $\quad H_2 + \frac{1}{2} O_2 \rightarrow H_2O$	Transportation, Portable applications
Alkaline (AFC)	Aqueous solution of potassium hydroxide soaked in a matrix	90-100	Anode : $H_2 + 2 OH^- \rightarrow 2H_2O + 2e$ Cathode : $\frac{1}{2} O_2 + H_2O + 2e \rightarrow 2 OH^-$ --------------------------------- Cell : $\quad H_2 + \frac{1}{2} O_2 \rightarrow H_2O$	Transportation
Phosphoric Acid (PAFC)	Phosphoric acid soaked in a matrix	175-200	Anode : $H_2 \rightarrow 2H^+ + 2e$ Cathode : $\frac{1}{2} O_2 + 2H^+ + 2e \rightarrow H_2O$ ----------------------------------- Cell : $\quad H_2 + \frac{1}{2} O_2 \rightarrow H_2O$	Stationary power plants
Molten Carbonate (MCFC)	Solution of lithium, sodium and/or potassium carbonates soaked in a matrix	600-1000	Anode : $H_2 + CO_3^{2-} \rightarrow H_2O + CO_2 + 2e$ Cathode : $\frac{1}{2} O_2 + CO_2 + 2e \rightarrow CO_3^{2-}$ ----------------------------------- Cell : $\quad H_2 + \frac{1}{2} O_2 \rightarrow H_2O$	Stationary power plants
Solid Oxide (SOFC)	Solid zirconium oxide with a small amount of yttria	600-1000	Anode : $H_2 + O^{2-} \rightarrow H_2O + 2e$ Cathode : $\frac{1}{2} O_2 + 2e \rightarrow O^{2-}$ ------------------------ Cell : $\quad H_2 + \frac{1}{2} O_2 \rightarrow H_2O$	Stationary power plants, transportations (auxiliary power supply)

University of Indonesia

2.2. Thermodynamic and Kinetic Consideration of Fuel Cell

The efficiency limit of energy conversion systems, which operate based on internal combustion, is determined by the Carnot cycle:

$$\varepsilon = \frac{T_h - T_1}{T_h} \tag{2.1}$$

which T_h being the higher temperature of the heat source and T_1 being the lower temperature, e.g. at the gas outlet. Combustion engines usually exhibit an efficiency of $\leq 40\%$. Fuel cell represent an attractive alternative as their efficiency is not limited by the Carnot cycle as described below and most of the chemical energy stored in the reactants can be converted into electricity [38].

2.2.1. Thermodynamic Consideration of Fuel Cell

The maximum electric energy obtainable in a fuel cell is determined by the product of the reversible cell potential E and the charge Q (Q = n.F), and is thus given by a change in the Gibbs free energy:

$$W_{el} = \Delta G = -n.F.E \tag{2.2}$$

n is the number of electrons participating in the electrochemical reaction and F is the Faraday's constant [38,39].

If all reactants and products are present in the standard state equation 2.2 can be rewritten as:

$$\Delta G^0 = -n.F.E^0 \tag{2.3}$$

Under reversible reaction conditions the Gibbs-Helmholtz reaction (2.4) describes the correlation between the Gibbs free energy of a reaction ΔG, the reaction enthalpy ΔH and the change in entropy $T\Delta S$ (which describes the amount of heat produced or consumed during irreversible reaction) [38-40]

$$\Delta G = \Delta H - T\Delta S \qquad (2.4)$$

ΔS^0 and ΔH^0 (i.e., the standard entropy and standard enthalpy) are available from several standard reference tables usually at a temperature of 298 K. Conversion factors to calculate the corresponding values for other given temperatures are also tabulated.

For an overall fuel cell reaction of: $H_2 + \frac{1}{2} O_2 \rightarrow H_2O$, the Gibbs free energy is expressed as:

$$\Delta G = \Delta G^0 + RT \ln \frac{P_{H_2O}}{P_{H_2} \cdot P_{O_2}^{1/2}} \qquad (2.5)$$

Where R represents the molar gas constant, T the absolute temperature (in K) and P_x describes the partial pressures of the reactants and products. By substituting equations 2.2 and 2.3 into equation 2.5 one obtains the general form of the Nernst equation:

$$E = E^0 + \frac{RT}{nF} \ln \frac{P_{H_2} \cdot P_{O_2}^{1/2}}{P_{H_2O}} \qquad (2.6)$$

Regarding a given reaction at a constant pressure the reversible potential E depends on the temperature. From equation 2.2 and 2.4 the temperature dependence can be expressed as:

$$\left(\frac{\partial E}{\partial T} \right)_p = \frac{\Delta S}{n.F} \qquad (2.7)$$

For reactions with negative (positive) overall ΔS the reversible cell potential decreases (increases) with increasing T. When both reactants are offered in the gaseous form, ΔS for the build up of liquid water from hydrogen and oxygen amounts to -163 $Jmol^{-1}K^{-1}$ and E decreases by 0.85 mV when increasing the temperature by 1 K [40].

This result in a generally lower reversible cell potential for high temperature fuel cells compared to low temperature fuel cells. However, fuel cells are practically operated far from their equilibrium potential. Thus the actual cell voltage of fuel cells is influenced by parameters different from the reversible cell potential.

2.2.2. Kinetic Consideration and Cell Polarization

The performance of fuel cell is usually determined by obtaining a polarization curve (I-V curve), where cell voltage is plotted as a function of current density.
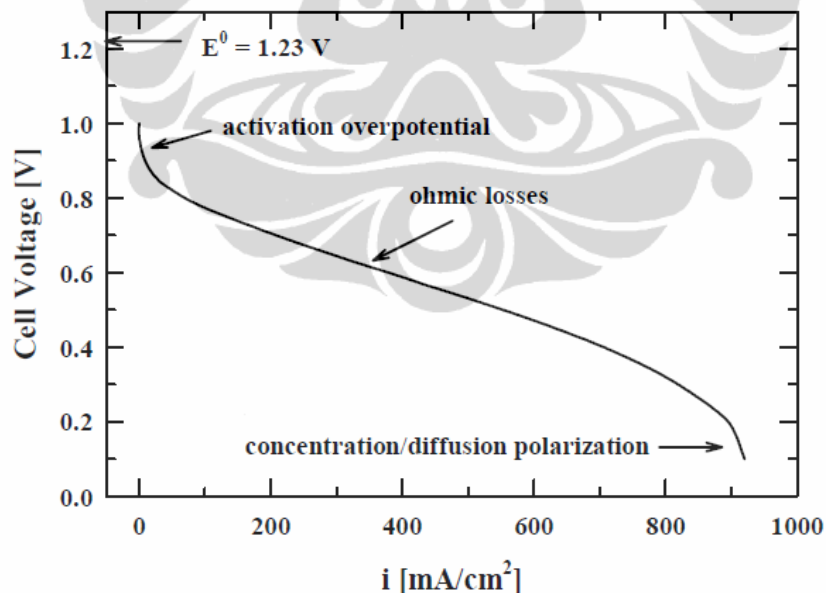
Figure 2.3. Typical Power Curve for Fuel Cell [37]

Naturally, a higher cell voltage at a specific current indicates better performance. From the polarization curve, we can get information about factors that affect cell performance. Performance losses caused by slow kinetics, ohmic resistance and mass transport can all be diagnosed from a polarization curve. Figure 2.3 shows a typical polarization curve for fuel cell.

Generally, there are three types of polarization losses can be identified, as follow:

1. Ohmic Polarization

   Ohmic polarization is caused by both the resistance due to the migration of ions within the ion conducting electrolyte and resistance due to the flow of electron

2. Concentration Polarization

   Concentration polarization occurs at high reaction rates, when the reactants are consumed rapidly and a concentration profile is build up between the reactant concentration at the electrode surface and in the bulk. Fuel cell operation is mainly influenced by concentration polarization losses at high current densities. In that case the transport of reactants to the electrode surface is limited by diffusion in the pores and the consumptions of reactants are fast.

3. Activation Polarization

   Activation polarization plays an important role if the reaction rate on the electrode surface is restricted by sluggish electrode kinetics. Similar to a chemical reaction the electrochemical reaction has to overcome an activation barrier. The barrier usually depends on the electrode material (electrocatalyst). It is influenced by process involving the adsorption/desorption of reactant species and/or product species, the transfer of electrons across the double layer and the nature of the electrode surface (rough or smooth surface)

2.3. Electrocatalyst and Structural Characterization

2.3.1. General Feature of Electrocatalyst

A catalyst is defined as a substance, usually used in small amounts relative to the reactants, that modifies and increases the rate of a reaction without being consumed in the processes [41].

The requirements for a practical catalyst for fuel cells include high intrinsic activity for the electrochemical oxidation of a fuel at the anode side and for the reduction of di-oxygen at the cathode side. It is also required good durability and should have good electrical conductivity to minimize resistive losses in the catalyst layer, be inexpensive to fabricate and be manufacturable at high volume with good reproducibility [36].

Catalyst plays an essential role in many chemical processes. The selection of a catalyst or catalyst system for a new catalytic process requires that many important technical parameters be considered. Catalyst should have properties such as high activity, high selectivity, high recycle capability and filterability.

Considering the requirements of suitable catalyst material for PEMFCs, platinum and platinum-containing catalysts are found to accord with these requirements, in both activity and stability. Catalyst exhibits great influence on both the cost and the durability of PEM fuel cells. Most of the presently used catalysts are Pt-based and are usually supported on porous conductive materials with a high specific surface area.

2.3.2. Electrocatalyst for Oxygen Reduction Reaction

Two reaction paths are assumed for the oxygen reduction depends on the pH of the electrolyte [42].
Direct reduction:

$$O_2 + 4H^+ + 4e^- \rightarrow 2\ H_2O \qquad\qquad E^0 = 1.23\ V \qquad\qquad (2.8)$$

University of Indonesia

Indirect reduction:

$$O_2 + 2H^+ + 2e^- \rightarrow H_2O_2 \qquad E^0 = 0.682 \text{ V} \qquad (2.9)$$

followed by a further reduction via

$$H_2O_2 + 2H^+ + 2e^- \rightarrow 2H_2O \qquad E^0 = 1.77 \text{ V} \qquad (2.10)$$

or a chemical decomposition via

$$2H_2O_2 \rightarrow 2H_2O + O_2 \qquad (2.11)$$

Several different models were developed during the last decades to describe the interplay between the two competing reactions. The following figure presents a simplified reaction scheme for the oxygen reduction reaction, based on the reaction schemes introduced by Wroblowa et al [43] and Bagotskii et al [44].

The scheme distinguishes between the pre-adsorbed oxygen being reduced through a direct four electron reduction resulting in the formation of water (k_1) or through a series pathway forming H_2O_2 as an intermediate (k_2) which is further reduced to water (k_3). In addition H_2O_2 can either chemically decompose to water and O_2 (k_4) or be desorbed into the solution (k_5).
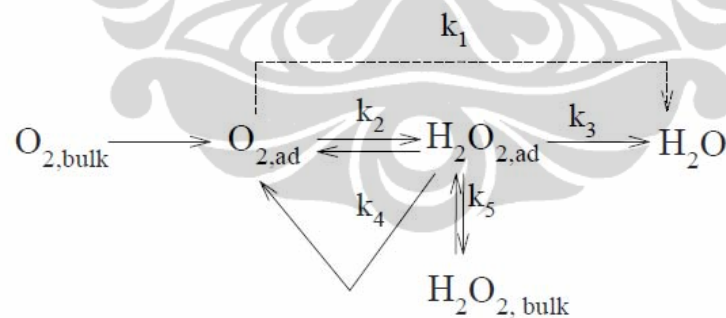
Figure 2.4. The ORR Pathway Based on the Scheme Suggested by Wroblowa [43]

The different reaction pathways are interpreted as the consequence of different adsorption state. The assumed adsorption possibilities for oxygen are schematically presented in Figure 2.5 and the resulting possible reaction pathways are shown in Figure 2.6.

A) Griffiths model   B) Pauling Modell   C) Bridge Modell
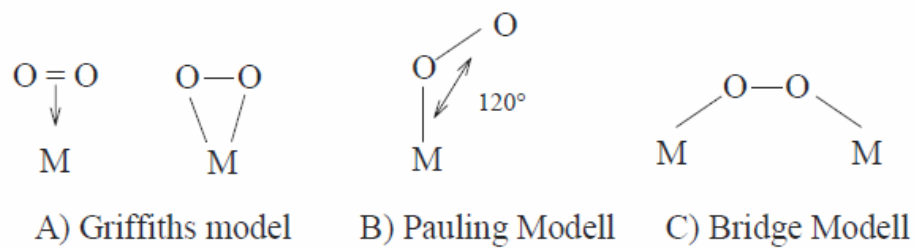
Figure 2.5. Models for the Adsorption of Oxygen on Catalyst Surface [42]

Once oxygen is adsorbed one sided (Pauling model) the O-O binding remains almost unchanged. Therefore pathway II is preferred and thus the formation of H_2O_2 is favored. Adsorption on both sides (Griffiths model, bridge model), however, stretches the O-O binding and thus prepares the decomposition of the O_2 molecule. Consequently the four electron reduction to water according to pathway I or III is favored [42, 45].
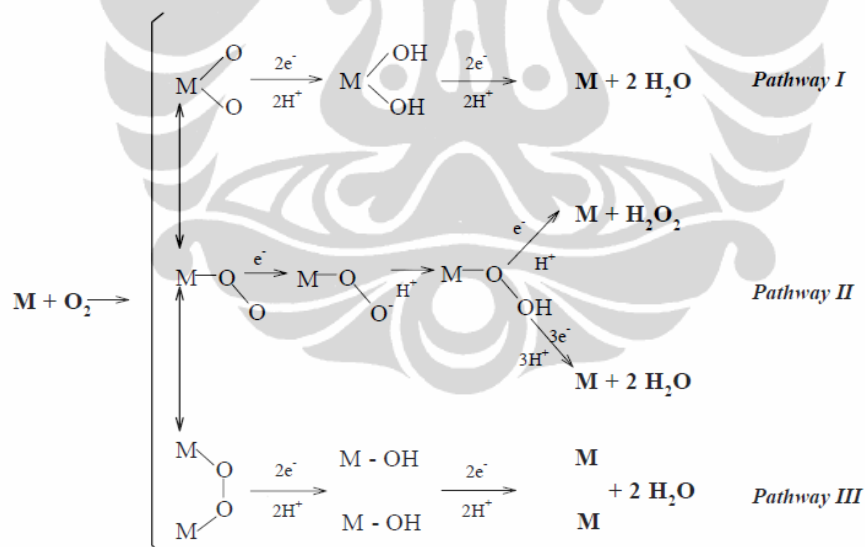
Figure 2.6. Reaction Pathways for the Oxygen Reduction in an Acid Surrounding [45]

When dealing with fuel cells the ORR is preferred to take place via the four electron reduction (either in a direct or a series pathway). The two electron reduction

with H_2O_2 as main product leads to a decreased utilization of the cathode feed gas and even more important to an accelerated degradation of the polymer electrolyte membrane. The oxygen reduction reaction suffers from poor kinetics and this results in high polarization losses of 0.3 to 0.4 V. Improvements in the PEMFC voltage output and thus improvements in the PEMFC efficiency will require finding a catalyst more active than platinum for ORR. Besides that, the requirement for the catalyst material like stability at temperature of up to 120 ^{o}C and stability in a highly corrosive surrounding make noble metals most suitable. Among the pure noble metals platinum shows the lowest overpotential and the ORR proceeds mainly via the four electrons pathway. Therefore, it is evident that platinum serves as the state of the art electrocatalyst in the oxygen electrode of PEMFCs [10].

Many researchers have demonstrated that activity of electrocatalyst advocated for ORR is strongly dependent on numerous factors such as particle size and particle size distribution [46], morphology of catalyst [47], catalyst composition and in particular its surface composition, oxidation state of Pt and second metal atom [48], and surface structure of the catalyst [49]. Several efforts have been made to improve the dispersion and stability of Pt nanoparticles [50-53], creating near-surface region with a Pt skin structure in Pt alloys via acid treatment [54-57], and core shell structure [58-61].

Pt based alloys have been extensively studied during the past decade. A vary of enhancement of the ORR kinetic by Pt based alloy are reported. Enhancement factor of 2-5 times were observed by Mukerjee et al [16], Paulus et al [13] and Stamenkovic et al [62], whereas factor up to 10 times was reported by Toda et al [63]. However, there is no consensus on why the Pt-based alloys have shown better activity toward ORR than that of Pt.

Toda et al [64] in the study of Pt/Fe alloys, attributed the ORR improvements to an increased Pt 5d-band vacancy, which strengthened the Pt-O_2 interaction and thus weakened and lengthened the O-O bond, facilitating O-O scission. Beard et al [65] attributed the ORR activity improvement to an increase in the catalyst surface roughness for the Pt_3Co alloy supported carbon in phosphoric acid media.

Alternatively, Arico et al [48] and Shukla et al [66] have proposed that the ORR enhancement was due to a decrease in surface oxides and an enrichment of Pt active sites of the catalyst surface. Finally, Mukerjee et al [16] suggested that the increased activity was due to a decrease in the Pt-Pt distance and in the Pt-Pt coordination number.

Pt-Co catalyst of various Pt:Co ratios have been reported to exhibit promising ORR activities relative to Pt nanoparticles. Stamenkovic et al [54-56] have shown that the polycrystalline Pt_3Co nanocrystals with a Pt skin layer is more active than polycrystalline Pt and bimetallic Pt_3M surfaces (M = Fe, Ni, V and Ti) and the Pt_3Ni (111) surface is 10 and 90 fold more active for the ORR than corresponding Pt (111) and Pt/C catalyst for PEMFC, respectively. The Pt_3Ni demonstrated unusual electronic structure (d band center position) and arrangement of surface atoms in the near surface region. It exhibits a Pt rich in the outmost and third layers, and Ni rich in the second atomic layer.

Duong et al [67] investigated oxygen reduction of Pt_3Co alloy in alkaline and acidic media by X-ray photoelectron spectroscopy and electrochemical methods. The XPS data show that two species of cobalt, metallic cobalt and cobalt oxides, coexist in the as received Pt_3Co sample. In combination with the voltammetric results, the XPS data demonstrate that there is dissolution of cobalt upon exposure of the sample to acidic media, whereas the cobalt forms in the catalyst are stable in alkaline media. In acids, Pt_3Co alloy has a slightly but demonstratively higher activity than Pt black toward ORR, while in alkaline media a decrease in the ORR activity was found.

Chen et al [57] demonstrated the chemical composition of Pt_3Co nanoparticle investigated by the atomic scale using aberration corrected scanning transmission electron microscopy (STEM), from which the origin of ORR activity enhancement of Pt alloy nanoparticle is postulated. The formation of percolated Pt skin regions in acid treated Pt_3Co nanoparticles was observed. Upon annealing of such acid treated sample, Pt sandwich segregation surface of order Pt_3Co nanoparticles was formed. The ORR activity of Pt_3Co and Pt nanoparticle was measured by sweep voltammetry in O_2 saturated $HClO_4$ electrolyte using a rotating disk electrode. The specific activity

of the annealed Pt_3Co at 0.9 V vs reversible hydrogen electrode (RHE) was increased four times than of Pt after annealing.

Recently, Strasser et al succeeded in the preparation of carbon supported, base metal rich $PtCu_x$ [60] and $PtCo_xCu_y$ [61] nanoparticles that show higher activities for oxygen reduction than commercial $PtCo_x/C$ catalysts. The electrochemical surface area of the alloy catalyst shows that the alloying process resulted in an almost twofold increase in active particle surface area compared to the standard catalyst. Once dissolution, it might be caused by surface roughening or particle break up. It is suspected that more favorable structural characteristics, such as Pt-Pt surface interatomic distances of the dealloyed particles, play a key role in the enhancement mechanism.

Recently, Markovic group has studied intrinsic catalytic of Pt_3Ni and Pt_3Co alloy catalyst with model bulk alloys characterized in UHV. The ORR of the Pt_3Ni and Pt_3Co catalyst has been studied in acid electrolyte using the rotating ring disk electrode method. In their studies Pt_3Ni and Pt_3Co catalysts with surface composition of 75% and 100% Pt were prepared. They observed that the ORR activity order on this catalyst is dependent on the nature of supporting electrolytes. It was found that the activity increases in the order $Pt_3Ni > Pt_3Co > Pt$ in H_2SO_4. However, in $HClO_4$ at 333 K, the ORR activity increases in the order Pt skin $> Pt_3Co >$ formation on Pt sites surrounded by oxide covered Ni and Co atoms beyond 0.8 V.

In an effort to increase the catalytic activity of Pt-Co, Zhang [68] prepared $PtCo_x/C$ core-shell catalysts by the underpotential deposition of a copper monolayer onto $PtCo_3$ nanoparticles, subsequent galvanic displacement of copper leads to a Pt shell on a $PtCo_3$ core.

PtCo/C as an electrocatalyst for ORR was also investigated by Lai et al [69]. In their study, PtCo/C nanoparticle was prepared by modified Watanabe method and was investigated by XAS. The relationship between the variations in alloying extent and Pt d band vacancy in PtCo/C electrocatalyst has been established, which is tunable with Pt and Co composition and has a strong impact on the catalytic activity for ORR. It is found that the catalytic activity of PtCo/C for ORR is higher when

compared to that of Pt/C, PtCo$_3$/C and Pt$_3$Co/C due to its higher alloying extent, smaller particle size and proper composition.

Very recently, Jayasayee et al [70] investigated stability of PtCo/C as a function of Pt-Co composition. In this work, the ORR and stability of unsupported Pt-Co bimetallic alloys with various Pt:Co ratios prepared through electrodeposition were investigated. Pt$_{10}$Co$_{90}$ electrodes showed superior activity and stability compared to all other compositions.

In recent years, many efforts to develop an alternative catalyst to Pt focused primarily on Pt based bimetallic alloys, in which platinum is partially replaced by other less expensive metals.[71-72] Numerous studies have highlighted the alloying of Pt with transitional metal such as Co [48,73], Ni [13,48,73-75], Fe [16], Mn [16], Cr [46,76-77] and V[78] as a promising approach toward improving ORR electrocatalyst in acidic solutions. A number of explanations for the improvement in activity by the addition of transition metals to Pt have been ascribed, including the lowering of the Pt oxidation state, the suppression of Pt oxide formation, the formation of a new electronic structure with higher Pt 5d orbital vacancies, a decrease in the Pt-Pt distance and therefore a more favorable adsorption of O$_2$ and the formation of a catalytic and thin Pt skin on the surface of the alloy [72]. Among these Pt catalysts, Pt-Co alloys were extensively studied and showed enhanced catalytic activity where Pt:Co ratios of 1:1 to 3:1 are most studied. Very recently, a study has been published in which alloy catalysts with a wide variety of Pt:Co of 9:1 to 1:9 compositions were electrodeposited on a carbon sub-layer and tested for their activity in PEM fuel cell [79]. Catalysts with a high Pt content were shown to be the most active in this study.

It should be noted that, although the Pt alloy electrocatalysts have shown an enhanced ORR activity in acidic media as compared to pure Pt, there is dissolution of base metals from the alloys. It was discovered that transition metals in Pt alloys leach out from their surfaces, resulting in a transition metal Pt core shell or in the formation of a so called Pt skin, where transition metal atoms in the bulk are protected by a pure Pt shell of a few atomic layers thickness [63,64].

University of Indonesia

In term of stability, Antolini et al [80] have reviewed the result of different test on the stability of Pt-M alloy catalyst under fuel cell conditions. Beard and Ross [65] and Travitsky et al [15] investigated the stability of Pt-Co catalyst (Co loss, change in the lattice parameter and in the surface area) but did not investigate its effect on the ORR activity. Watanabe et al [17] compared the ORR activity of ordered and disordered Pt-Co alloys after durability test (the disordered alloy was found to be more stable than the ordered alloy) but no comparison was made with pure Pt. Yu et al [81] investigated the durability of Pt/C and PtCo/C cathode catalyst in a dynamic fuel cell environment with continues water fluxing on the cathode. A potential cycling test between 0.87 and 1.2 V vs RHE was applied to the system to illustrate how cobalt or platinum dissolution affect the cell performance. They found that cobalt dissolution neither detrimentally reduces the cell voltage nor dramatically affects the membrane conductance. Colon Mercado and Popov [82] investigated the corrosion and surface area changes of platinum based catalyst supported on carbon and found a strong correlation between the amount of the alloying metal dissolved and the ORR activity of the Pt alloy catalysts.

Recently, Zignani [11] investigated the stability and durability of Pt and PtCo/C. In this work, Pt and Pt-Co were prepared by reduction of the corresponding metal precursors with $NaBH_4$ at room temperature. The durability of Pt and Pt-Co electrocatalyst then was investigated by correlating the change of electrocatalyst characteristics (Co content, lattice parameter, particle size) and the loss of ORR activity observed after various types of testing.

2.3.3. Heat Treatment on Pt Alloy (PtM/C) Electrocatalyst

Pt alloys with various transition metals have been extensively studied in order to reduce catalyst cost and also to improve both the resistance to sintering and the electrocatalytic activity toward ORR [6,80]. The alloying of a second metal into the Pt can cause a change in the Pt lattice parameters, which can be directly observed by XRD. A concentration in the lattice spacing or a shift in the position of the reflection

peaks is indicative of the second metal being dissolved and of the formation of an ordered Pt-M phase.

The particle size and lattice constant of the alloy are also dependent on the preparation method. Heat treated PtCo/C alloy prepared in acidic media (pH=2) showed larger particle size, more significant ordering and greater alloying degree than those prepared in the basic media (pH=11) [65].

Cambanis and Chadwick [83] prepared heat treated PtV/C catalyst with different Pt/vanadium ratios. The heat treatment was performed at 830 and 930 ^{o}C. They observed that heat treatment resulted in crystalline sizes in the range of 3.3-3.5 nm when treated at 830 ^{o}C and 4.0-4.5 nm when treated at 930 ^{o}C, independent of the vanadium content. It was also found that the catalyst heat treated at 930 ^{o}C had less activity, which was attributed to the sintering effect. Heat treatment on PtV/C was also investigated by Santos et al [84]. In their work, catalyst was treated at 300, 500 and 850 ^{o}C for 1 h. They found that increasing the heat treatment temperature resulted in an increase of the Pt 5d band occupancy for Pt/C, consequently leading an enhancement of the ORR kinetics. No changes in the electronic properties were noted for PtV/C with an increase of heat treatment temperature.

Antolini et al [78] heat treated Pt-V alloy catalyst under Ar + 10% H_2 atmosphere for 2 h at 500 and 850 ^{o}C in effort to evaluate the effect of particle size and lattice parameters on the catalytic ORR performance in a PEM fuel cell. It was found that a decrease lattice parameter and an increase particle size (from 3.4 to 5.4 nm) with an increase in heat treatment temperature.

Min et al [46] prepared three carbon supported alloy catalyst, PtCo, PtNi and PtCr and heat treated each of them separately at 600, 700, 900 and 1100 ^{o}C in a reducing atmosphere. From their study showed that catalytic activity increased with increasing heat treatment temperature, the amount of increased activity was dependent on the nature of the second metal used in the alloying process, particle size and alloying degree with Pt.

Santiago et al [85] prepared $Pt_{70}Co_{30}$ nanoparticle catalyst using a polyol process. The first sample was treated at 400 ^{o}C for 2 h in H_2 atmosphere and the other

was first treated at 200 ^{o}C for 1 h in air, and then followed by a 300 ^{o}C treatment for 1 h in H$_2$ atmosphere. The ORR performance catalyzed by both as prepared and heat treated PtCo catalyst was better than that of commercially available Pt/C and PtCo/C catalyst. Both heat treated catalyst also showed an increase in the crystallite size compared to as prepared Pt$_{70}$Co$_{30}$/C.

Beard and Ross [65] prepared Pt-Co/C alloy with 3:1 atomic ratio, by using two methods: in acidic (pH=2) and alkaline (pH=11) aqueous medium. The synthesized catalysts were then heat treated at 700, 900 and 1200 ^{o}C under an inert atmosphere for 2 h. It found that heat treatment improves the catalyst activity in the whole temperature range, and that PtCo/C treated at 1200 ^{o}C showed slightly higher specific activity than Pt/C. An important observation was the effect of the heat treatment on Co loss. Catalyst synthesized by both methods showed a Co loss of more than 80% for untreated catalyst, and 15% for sample treated at 1200 ^{o}C and 28.4% for acidic and alkaline routes.

Watanabe et al [17] prepared Pt-Co/C catalyst and investigated the effect of heat treatment on their ORR catalytic activity and stability under the operating conditions of a phosphorous acid fuel cell. Heat treatment was conducted in a reducing atmosphere at several temperatures ranging from 400 to 900 ^{o}C for different time intervals under 20 h. The highest ordered structure was achieved with catalyst heat treated at temperature between 600 and 650 ^{o}C for more than 5 h. It was found that the mean diameters of the Pt-Co alloy crystallites increased linearly with increasing heat treatment temperature.

Salgado et al [86] investigated the effect of heat treatment on the structural and activity properties of PtCo/C alloy. The catalyst was heat treated at 550 and 900 ^{o}C under a hydrogen atmosphere for 3 h. It is observed that increased in particle size and contraction of the lattice, as a result of increasing temperature. However, through ORR kinetic analysis, it was found that sample treated at 550 was more active than treated at 900 ^{o}C, although its alloying degree was poorer.

In an attempt to avoid alloy particle growth, Xiong et al [87] prepared carbon supported Pt-M alloys (M = Fe, Co, Ni and Cu) using a low temperature (70 ^{o}C)

method and investigated their ORR catalytic activity in a half cell containing a sulphuric acid solution and in a PEM fuel cell cathode. Two alloy catalysts, PtCo/C and PtFe/C were separately heat treated at 200 and 900 $^{\circ}$C in an atmosphere of a flowing mixture Ar + 10% H_2. They observed that the particle size increased with increasing heat treatment temperature and time. The ORR activities of these two catalysts were improved by heat treatment at lower temperature (200 $^{\circ}$C). However, both catalysts treated at the higher temperature of 900 $^{\circ}$C catalysts showed a dramatic degradation in ORR activity, which was attributed to the increase in particle size.

An investigation on PtCo/C nanoparticle was also carried out by Fernandez et al [88]. He has demonstrated that the thermal treatment of PtCo/C plays a key role in the performance of the samples in the ORR. Fresh and 300 $^{\circ}$C hydrogen treated samples proved to be moderately active electrocatalysts. However, after thermal treatment at 875 $^{\circ}$C under hydrogen, PtCo/C surpassed the performance of the state of the art Pt/C catalyst in the ORR

Recently, Schulenburg et al [89] treated $PtCo_3$ nanoparticles at temperature of 350 to 1000 $^{\circ}$C and were characterized by chemical and electrochemical method. It was found that $PtCo_3$ treated at 800 $^{\circ}$C leads to the highest mass activity for oxygen reduction and it was 2.4-fold higher than that for commercial PtCo/C.

Mayrhofer et al [25] has introduced novel preparation procedure of such core shell nanoparticle with a platinum shell by using an adsorbate-induced surface segregation effect. This effect is additionally dependent upon the chemical potential of the gas phase since the strong bonding of adsorbates will result in a gain in energy of the system. Consequently, for bimetallic systems, enrichment at the surface of the component that binds a certain adsorbate more strongly may occur. For this purpose, the catalyst was subject to either a gas phase treatment or an electrochemical treatment. In a gas phase treatment, catalyst powder was placed into a rotary evaporator, which was then repeatedly evacuated and filled with CO to eliminate residual oxygen. The distiller was then filled with ambient pressure of CO and heated to 200 $^{\circ}$C for three hours.

The state of the art of the research on heat treatment on Pt-M/C electrocatalyst is summarized in the Table 2.2. From the Table 2.2 it is clearly seen that when temperature is increased, the lattice constant decreased. According to Vegard's law, when the temperature is fixed, the lattice parameters are linear function of the alloy composition. Thus, the degree of alloying can be determined by the value of these lattice parameters. It also can be seen from the Table 2.2 that the degree of alloying formation is a function of the temperature. Therefore, heat treatment temperature may be used to adjust the degree of alloying.

In summary, heat treatment of as prepared Pt-M/C catalyst increases the catalyst particle size, and at the same times, changes the catalyst lattice structure from a disordered one to a partially ordered one. It seems that the lattice structure change effectively improves the ORR catalytic activity and catalyst stability, although the catalyst active area is reduced by the growth of particle size.

2.4. Surface Segregation

Surface segregation is a phenomenon that one or more types of elements enrich in the surface region, resulting in the surface composition becoming higher than the bulk composition. This phenomenon is of great importance, especially for catalyst study, because it may either improve or block desirable and undesirable reactions

The thermodynamics of surface segregation was first studied by Willard Gibbs [90]. Nowadays there are many experimental methods has been developed to obtain the surface concentrations, such as ion scattering spectroscopy (ISS), auger electron spectroscopy (AES) and X-ray photoemission spectroscopy (XPS). Although the development of experimental techniques enables us to conduct a wide and deep exploration of surface segregation for catalyst, there are still limitation due to the expensive cost of those equipments and difficulties in preparing experimental sample. Therefore, theoretical modeling for surface segregation has been widely applied.

University of Indonesia

There are two factors influence in determining which element of the binary alloy system may segregate to the surface or move away from the surface. The first one is size effect. The differences in atomic size between the two elements in the binary alloy effect on mismatch strain energy of the system. It might be decreased when one element diffuse towards the surface, compared to when the two elements are randomly distributed in the alloy system. The second factor is the different between surface energies of pure elements. The element with lower surface energy will diffuse towards the surface and thus decrease the total surface energy of the binary alloy system.

Surface segregation phenomena in binary alloy systems have been investigated by many groups. Gauthier et al [91] observed surface sandwich segregation at the (111) surfaces of disordered $Pt_{50}Ni_{50}$ and $Pt_{78}Ni_{22}$ alloy by low energy electron diffraction (LEED). It was found that the concentration of Pt in the first, second and third layers are 88±2, 9±5 and 65±10 % respectively. A near pure Pt top layer was found in $Pt_{78}Ni_{22}$ alloy with first layer containing of 99±1 % Pt. In another paper, Gauthier et al [92] reported a segregation reversal on $Pt_{50}Ni_{50}$ (110) surface. Enrichments of 100 % Ni, 95 % Pt and 83 % Ni were found in the first three layers.

Theoretically, it is difficult to predict surface segregation for Pt based alloy system. Sometimes, it is orientation dependent and lack of reliable experiment technique to obtain the quantitatively reliable segregation energies. Photoemission spectroscopy of surface core level shifts (SCLS) is more reliable technique, but it only feasible for very restricted set of dilute alloys. While for other alloys, estimation should be based on the Langmuir-McLean relation between bulk and surface composition, which is very sensitive to the environmental condition and invalid if the ordering effects in the system can't be neglected [93].

Nilekar et al [94] conducted a systematic test of surface energies for various bimetallic transition metal alloys. In this work, which is focused on the low index (100) surface, the surface segregation energy for impurity Co atom in the host of Pt atoms was found to be 0.29 eV, indicated Pt atoms would segregate to the outmost

layer and Co may stay at the subsurface. Ma et al [95] studied the surface segregation energies of (111) surface for a series Pt_3M alloy system by density functional theory (DFT) calculations. The results showed segregation energy for Pt_3Co, Pt_3Fe and Pt_3Ni are -0.61, -0.41 and -0.38 eV respectively, indicated Pt segregation in all three alloys. The tendency of segregation is stronger, when the energy is more negative.

2.5. Structural Model and Atomic Distribution of Bimetal Nanoparticles as Investigated by X-ray Absorption Spectroscopy
2.5.1. X-ray Absorption Spectroscopy

X-ray absorption spectroscopy (XAS) has become a widely used technique to determine the local atomic structure of materials since last two decades. The increasing use of XAS may be attributed to its unique potential to provide information regarding the oxidation state and local coordination numbers as well as the identity of neighbors, and absorbing atom. The advantage of XAS over other characterization methods lies in the ability to conduct the measurement in situ. XAS technique can provide information on the morphology of the considered species, as well as the distribution of the two metals insides the species [27,28]. With the development of XAS, researchers have obtained a tool which is particularly well suited for the structural investigation of bimetallic NPs. XAS consists of X-ray absorption near edge structure (XANES) and extended X-ray absorption fine structure (EXAFS).

The XANES spectra which is conventionally from below the edge up to ~ 30-50 eV provide information about the oxidation state, fractional d-electron density and electronic environment of absorbing atom, while the EXAFS spectra which is above the edge ~30-50 eV, either the L edge or K edge of transition metals, yield information on the number, type and distance of the backscattering atom surrounding the central absorbing atom and allow investigation on the short ordering and provide geometric information.

The principle concern of XAS measurements is how the absorption coefficient μ, varies with the X-ray energy (μ depends strongly on atomic number Z, and on the density ρ and atomic mass A,). This absorption coefficient gives the probability of the absorption of X-rays and is related to the X-ray intensity by Beer's law [99]:

$$I_t = I_0 \, e^{-\mu t} \qquad\qquad (2.12)$$

Where I_0 is the incoming X-ray intensity to the sample, I_t is the intensity transmitted through the sample and t is the sample thickness.

The actual experimental set up and data acquisition required to perform XAS experiments is quite simple but usually involve X-rays sources with high energy and with very collimated beams (synchrotron radiation)
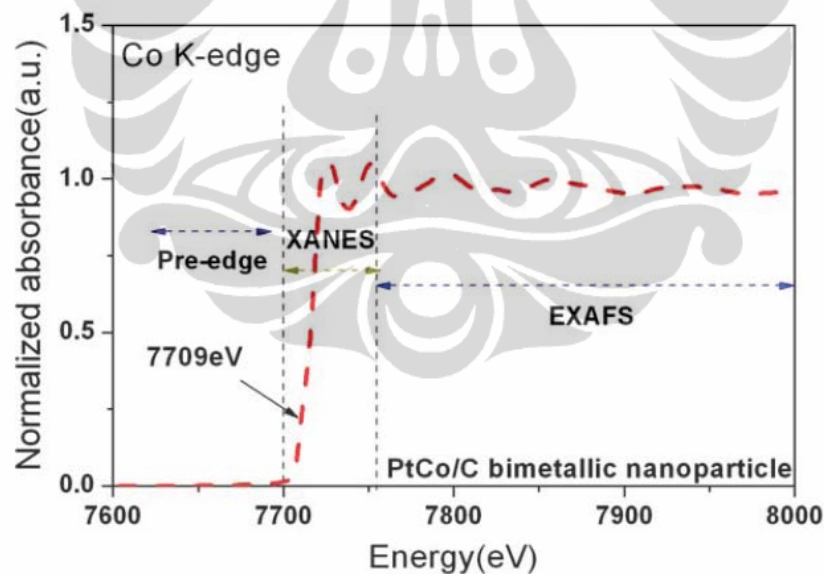
Figure 2.7. X-ray Absorption Spectrum of Co K-edge for Pt-Co/C
Electrocatalyst[100]

2.5.2. Identification of Structural Model and Atomic Distribution by X-ray Absorption Spectroscopy

The structure of bimetallic nanoparticles (NPs), which contains two kinds of metal elements, may possess the crystal structure similar either to the bulk alloy or another type in which the distribution of each metal element is different from the bulk. Applicability of XAS to derive structural models for bimetallic NPs has been reported. However, researchers have proposed only qualitatively the structural model of bimetallic NPs such as random alloy, alloy with an intermetallic compound type, cluster in cluster and core shell structure [101]. It is rather scarce that literature describing the quantitative extent of alloying or atomic distribution of bimetallic NPs. Therefore, it is of interest to estimate the extent of alloying or atomic distribution of elements in bimetallic NPs to get more detail about the structure as well as their real application. In this direction, we have analyzed the bimetallic NPs by XAS. By estimating the ratio of the coordination number of atom A around atom B and also the coordination number of atom B around atom A to the total coordination numbers, we have deduced the quantitative parameters alloying extent, J_A and J_B, in A-B bimetallic NPS.

The quantitative of alloying extent or atomic distribution in bimetallic NPs can be evaluated by deriving the XAS structural parameters. The parameters that are needed to derive the alloying extent are represented as $P_{observed}$, $R_{observed}$, P_{random} and R_{random}. The parameter $P_{observed}$ can be defined as a ratio of the scattering atoms B coordination number around absorbing A atoms (N_{A-B}) to the total coordination number of absorbing atoms $(\sum N_{A-i})$.

$$P_{observed} = \frac{N_{A-B}}{\Sigma N_{A-i}} \qquad (2.13)$$

Similarly, $R_{observed}$ can be defined as a ratio of the scattering atoms A coordination number around absorbing B atoms $(N_{B\text{-}A})$ to the total coordination number of absorbing atoms $(\sum N_{B\text{-}i})$.

$$R_{observed} = \frac{N_{B-A}}{\Sigma N_{B-i}} \qquad (2.14)$$

Whereas, P_{random} and R_{random} can be taken as 0.5 for perfect alloyed bimetallic NPs if the atomic ratio of A and B is 1:1. This value can be achieved by assuming $N_{A\text{-}A} = N_{A\text{-}B}$ and $N_{B\text{-}B} = N_{B\text{-}A}$, which is generally true for perfect alloyed bimetallic NPs.

This methodology can be easily extended to the other NP systems of interest. In similar way P_{random} can be taken as 0.67 and 0.8 for 1:2 and 1:4 bimetallic NPs respectively. The parameter R_{random} can be taken as 0.33 and 0.2 for 1:2 and 1:4 bimetallic NPs. In this contribution, we focus on 1:1 bimetallic NPs system. From the ratio of $P_{observed}$ to P_{random}, we can evaluate the alloying extent of the A element in NPs and similarly, from the ratio of $R_{observed}$ to R_{random} we can estimate the alloying extent of the B element in NPs.

The alloying extent of element A (J_A) and element B (J_B) for 1;1 A-B bimetallic NPs can be calculated quantitatively by using the following equations respectively.

$$J_A = \frac{P_{observed}}{P_{random}} x100\% \qquad (2.15)$$

$$J_B = \frac{R_{observed}}{R_{random}} x100\% \qquad (2.16)$$

It is possible to construct the structural models emphasizing the atomic distribution in the bimetallic NPs with the knowledge of the $\sum N_{A\text{-}1\text{.}}$, $\sum N_{B\text{-}1}$, J_A and J_B values derived

from XAS. It is also possible to predict the structure models of NPs, with the help of the alloying extent and structural parameters extracted from EXAFS.

Actually there are unlimited cases possible which really depend on the alloying extent, but herein we will discuss seven possible cases as presented in Figure 2.8.

1. Case 1 : if $J_A = 0$ and $J_B = 0$,

   Then both A and B particles are not involved in the alloying and resulted in separated cluster particles. In this case, if $N_{A-A} = N_{B-B}$, this means that the particle size of both A and B is same, but $N_{A-A} > N_{B-B}$ means the particle size of A is larger than that of B. Only at the equilibrium state, is it possible to know the nature of metallic interaction. For bimetallic NPs systems, which have not reached the kinetic barrier, it is not possible to assess the extent of metallic interactions. In this case, homoatomic interaction of A atoms (H_{A-A}) and homoatomic interaction of B atoms (H_{B-B}) >> bimetallic (A-B) heteroatomic interaction (H_{A-B}) and means that there are no heteroatomic interactions in the NPs.

2. Case 2 : if $J_A = J_B = 100\ \%$

   Then both the A and B atoms are involved completely in the alloying process and resulted in perfect alloyed NPs. If the bimetallic system is in the equilibrium state, then the interactions will be $H_{A-A} = H_{B-B} = H_{A-B}$, which means that there are equal bimetallic interactions in the NPs.

3. Case 3 : if $J_A < 100\ \%$ and $J_B < 100\ \%$

   Then both A and B atoms are not preferred to be alloyed, and it indicates that a higher extent of A/B atoms prefer A/B atoms and prefer only to a lesser alloying extent between A and B atoms. If $J_B > J_A$, it appears that the core is rich in A atoms and the shell is rich in B atoms. The $\sum N_{A-I}$ will be greater than that of $\sum N_{B-I}$. At equilibrium conditions we can see the order of interaction will be $H_{A-A}, > H_{B-B} > H_{A-B}$. On the contrary, if $J_A > J_B$, then in the resulting bimetallic NPs, B atoms are rich in the core and A atoms are rich in the shell.

University of Indonesia

In this case $\sum N_{B\text{-}I} > \sum N_{A\text{-}I}$. At the equilibrium state, the interaction follows the order $H_{B\text{-}B} > H_{A\text{-}A}, > H_{A\text{-}B}$.

4. Case 4 : if $J_A > 100\%$ and $J_B < 100\%$

Then B atoms prefer B atoms rather than A, and A atoms prefer B atoms rather than A atoms. As a result, atomic distribution of A atoms is better than that of B atoms. In other word, we can say segregation of A atoms is less pronounced than that of B atoms. At equilibrium state the interactions are in the following order $H_{B\text{-}B} > H_{A\text{-}B}, > H_{A\text{-}A}$. In this type the bimetallic NPs adopts a structure similar to B rich in core - A rich in shell.

Here $\sum N_{B\text{-}I} > \sum N_{A\text{-}I}$. Even though the structures describe in case 3 and case 4 are similar in nature, but the atomic dispersion of A atoms in NPs of case 4 is better, indicating J_A value role in providing the degree of atomic dispersion in NPs quantitatively which we can't simply obtain from coordination numbers. In case if $J_A < 100\%$ and $J_B > 100\%$ the situation is reverse to the case 4, i.e. the atomic distribution of B atoms is better when compared to that of A atoms. As a result the structure will be similar to A rich in core – B rich in shell. At equilibrium state the interactions are in the order $H_{A\text{-}A}, > H_{A\text{-}B} > H_{B\text{-}B}$.

5. Case 5 : if $J_A > 100\%$ and $J_B > 100\%$

Then the atomic distribution of both A and B atoms is improved, and in the resulting structure, we can expect more heteroatomic interactions than homoatomic interactions. At equilibrium, the interactions will be in the following order $H_{A\text{-}B}, > H_{A\text{-}A} > H_{B\text{-}B}$. By comparing the different models described above (from case 4 to case 5) we can provide atomic distribution quantitatively which is very important for nanoparticles application.

6. Case 6 : if $J_A < 50\%$ and $J_B < 50\%$

Then the resultant structure A particles are in the core and B particles are in the shell. The total coordination number, $\sum N_{A\text{-}I}$ will be greater than that of $\sum N_{B\text{-}I}$. At the equilibrium state, the interactions follows the order $H_{A\text{-}A}, > H_{B\text{-}B} > H_{A\text{-}B}$. In case $J_A < 50\%$ and $J_B < 50\%$ the bimetallic NPs adopts a structure

similar to B core − A shell. In this case $\sum N_{A-I} > \sum N_{B-I}$ and the interactions at equilibrium state are in the following order $H_{B-B} > H_{A-A}, > H_{A-B}$.

7. Case 7 : if $J_A = 200\,\%$ and $J_B = 200\,\%$

Then A atoms always prefer B atoms and vice versa, and the resulting structure looks like an onion ring, in which one layer is occupied by A atoms and the other layer by B atoms.

The methodology will be useful to deduce the structural model and alloying extent or atomic distribution of nanoparticles systems. It is possible to understand and control the structure of bimetallic NPs based on these structural parameters.
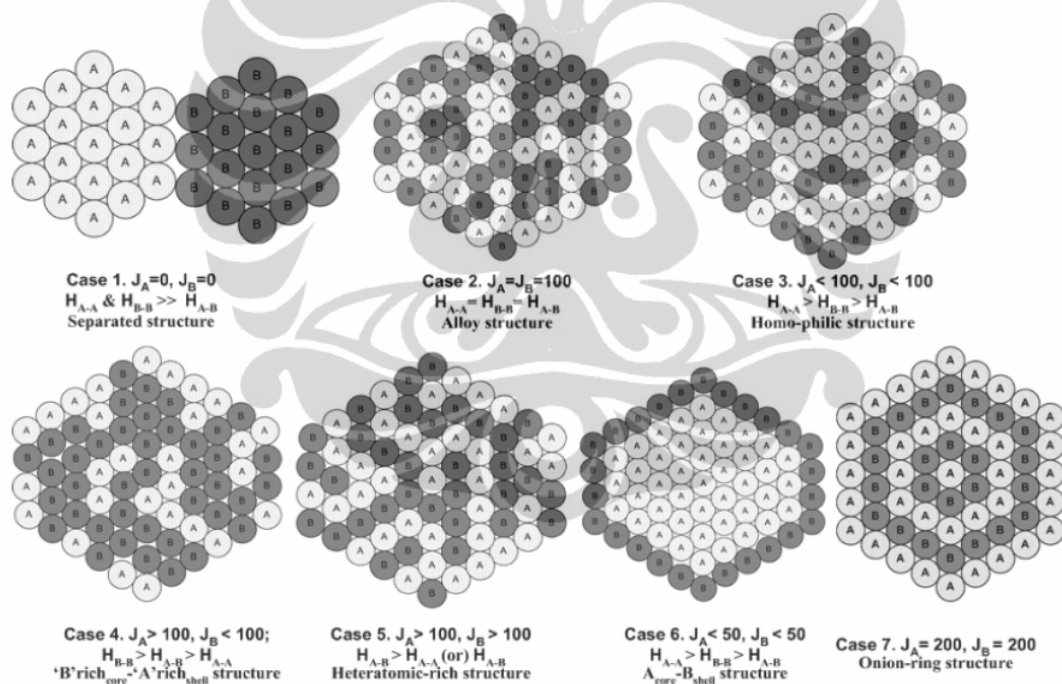
Figure 2.8. Schematic of Bimetallic Nanoparticles at Various Degrees of Alloying [27]

Table 2.2. State of the Art of Research on Heat Treatment on Pt-M/C Electrocatalyst

Second Metal in Pt-M/C	Heat Treatment Condition	Remarks	Reference
V (1:1)	500 ^{o}C and 850 ^{o}C, 2 h with Ar/H$_2$	Particle size : 3.9 and 5.4 nm for 500 ^{o}C and 850 ^{o}C respectively Lattice constant (Å) : 3.880 and 3.8686 for 500 ^{o}C and 850 ^{o}C respectively Alloying degree (%) : 25 and 33 for 500 and 850 oC respectively	Antolini et al [78]
Co (3:1)	600, 700, 900 and 1100 ^{o}C, 2.5 h with N$_2$/10% H$_2$	Particle size : 3.83, 2.95, 6.60, 8.63 for 600, 700, 900 and 1100 ^{o}C respectively Lattice constant (Å) : 3.855, 3.876, 3.866, 3.868 for 600, 700, 900 and 1100 ^{o}C respectively Alloying degree (%) : 61, 79, 75 for 700, 900 and 1100 ^{o}C respectively	Min et al [46]
Cr (3:1)	700, 900 and 1100 ^{o}C, 2.5 h with N$_2$/10% H$_2$	Particle size : 4.23, 6.23, 10.4 for 700, 900 and 1100 ^{o}C respectively Lattice constant (Å) : 3.903, 3.884, 3.883 for 700, 900 and 1100 ^{o}C respectively Alloying degree (%) : 39, 78, 81 for 700, 900 and 1100 ^{o}C respectively	
Ni (3:1)	700, 900 and 1100 ^{o}C, 2.5 h with N$_2$/10% H$_2$	Particle size : 4.62, 6.35, 10.2 for 700, 900 and 1100 ^{o}C respectively Lattice constant (Å) : 3.858, 3.841, 3.836 for 700, 900 and 1100 ^{o}C respectively Alloying degree (%) : 53, 70, 75 for 700, 900 and 1100 ^{o}C respectively	

University of Indonesia

Co (3:1)	Acidic route : 700, 900 and 1200 ^{o}C, 2 h	Particle size : 8.4, 8.0, 12.0 for 700, 900 and 1200 ^{o}C respectively Lattice constant (Å) : 3.870, 3.867, 3.864 for 700, 900 and 1200 ^{o}C respectively	Beard and Ross [65]
Co (3:1)	Alkaline route : 700, 900 and 1200 ^{o}C , 2 h	Particle size : 2.5, 4.1, 10.4 for 700, 900 and 1200 ^{o}C respectively Lattice constant (Å) : 3.894, 3.907, 3.910 for 700, 900 and 1200 ^{o}C respectively	
Co (3:1)	550 and 900 ^{o}C, 3 h with H$_2$	Particle size : 3.9 and 6.8 for 550 and 900 ^{o}C respectively Lattice constant (Å) : 3.911 and 3.897 for 550 and 900 ^{o}C respectively Alloying degree (%) : 7 and 35 for 550 and 900 ^{o}C respectively	Salgado [86]
Co (3:1)	400 ^{o}C, 2 h 200 ^{o}C, 1 h (air) + 300 ^{o}C, 1h (H$_2$)	Particle size and lattice constant : 9.6 nm and 3.90 Å for first condition respectively Particle size and lattice constant : 8.3 nm and 3.90 Å for second condition respectively	Santiago et al [85]
Co (5:1)	200 and 900 ^{o}C, 1 h with Ar/10% H$_2$	Particle size : 4.9 and 6.6 for 200 and 900 ^{o}C respectively	Xiong et al [87]
Cu (3:1)	300, 600 and 900 ^{o}C, 1 h with Ar/10% H$_2$	Particle size : 6.9, 17.1, 29.6 for 300, 600 and 900 ^{o}C respectively Lattice constant (Å) : 3.86, 3.88 and 3.85 for 300, 600 and 900 ^{o}C respectively	Tseng et al [96]
Fe (1:1)	500, 600 and 800 ^{o}C, 1 h with Ar/10% H$_2$	Particle size : 6.3, 6.5 and 6.8 for 500, 600 and 800 ^{o}C respectively Lattice constant (Å) : 3.847, 3.845 and 3.848 for 500, 600 and 800 ^{o}C respectively	Xiong et al [97]

University of Indonesia

Co (1:1)	650 °C with Ar/10% H_2	Particle size and lattice constant : 5.8 nm and 3.780 Å respectively	Xiong et al [97]
Ti	700, 900 and 1200 °C, 2 h with He (methanol :water solution = 1:1)	Particle size : 11.0, 12.5, 14.4 for 700, 900 and 1200 °C respectively Lattice constant (Å) : 3.916, 3.907, 3.906 for 700, 900 and 1200 °C respectively	Beard and Ross [98]
Ti	700, 900 and 1200 °C, 2 h with He, (methanol :water solution = 1:1, pH :10)	Particle size : 5.0, 7.0 and 28.0 for 700, 900 and 1200 °C respectively Lattice constant (Å) : 3.922, 3.922 and 3.908 for 700, 900 and 1200 °C respectively	
Co	300 and 875 °C under H_2	PtCo/C treated in hydrogen at 875 °C is more active for ORR than the commercial sample Pt/C	Fernandez et al [88]
Co	350 - 1000 °C	Heat treatment at 800 °C leads to the highest mass activity, yield 2.4 times higher activity than commercial Pt-Co/C TEM images revealed that particle size remains constant until temperature of 600 °C	Schulenburg [89]
Co	Treated with CO at 200 °C for 3 h	Nanoparticles consisting of a Pt shell around a PtCo core were formed by utilizing an adsorbate-induced surface segregation effect, resulting in a highly active catalyst with a low amount of noble metal	Mayrhofer et al [25]

University of Indonesia

CHAPTER 3
EXPERIMENTAL METHODS

This chapter provides an overview of the experimental methods applied in the current work. The PtCo/C commercial catalyst was treated in two different ways, which are treatment using nitrogen with various of temperatures and treatment using carbon monoxide with various of times.

Catalyst then was characterized by X-ray diffraction (XRD), transmission electron microscopy (TEM), and X-ray absorption spectroscopy (XAS). Electrochemical characterization then was applied to observe the electrocatalytic activity toward ORR by cyclic voltammetry and linear sweep voltammetry measurement. Finally, the catalyst was applied in single cell to obtain the electrocatalyst performance.

3.1. Material and Chemicals

The following chemicals were used during the period of study:
- Sulfuric Acid, H_2SO_4 95-97% : ACROS
- Commercial PtCo/C 30 wt% electrocatalyst from E-TEK
- Commercial PtCo/C 20 wt% electrocatalyst from PREMETEK
- Commercial Pt/C 40 wt% electrocatalyst from ETEK
- Nafion Solution, 5wt% : ALDRICH
- Methanol, CH_3COOH p.a : ACROS
- Sodium hydroxide, NaOH
- Isopropanol from Merck
- Methanol from Merck
- Pure water : Millipore pure water systematic Milli RO60
- Carbon Paper
- Nafion 117 from DuPont
- Nitrogen

- Hydrogen (ultra high purity)
- Oxygen (ultra high purity)

While, the following equipments were used for measurement, analysis and characterization:

- XRD
- TEM
- XAS
- Three Electrodes Electrochemical Cell
- PEM Single Cell
- Electronic Discharge Meter ®Prodigit 3311D 60 V/60 A, 300 V
- Termometer
- Flowmeter
- Humidifier
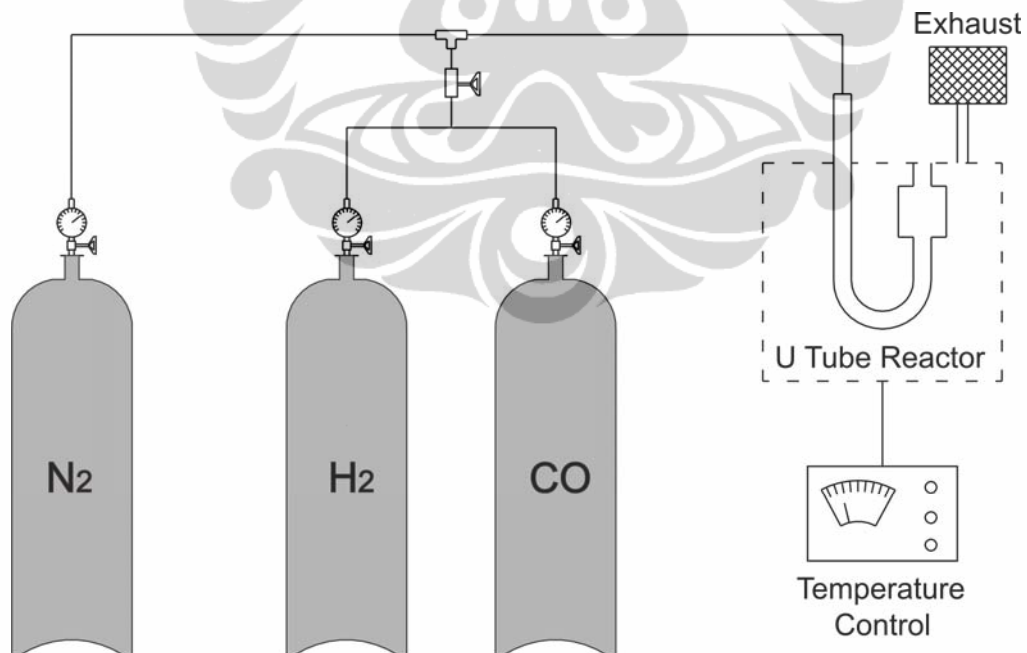
The treatment was done with the following diagram:

Figure 3.1. Flow Diagram of Heat Treatment of PtCo/C Electrocatalyst

University of Indonesia

3.2. Catalyst Treatment

A commercial E-TEK PtCo/C (30 wt% Pt) catalyst was used for the nitrogen treatment studies. To obtain a reliable comparison, sample from the same batch with homogenous mixing were used. First, the as received catalyst powder was pre-treated by flowing H_2 for 2 h at 300 ^{o}C. The sample then was allowed to cool temperature under N_2 atmosphere. In the case of N_2 thermal treatment experiments, pure N_2 gas was introduced into the sample chamber with a flow rate of 60 mL min^{-1} for about 2 h at various temperatures i.e. 300, 400, 500, 600 and 700 ^{o}C. Again, the catalyst was allowed to cool temperature under N_2 atmosphere. H_2 was flowed to clean any existing impurities and to eliminate the oxide contribution.

In the case of CO thermal treatment, a commercial PREMETEK PtCo/C (20 wt% Pt) was used. First, catalyst was purged by flowing H_2 at 300 ^{o}C for 2 h. The sample then was allowed to reduce to 200 ^{o}C then purged by flowing 20% CO at various times i.e. 1, 3, 5, 7, 10 and 15 h. Later, the sample was allowed to cool temperature. H_2 was flowed to clean the impurities if present any and to eliminate the oxide contribution.

Description of the samples code is described as following:

Table 3.1. Description of Catalyst Samples

No. of sample	Description
(1)	PtCo/C commercial (E-TEK)
(2)	PtCo/C - N_2 treatment 300 ^{o}C
(3)	PtCo/C - N_2 treatment 400 ^{o}C
(4)	PtCo/C - N_2 treatment 500 ^{o}C
(5)	PtCo/C - N_2 treatment 600 ^{o}C
(6)	PtCo/C - N_2 treatment 700 ^{o}C
(7)	PtCo/C commercial (PREMETEK)
(8)	PtCo/C - CO treatment 1 h
(9)	PtCo/C - CO treatment 3 h
(10)	PtCo/C - CO treatment 5 h
(11)	PtCo/C - CO treatment 7 h
(12)	PtCo/C - CO treatment 10 h
(13)	PtCo/C - CO treatment 15 h

3.3. Physical Characterization

3.3.1. X-ray Diffraction

X-ray diffractograms of the electrocatalyst were obtained with a universal Rigaku Dmax-B, Japan diffractometer operating with a Cu Kα radiation (λ = 0.15406 nm) generated at 40 kV and 100 mA. Scans were done at 0.05 deg s^{-1} for 2θ values between 20 and 90°. An average value of the lattice parameter was obtained from the Pt (111), (200), (220) and (311) peaks. The crystalline sizes were obtained from the Pt (220) reflection using Scherrer's equation:

$$D = \frac{k\,\lambda}{\beta\,\cos\theta} \tag{3.1}$$

Where D is the average particle size in Å, k is a coefficient taken here as 0.9, λ is the wavelength of the X-rays used, β is the width of diffraction peak at half height in radians, and θ is the angle at the position of the peak maximum.

3.3.2. Transmission Electron Microscopy

Transmission electron microscopy (TEM) and electron diffraction measurements were carried out on Phillips TEM. High angle annular dark field scanning transmission electron microscopy images were obtained with Tecnai G2 F20 operated at 300 kV. Samples were prepared by sonicating a small amount of the catalyst NPs in ethanol. A drop of this slurry was deposited onto a holey carbon-copper grid followed by drying in the oven.
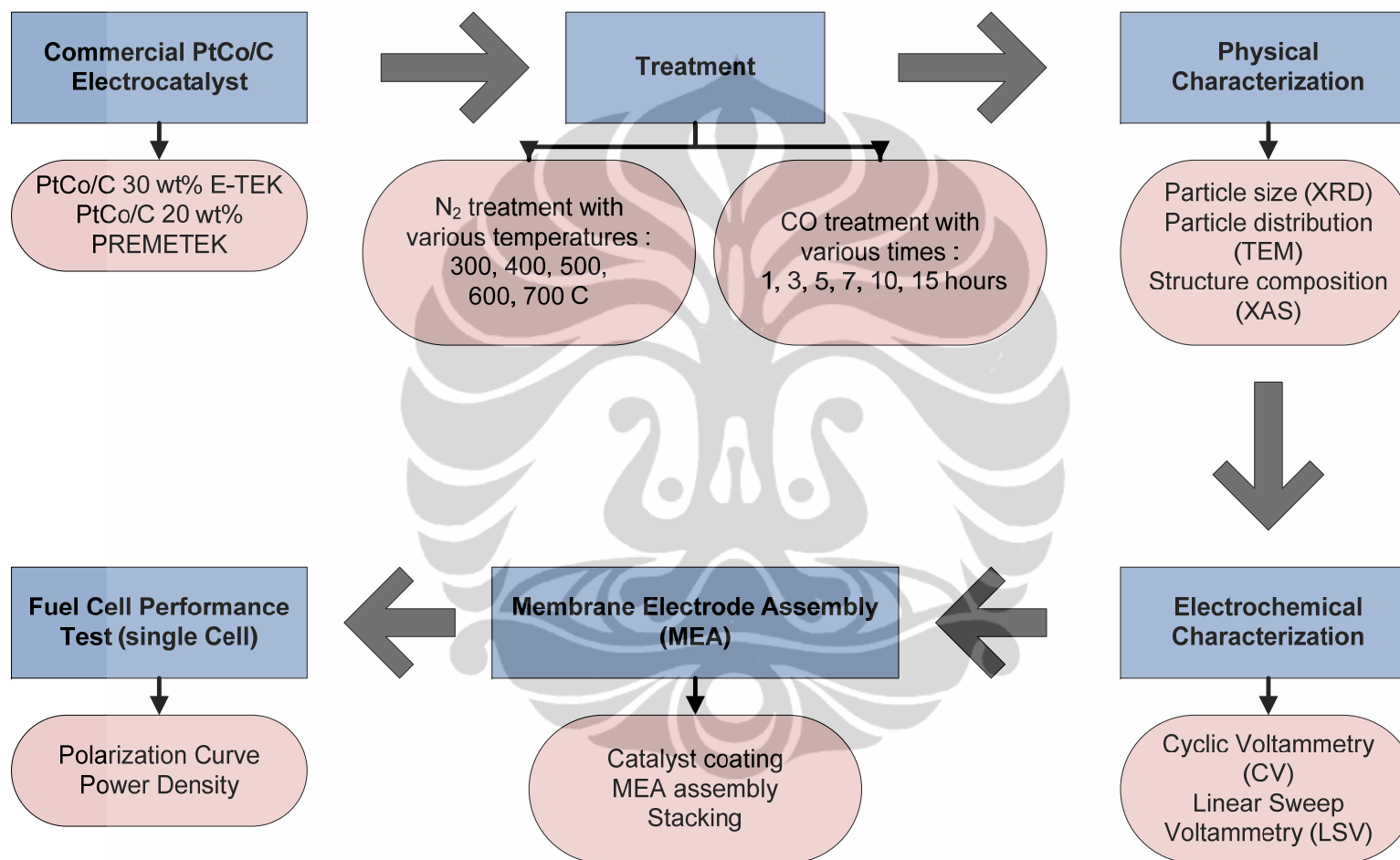
Figure 3.2. Flow Diagram of Research Experiment

3.3.3. X-ray Absorption Spectroscopy

The X-ray absorption spectra were recorded at the beamline 17C1, National Synchrotron Radiation Research Centre, Hsinchu, Taiwan. The electron storage ring was operated at 1.5 GeV with a current of 300 mA. A Si (111) double crystal monochromator was employed for the energy selection with a resolution $\Delta E/E$ better than 2 x 10^{-4} at both the Pt L_{III}-edge (11564 eV) and the Co K-edge (7709 eV). All of the experiments on bimetallic nanoparticles were conducted on homemade cells fabricated with stainless steel for an XAS powder study. Prior to the XAS measurements, samples were reduced with 10% H_2 for 1 h at 300 ^{0}C to remove any oxidized species remaining on the catalyst surface. The total amount of the sample was adjusted to reach the optimum absorption thickness ($\Delta\mu x = 1.0$, $\Delta\mu$ is the absorption edge, x is the thickness of the sample) so that the proper edge jump step could be achieved during measurements. All of the spectra were recorded at room temperature in a transmission mode. Higher harmonics were eliminated by detuning the double crystal Si(111) monochromator. A series of three gas filled ionization chambers were used to measure the intensities of the incident beam (I_0), the beam transmitted by the sample (I_t) and the beam subsequently transmitted by the reference foil (I_r). The third ion chamber was used in conjunction with the reference samples, which were a Pt foil for Pt L_{III}-edge measurements and a Co foil for the Co K-edge measurements. The control of parameters for EXAFS measurements, data collection modes, and calculation of errors were all carried out according to the guidelines set by the International XAFS Society Standards and Criteria Committee.

EXAFS Data Analysis. The XAS experimental data were treated by utilizing the standard procedures. The EXAFS function, χ , was obtained by subtracting the post edge background from the overall absorption and then normalized with respect to the edge jump step. The normalized $\chi(E)$ was transformed from energy space to k-space, where "k" is the photoelectron wave vector. The $\chi(k)$ data were multiplied by k^2 to compensate for the damping of EXAFS oscillations in the high k-region.

Subsequently, k^2 weighted $\chi(k)$ data in k-space ranging from 3.53 to 13.95 $\text{\AA}^{-1}$ for the Pt L $_{III}$-edge and from 3.53 to 10.36 $\text{\AA}^{-1}$ for the Co K-edge were Fourier transformed (FT) into r-space to separate the EXAFS contribution from the different coordination shells. A non linear least squares algorithm was applied to the curve fitting of an EXAFS in the r-space between 1.8 and 3.2 Å for both Pt and Co depending on the bond to be fitted. The PtCo reference file was determined by a theoretical calculation. Reference phase and amplitude for the Pt-Pt absorber scatter pairs were obtained from a Pt foil. For the Co-Co and Co-O absorber scatter pairs, the phase and amplitude were obtained from the reference Co foil and CoO, respectively. All of the computer programs were implemented in the UWXAFS 3.0 package [102], with the backscattering amplitude and the phase shift for the specific atom pairs being theoretically calculated by using the Feff7 code [103]. From this analysis, structural parameters such as coordination numbers (N), bond distance (R), Debye-Waller factor ($\Delta\sigma_j^2$) and inner potential shift (ΔE_0) have been calculated. For the amplitude reduction factor, S_0^2, values for the Pt and Co were obtained by analyzing the Pt and Co foil reference samples respectively, and by fixing the coordination number in the FEFFIT input file.
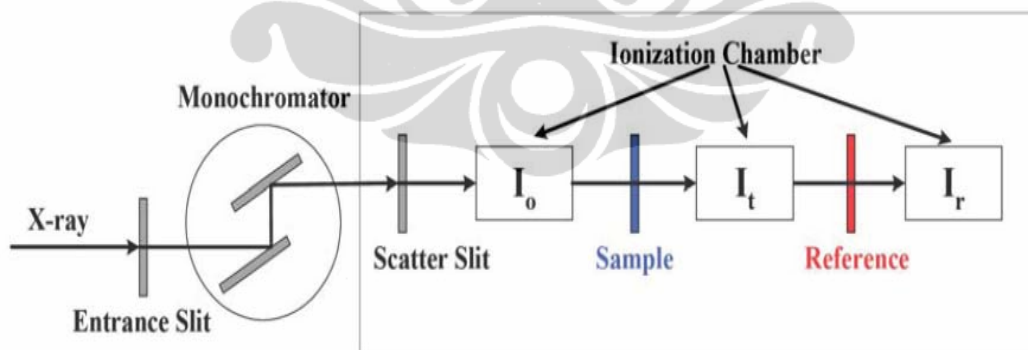

Figure 3.3. Experimental Setup for XAS Measurements [100]

University of Indonesia

3.4. Electrochemical Methods and Setup

3.4.1. Cyclic Voltammogram

Cyclic voltammetry is the most widely used technique for acquiring qualitative information about electrochemical reaction. Cyclic voltammetry describes the imposition of a triangular potential time waveform on the working electrode. The working electrode potential is varied periodically between the lower turning potential E_{t1} and the upper turning potential E_{t2} with a constant scan rate $v = dE/dt$ as shown in Figure 3.4. The obtained current-potential values are recorded and displayed as cyclic voltammogram. Anodic current are plotted in positive while cathodic currents in negative direction.

In the absence of redox active substances in the electrolyte in the potential region between the two turning potentials E_{t1} and E_{t2}, the observed current-potential behavior is exclusively determined by the formation and dissolution of hydrogen ad-layers and oxygen ad-layers on the working electrode surface. Figure 3.5 shows polycrystalline platinum in argon saturated 0.5 M H_2SO_4. The potentials refer to the reversible hydrogen electrode (RHE) in the same solution, i.e. the equilibrium potential for the hydrogen evolution/oxidation reaction is defined to be 0 in any case.
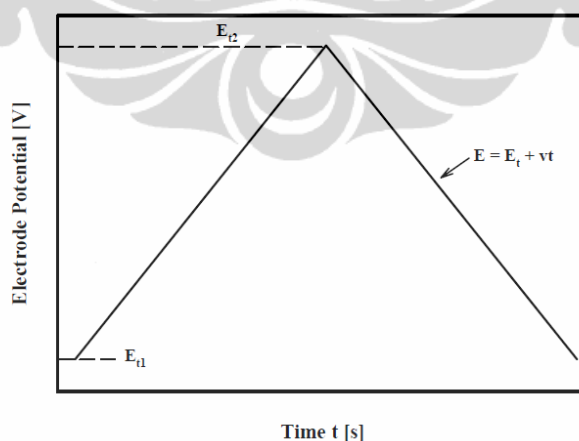
Figure 3.4. Potential-time Behavior of The Working Electrode Typical for the Cyclic Voltammetry [104]

One can distinguish several regions of the voltammogram. In anodic direction between 0.35 and 0.8 V and in cathodic direction between 0.65 and 0.35 V one observes only the current flow required to charge the electrochemical double layer. Above 0.8 V this region is followed by oxide chemisorptions which proceeds in two steps

$$Pt + H_2O \rightarrow Pt\text{-}OH + H^+ + e^- \qquad (3.2)$$

$$2Pt\text{-}OH \rightarrow Pt\text{-}O + Pt + H_2O \qquad (3.3)$$

If the potential limit is further increased, oxygen evolution can be observed above ca. 1.4 V.
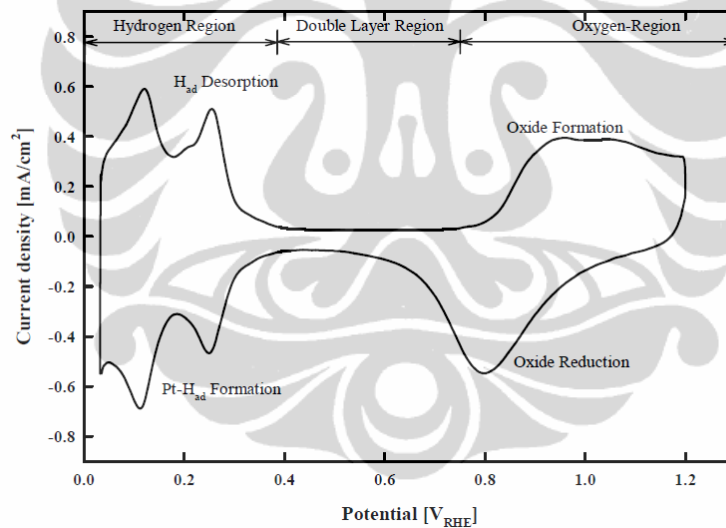
Figure 3.5. Cyclic Voltammogram of Polycrystalline Platinum in Argon-purged 0.5 M H_2SO_4 [105]

When reversing the sweep direction, reduction of the oxide layer is observed. Compared to the oxide formation the oxide reduction is shifted to lower potentials. Following the double layer charging, deposition of atomic hydrogen occurs (underpotential deposition, H_{upd}) according to:

$$Pt + H^+ + e^- \rightarrow Pt\text{-}H \qquad\qquad (3.4)$$

Close to the equilibrium potential of 0 V the onset of strong evolution of hydrogen is found, which is re-oxidized once the potential sweep direction is reversed again. The H_{upd} region shows two well-resolved peaks. The peak located around 120 mV is related to the adsorption/desorption process of hydrogen on low coordinated Pt surface atoms comparable to the H adsorption/desorption peak observed on Pt (110) single crystal surfaces. The second peak is located around 240 mV. At the same position a H adsorption/desorption peak can be observed on Pt(100) single crystal surfaces [105]. This peak therefore points to the H_{upd} process taking place on 100 facets.

The measured current density obtained from the cyclic voltammograms depends on the potential sweep rates. The manner of dependence, however, varies with the given electrochemical system. If the constitution of the equilibrium coverage e.g. of the H_{upd} film is fast compared to the sweep rate, then the current density, i , will be directly proportional to the sweep rate and increase with increasing sweep rate [42], i.e. i ~ v. The peak potential E_p is independent of the sweep rate : if the electrode reactions are, however, exclusively determined by diffusion of the reactants to the electrode surface and a subsequent electron transfer process at the surface, the current increases with the square root of the sweep rate according to equation 3.5 [42]

$$i \sim \sqrt{v}.c.\sqrt{D} \qquad\qquad (3.5)$$

where D is the diffusion coefficient and c is the concentration of the limiting species.

3.4.2. Determination of Electrochemical Active Surface Areas

The determination of the surface area of platinum metal electrodes using hydrogen adsorption has been one of the most widely used methods for determination

of the real surface of fuel cell electrodes. Two central assumptions of this method are:

- the potential at which the hydrogen forms a monolayer on the surface is at the onset of hydrogen evolution

- the relation between adsorbed hydrogen and platinum atoms is one to one.

Determination of exact potential where the hydrogen monolayer is formed was a very crucial aspect in experimental point of view. It has been concluded that the value for the charge of the hydrogen adsorbed and to refer to an area defined by the hydrogen adsorbing atoms. The most accepted value is 210 μC cm^{-2}, which is close to the calculated charge for Pt (100) surfaces.

The cyclic voltammetry is the most common method for determining the current-potential curve for adsorption and desorption of the hydrogen monolayer. The integration of the current in the anodic scan gives the amount of hydrogen desorbed, since the charge required to remove one hydrogen atom is 1, according to the reaction:

$$H_{ads} \rightarrow H^+ + e^- \tag{3.6}$$

In voltammetric cycle, with constant potential sweep change, the charge due to the double layer can be obtained, scanning the potential into double layer region and extrapolating to the hydrogen region. The integration that can be carried out is therefore:

$$Q_H = \frac{1}{v} \int (j - j_{dl})\, dE \tag{3.7}$$

Where

v : the sweep rate at which the cyclic voltammetry is recorded

j : the electric current density

j_{dl} : the current density due to the double layer charging
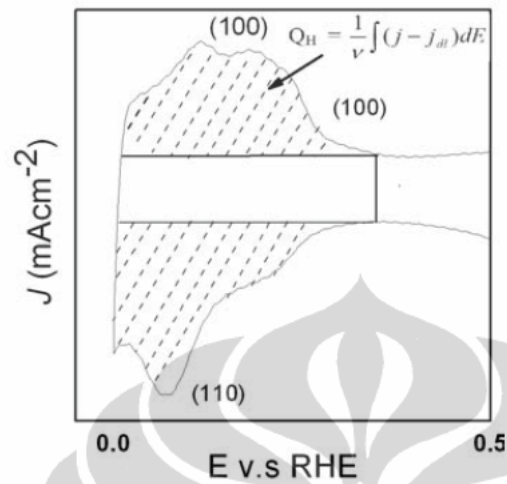
dE : the change in potential

Figure 3.6. Cyclic Voltammogram of Pt/Vulcan Dispersed Electrode [100]

The double layer current usually is small for pure electrodes, but it is very high for carbon dispersed electrodes. However, the current due to hydrogen can be distinguished and results quite similar to smooth electrode can be obtained. The differential capacity obtained from the i vs E curve for the carbon electrode (Vulcan XC 72) in the thin porous coating electrode was 13 μC cm^{-2}, taking the area measured by BET (230 m^{2}g^{-1}). This is a typical value for the capacitance for metal electrode.

3.4.3. The Rotating Disk Electrode Setup

Many electrochemical techniques are known involving electrodes which itself are in motion with respect to the electrolyte. These techniques include e.g. rotating disk, rotating rings, rotating wires, streaming mercury electrodes or rotating mercury electrodes. One convective mass transport is involved these techniques are also called hydrodynamic methods. The advantages of these methods are that the steady state is build up rather quickly. The mass transfer to the electrodes surface is faster than in case of stationary electrodes where mass transfer is determined solely by diffusion. Consequently, the influence of mass transfer to the electron-transfer kinetic is in

University of Indonesia

general smaller than in case of stationary electrodes [106]. The rotating disk electrode (RDE) system is a convective electrode system for which both the hydrodynamic equation (T. von Karman, 1921) and the convective-diffusion equation (V.G.Levich, 1942) have been solved for steady state condition [106]. Figure 3.7 gives a schematic overview of the RDE setup.

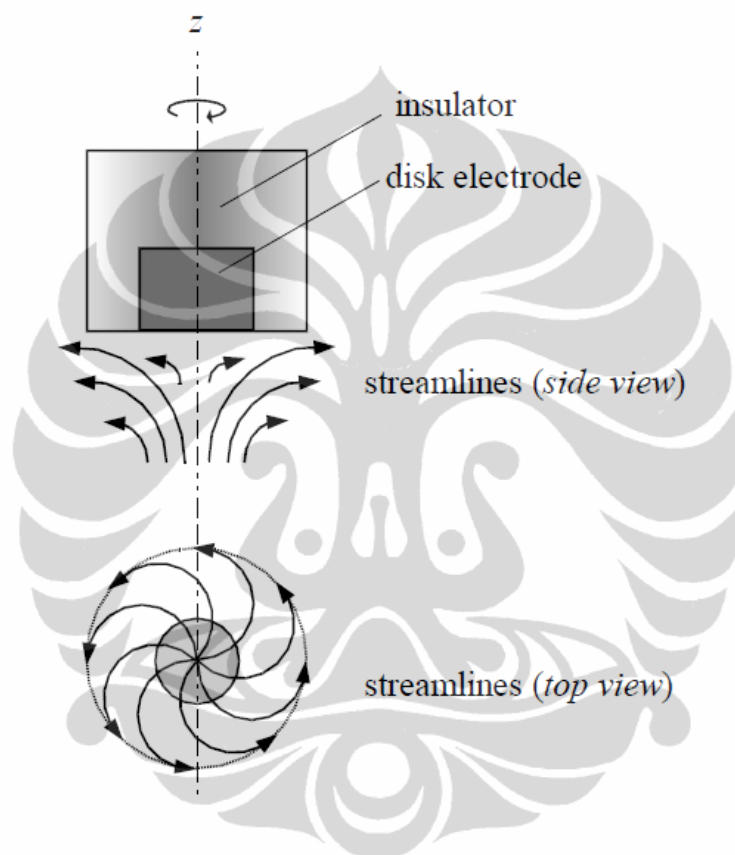Figure 3.7. Scheme of a Rotating Disk Electrode Setup [104]

The RDE consists of a circular electrode surrounded by an insulator. The electrode rotates with a defined constant velocity around the rotating axis z, which is perpendicular to the electrode surface. The electrode acts like a pump, which suck the electrolyte (and the reactants dissolved in the electrolyte) to its surface and propels it outwards radially.

3.4.4. Electrode Preparation and Electrochemical Analysis

Analytical grade Millipore water (18 MΩ) and sulfuric acid (ACROS) were used in this study. All of the experiments were carried out at ambient temperature of $25 \pm 1^{o}C$. A conventional three electrodes electrochemical cell was used for the CV measurements, with a high surface area Pt counter electrode and the saturated calomel electrode (SCE) as a reference electrode powered by a Solartron 1480 potentiostat/galvanostat. However, all potentials reported herein are referenced to the NHE. The working electrode was made of the carbon supported PtCo catalyst immobilized on a GCE surface ($0.1964 \, cm^{2}$).

The procedure for the electrode fabrication involves, first, preparation of a clear suspension by sonicating a known amount of PtCo/C catalyst powder dispersed in 0.5% Nafion, second, placing an aliquot of this suspension (7 μL) on the GCE disk, and, third, air drying about 5 minutes at room temperature and then at 80 ^{o}C to yield a uniform thin film of the catalyst. CV experiments were performed in 0.5 M H_2SO_4 solution at a scan rate of 10 mV/s. N_2 gas was purged for nearly 30 minutes before starting the experiment, and stable voltammogram recorded after two cycles were taken into account for all the CV experiments.

Stability measurements were recorded up to 2000 cycles, and were done every 500 cycles with a new solution. Linear sweep voltammetry was performed in the potential range from 0.856 to -0.244 V in 0.5 M H_2SO_4 solution with a scan rate of 1 mV/s and rotation of 1600 rpm.
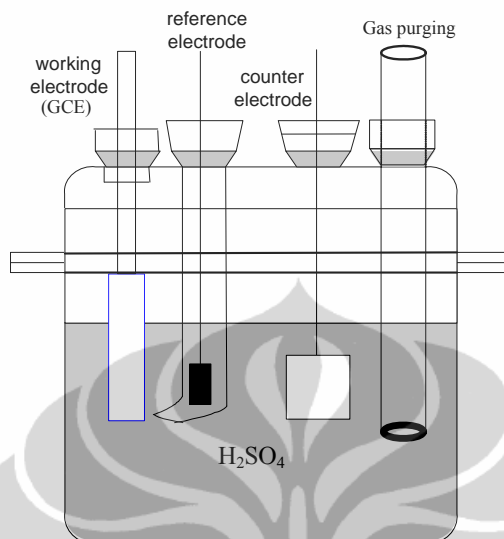
Figure 3.8. Three Electrodes Electrochemical Cell

3.5. Single Cell Performance Test

The obtained MEA was stacked to a homemade standard single stack PEM fuel cell with parallel plate that purchased from Fuel Cell Store, USA.

Single stack PEM fuel cell was firstly passed cross leak test before ready to use. The leak test was done by flowing inert gas to hydrogen inlet valve of PEM fuel cell then hydrogen outlet valve was closed, and oxygen inlet-outlet valve were monitored by soap bubbles. Tube of hydrogen and oxygen can be set for measurement after no leak was measured.

Prior to measurement of fuel cell performance, single stack PEM fuel cell was humidified. Conditioning was done by flowing hydrogen and oxygen to single stack PEM fuel cell at flow rate of 100 ml/min, temperature of 50 ^{o}C at ambient pressure for at least 3 hours. Performance of single stack was measured by electronic discharge meter 3300 C Electronic Load Mainframe Prodigit 3311D 60V/60A, 300 V.

University of Indonesia

Figure 3.9. Flow Diagram of Single Cell Performance Measurement

In this test, MEA was prepared by following procedure: catalyst ink was prepared by mixing the required amount of catalyst powder with 5% Nafion® solution (Du Pont) and then dilute with a mixture of millipore^{TM} water and 2-propanol. The resulting ink then placed in an ultrasonic bath until the catalyst powder had fully dispersed. This ink then is coated in a piece of carbon paper above a hot plate with temperature of 40 °C. The catalysts ink (anode and cathode catalyst) were coated in carbon paper with 25 cm^2 area. The catalyst layer on carbon paper then sandwiched with porous carbon paper to make the membrane electrode assembly (MEA) by pressing at 65 bar and 120 °C for 1 minutes. The catalyst for anode was Pt/C (E-TEK) as reference with wt 40%. Meanwhile, catalyst employed for cathode was Pt-Co/C. The loading of Pt for anode side is 0.5 mg/cm^2 and for cathode side is 0.5 mg/cm^2.

University of Indonesia

CHAPTER 4
RESULT AND DISCUSSION

The result of experiments will be presented and discussed in this chapter. The discussion was emphasized on the effect of particle size on its activity and stability of nitrogen-treated PtCo/C electrocatalyst and an adsorbate-induced surface segregation in bimetallic PtCo/C nanoparticles.

4.1. Effect of Particle Size on Activity and Stability of PtCo/C Electrocatalyst
4.1.1. Structure Characterization of Nitrogen-treated PtCo/C Electrocatalyst

The composition of commercial E-TEK PtCo/C electrocatalyst is 72:28 which was determined from the edge jump measurements of the Co K-edge and Pt L_{III}-edge X-ray absorption near edge spectra (XANES). It is found that the atomic composition of Pt-Co is very close to the nominal value (3:1).

Figure 4.1 shows the comparison of XRD patterns of a commercial E-TEK PtCo/C electrocatalyst with loading of 30 wt% and PtCo/C catalyst subjected to N_2 treatment at various temperatures. In all the catalysts, the peak appeared at 20-25° is attributed to the (002) plane of the hexagonal structure of the Vulcan XC 72 carbon [11]. As indicated in Figure 4.1, all the catalysts exhibit the main characteristic peaks of the face centre cubic (fcc) crystalline Pt with the peak positions of the (111), (200), (220), (311) and (222) planes appeared at 2θ value of ca. 40.25^o, 46.82^o, 68.36^o, 82.42^o and 86.96^o respectively according to XRD standard JCPDS No. 87-0647.

In this PtCo/C XRD pattern showed there is no superlattice reflection, which indicates the formation of only disordered solid solution. Also there is no peak for pure Co or its oxide was found. This presence can't be discarded because may be it present in a small amount or even in amorphous form [11]. The absence of characteristic peaks associated to the cobalt-species indicates that all the catalysts are single phase disordered structure [17].
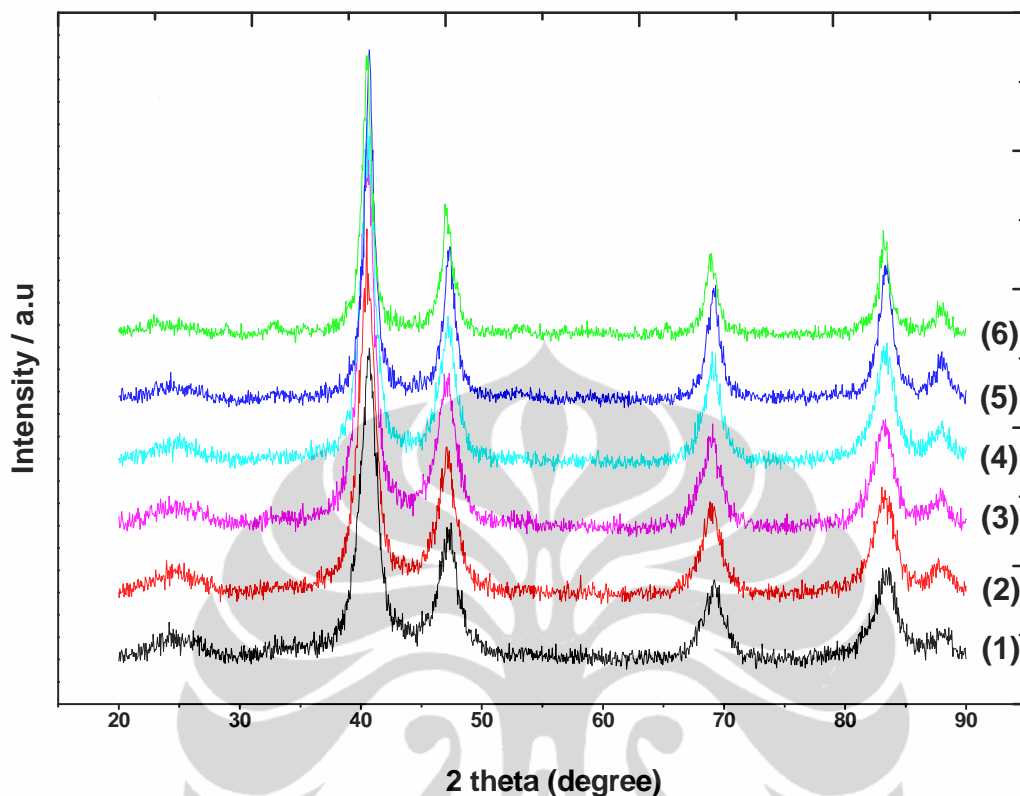
Figure 4.1. X-ray Diffraction (XRD) Patterns of PtCoC Electrocatalysts
(1) Commercial E-TEK PtCo/C, (2) PtCo/C N_2-treated 300 ^{o}C, (3) PtCo/C N_2-treated 400 ^{o}C, (4) PtCo/C N_2-treated 500 ^{o}C, (5) PtCo/C N_2-treated 600 ^{o}C, (6) PtCo/C N_2-treated 700 ^{o}C

The average grain size associated with the catalyst is calculated by using Scherrer's equation and full-width at half maximum of peak (220) is listed in Table 4.1. As can be seen from the results, the average grain size of commercial PtCo/C catalyst is increased with the increasing of temperature treatment.

Figure 4.2 presents the typical transmission electron microscopy (TEM) images of commercial and N_2-treated PtCo/C electrocatalyst. As can be seen, all the PtCo nanoparticles are well dispersed on the surface of carbon, the morphology and the size distribution of the catalysts are well with the higher particle size with the higher temperature treatment due to the agglomeration of the catalyst. The particle size derived from TEM images is in relation with the XRD measurement.

University of Indonesia

Table 4.1. E-TEK PtCo/C Grain Size Calculation from XRD Data

Sample	2θ	FWHM	Grain Size, nm	Lattice Parameter, Å
PtCo/C commercial	40.646	1.599	5.532	3.838
PtCo/C N_2-treated 300 °C	40.536	1.598	5.534	3.848
PtCo/C N_2-treated 400 °C	40.506	1.438	6.146	3.851
PtCo/C N_2-treated 500 °C	40.571	1.351	6.543	3.845
PtCo/C N_2-treated 600 °C	40.694	0.945	9.361	3.834
PtCo/C N_2-treated 700 °C	40.501	0.921	9.594	3.852

The composition and grain size of the commercial ETEK Pt-Co/C is described in the Table 4.2 as follows:

Table 4.2. Composition and Grain Size of the Commercial E-TEK PtCo/C Electrocatalyst

Catalyst	Pt : Co [a]	Grain size [b] nm, from XRD	Particle size (nm) from TEM
PtCo/C (E-TEK)	72 : 28	5.532	4-5

(a) Determined by the edge jump of the Co K-edge and Pt L_{III}-edge XANES spectra

(b) Grain size derived from XRD based on the Pt (220) peak

University of Indonesia
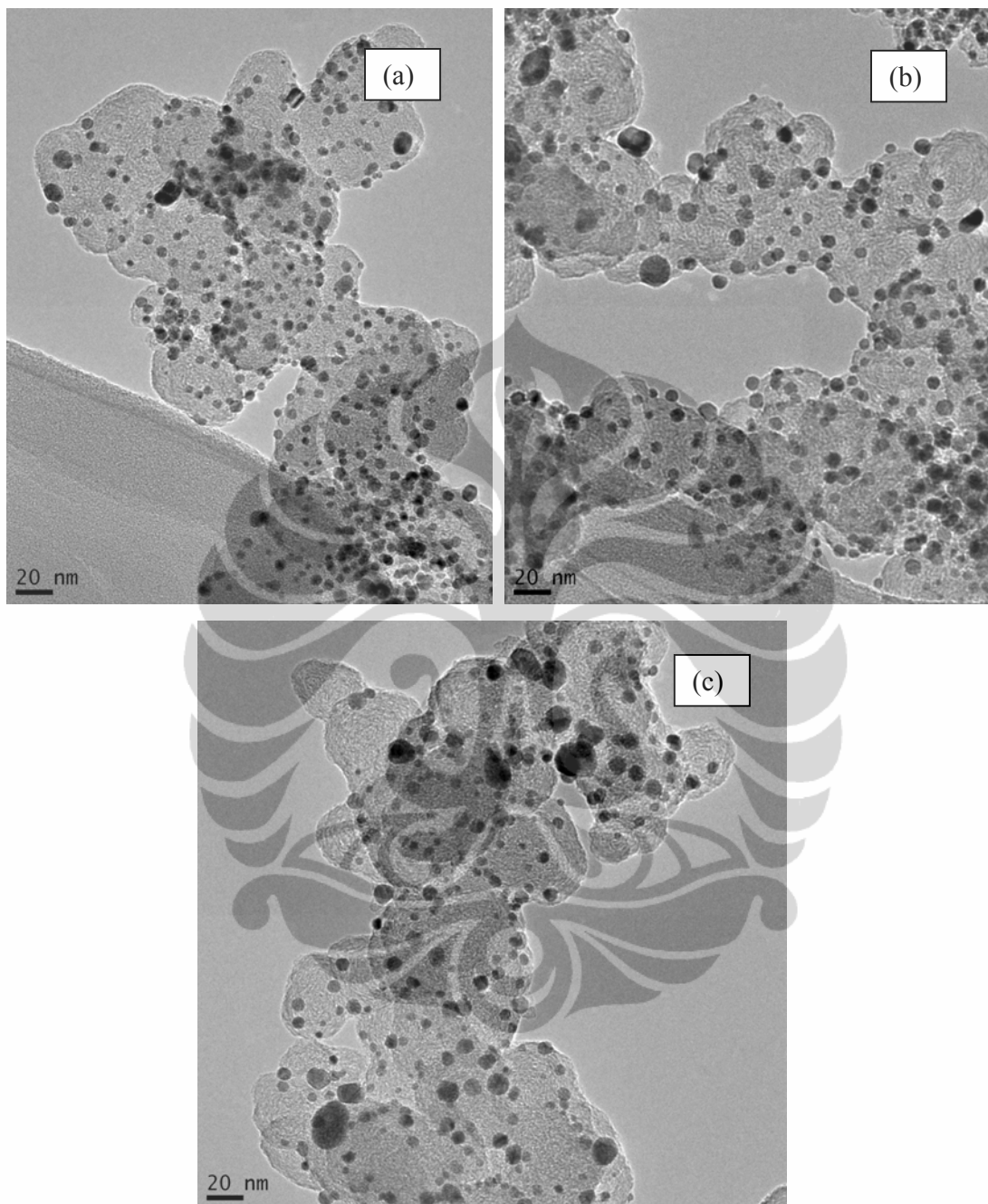
Figure 4.2. TEM Images of PtCo/C Electrocatalyst
(a) PtCo/C N_2-treated 300 ^{o}C, (b) PtCo/C N_2-treated 400 ^{o}C, (c) PtCo/C N_2-treated
600 ^{o}C

University of Indonesia

4.1.2. Electrochemical Property of Nitrogen-treated PtCo/C Electrocatalyst

Figure 4.3 shows a typical CV obtained for PtCo/C commercial catalyst. It can be seen, there are two peaks observed correspond to the oxidation-reduction of Pt and desorption-adsorption of hydrogen on the Pt surface. In the case of PtCo/C alloy indicates the creation of a weakly adsorbed oxide layer on the Pt surface, which is easier to reduce, consequently increases the ORR activity. This is in accordance with previously reported by Paulus [14].

Figure 4.3. Cyclic Voltammogram of a) Commercial E-TEK PtCo/C Electrocatalyst, b) PtCo/C N_2-treated 300 ^{o}C, c) PtCo/C N_2-treated 500 ^{o}C

University of Indonesia

According to Gasteiger et al [12] there are at least three possible causes for the leaching of base metal from a Pt alloy/C catalyst in PEMFCs : (i) excess base metal deposited onto the carbon support during preparation, (ii) incomplete alloying of these base elements to Pt due 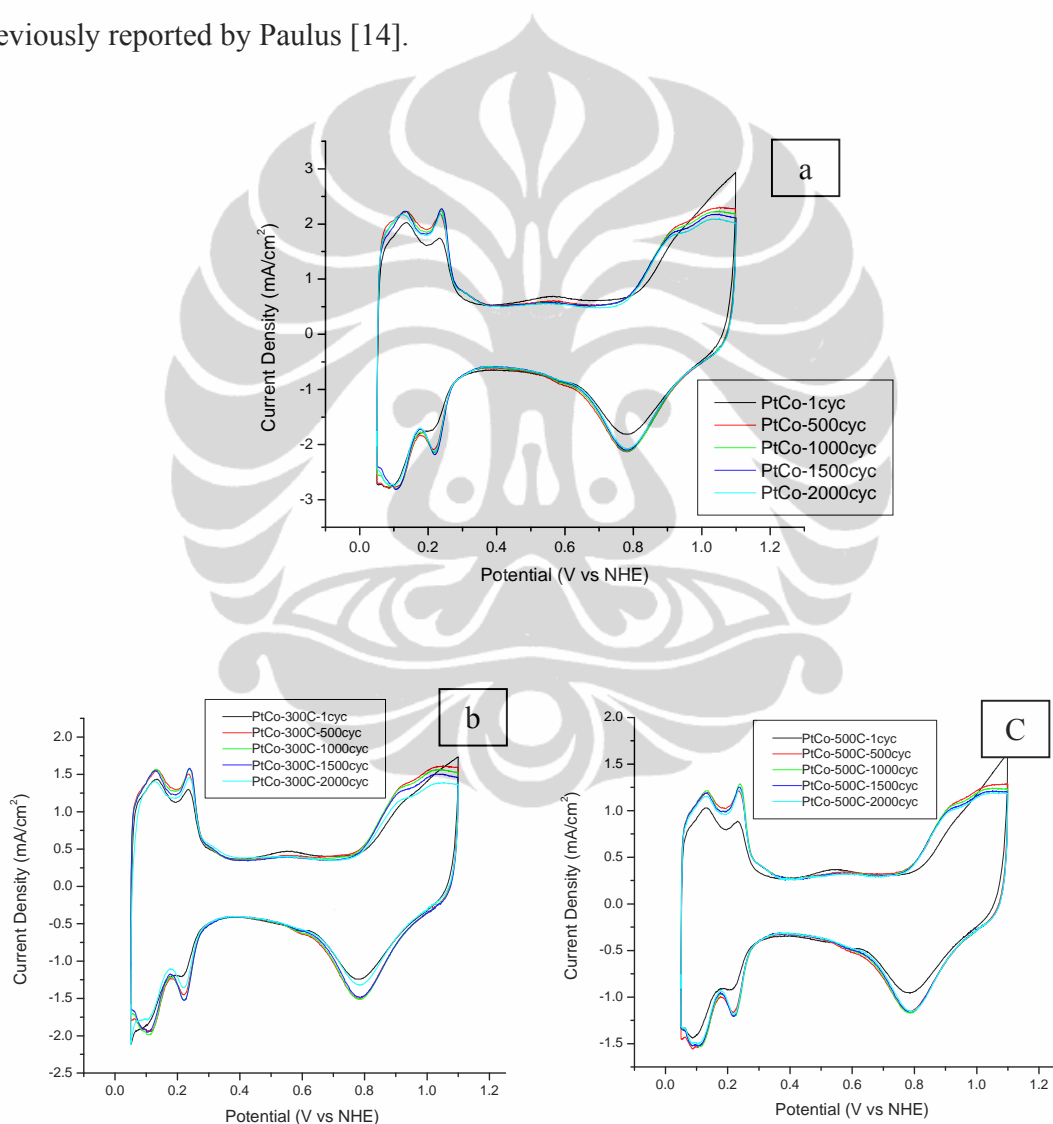to a low alloying temperature applied during formation of the alloy, (iii) even a well alloyed base metal may leach out of the surface under PEMFC operating conditions and leave a Pt enriched surface or skin since thermodynamically base metals are unstable under PEMFC potentials in acidic electrolytes.

Toda et al [64] on his experiment by XPS measurement found that most of the Ni, Co and Fe easily disappeared from all Pt alloys surface layer, probably by dissolution, by submitting the surface to an anodic potential or even in diluted acid solution at room temperature.

Figure 4.4 shows the LSV for the PtCo/C commercial catalyst. It is clearly observed that the performance of the system remain constant, there are no changes of the ORR even after several cycles, since there is no treatment on this commercial catalyst.
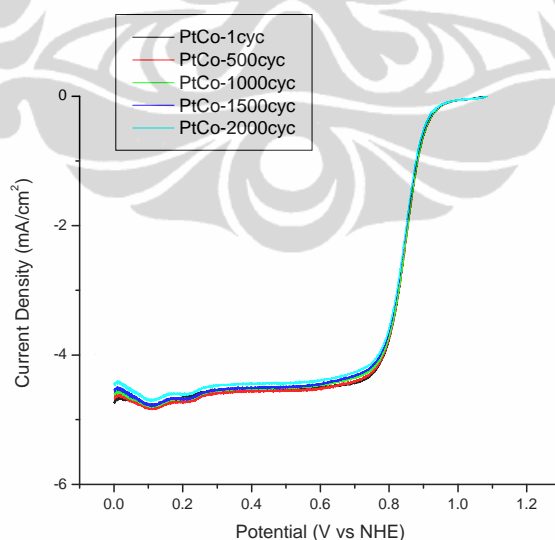
Figure 4.4. Linear Sweep Voltammogram of Commercial E-TEK PtCo/C Electrocatalyst

Figure 4.5 shows the linear sweep voltammetry for N_2-treated PtCo/C electrocatalyst. It is clearly seen that the ORR on all the catalysts is diffusion controlled when the potential is less than 0.75 V and is under a mixed control region of diffusion kinetics from 0.75-0.9 V. It is observed that the activity of catalyst decreased with increasing of temperature of treatment
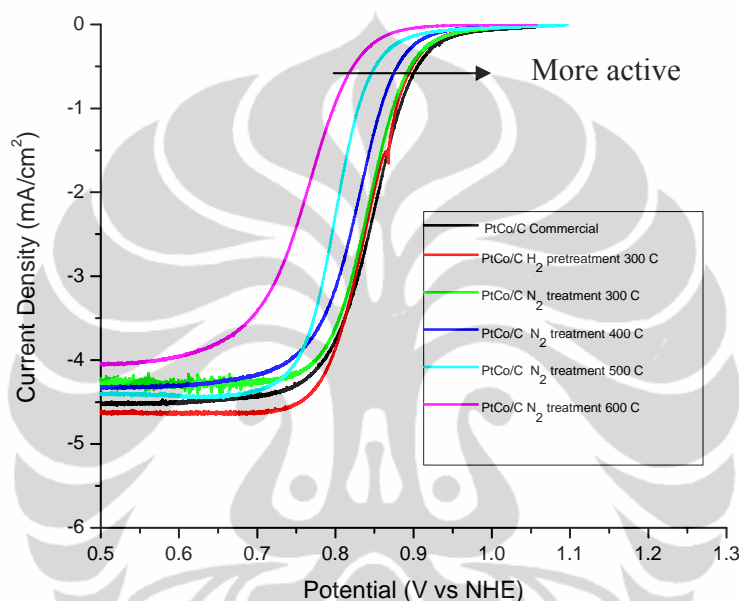
Figure 4.5. Linear Sweep Voltammogram of N_2-treated PtCo/C Electrocatalyst

This phenomenon is in relation with previously study reported by Antolini et al [80] that metal particle size of the Pt alloy influences the dissolution of the base metal in acid environment. The higher temperature treatment will effect on the particle agglomeration, consequently it will loss the active surface area. However, higher stability of PtCo/C alloy with large particle sizes than that of catalyst with small particle sizes was observed.

N_2-treated PtCo/C electrocatalyst results in the base voltammogram become more Pt like, which is probably indicative of leaching of Co from the surface. This phenomenon is in accordance with Antolini et al [80] who reported that the metal

particle size of the Pt alloy influences the dissolution of the base metal in an acid environment. The higher temperature treatment will affect the particle agglomeration, causing it to lose the active surface area.

Table 4.3. Specific Surface Area of Commercial and N_2-treated PtCo/C Electrocatalyst

Sample	Specific surface, m^2/g
PtCo/C commercial	74.605
PtCo/C N_2-treated 300 ^{o}C	50.311
PtCo/C N_2-treated 400 ^{o}C	47.378
PtCo/C N_2-treated 500 ^{o}C	38.526
PtCo/C N_2-treated 600 ^{o}C	36.471
PtCo/C N_2-treated 700 ^{o}C	34.636

4.2. Adsorbate-Induced Surface Segregation in Bimetallic PtCo/C Nanoparticles
4.2.1. Structure and Atomic Distribution of CO-treated PtCo/C Electrocatalyst

The composition of the commercial PREMETEK PtCo/C electrocatalyst is 49:51 which was determined from the edge jump measurements of the Co K-edge and Pt L_{III}-edge X-ray absorption near edge spectra (XANES). It is found that the atomic composition of Pt-Co is very close to the nominal value (1:1).

Figure 4.6 shows the comparison of XRD patterns of a commercial PREMETEK PtCo/C electrocatalyst with loading of 20 wt% and PtCo/C catalyst subjected to CO treatment at various times.

In all the catalysts, the peak appeared at 20-25° is attributed to the (002) plane of the hexagonal structure of the Vulcan XC 72 carbon [11]. As indicated in Figure 4.6, all the catalysts exhibit the main characteristic peaks of the face centre cubic (fcc) crystalline Pt with the peak positions of the (111), (200), (220), and (311) planes appeared at 2θ value of ca. 40.25^o, 46.82^o, 68.36^o and 82.42^o respectively according to XRD standard JCPDS No. 87-0647. From the figure, it is also clearly observed that for sample number (10), (11), (12) and (13) which are subjected to CO treatment for 5, 7, 10 and 15 h respectively show diffraction peaks namely (400), (331) and (531)

planes characteristic to Co-related species according to XRD standard JCPDS No. 01-1259. The appearance of Co-related species after CO treatment indicates the presence of segregation in CO-treated catalysts.
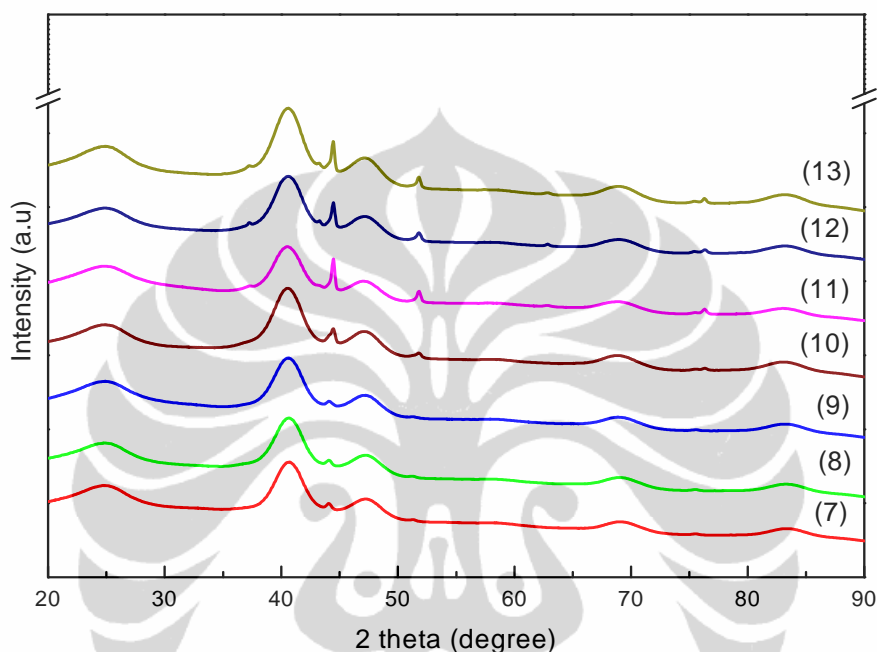
Figure 4.6. X-ray Diffraction (XRD) Patterns of PREMETEK PtCo/C Electrocatalysts.
(7) Commercial PREMETEK PtCo/C, (8) PtCo/C CO-treated 1 h, (9) PtCo/C CO-treated 3 h, (10) PtCo/C CO-treated 5 h, (11) PtCo/C CO-treated 7 h, (12) PtCo/C CO-treated 10 h, (13) PtCo/C CO-treated 15 h.

The average grain size associated with the catalyst is calculated by using Scherrer's equation and full-width at half maximum of peak (220) is listed in Table 4.4. As can be seen from the results, the average grain size of commercial PtCo/C catalyst has not varied much even after the CO treatments for various times.

Although the commonly available X-ray powder diffraction technique is capable to predict the atoms arrangement preferably in single crystals or polycrystals with sufficient long range order, but it lacks of providing information about the

University of Indonesia

structural parameters required to understand the atomic distribution in bimetallic nanoparticles. Therefore, information about the alloy structure related to nanoparticle where short range order exists is incomplete from XRD results [26]. Since XRD is very sensitive to grain size, the larger grain would produce the narrow diffraction peaks. Thus, the broad diffraction peaks appeared for the present catalysts suggest that the grain size is small.

Table 4.4. PREMETEK PtCo/C Grain Size Calculation from XRD Data

Sample	$2\theta^o$	FWHM	Grain Size, nm	Lattice Parameter, Å
PtCo/C commercial	40.832	2.899	3.052	3.822
PtCo/C- CO-treated 1 h	40.749	2.931	3.018	3.842
PtCo/C- CO-treated 3 h	40.573	3.039	2.909	3.845
PtCo/C- CO-treated 5 h	40.623	3.013	2.935	3.841
PtCo/C- CO-treated 7 h	40.647	2.878	3.073	3.838
PtCo/C- CO-treated 10 h	41.047	2.968	2.984	3.802
PtCo/C- CO-treated 15 h	40.752	2.896	3.055	3.828

X-ray absorption spectroscopy (XAS) comprises of x-ray absorption near edge structure (XANES) and extended x-ray absorption fine structure (EXAFS) regions was measured on commercial as well as on CO-treated PtCo/C electrocatalysts. The electronic properties in terms of the oxidation state, the fractional d-electron density and electronic environment of the absorbing atom of PtCo/C catalyst nanoparticles are investigated by XANES spectra. XANES is a powerful tool in providing information about the electronic state of the atoms in the material [28].

Figure 4.7 shows the XANES features obtained at the Co K-edge for the commercial and CO-treated PtCo/C electrocatalysts and reference Co foil. In the case of Co, a pre-edge feature originating from the 1s to 3d transition is observed at 7709 eV, which is a finger print for the tetrahedral site symmetry of cobalt species in a Co metal foil [72]. The absorption at 7709 eV corresponds to an electronic transition from 1s to 3d orbital [69], and the absorption hump at 7725 eV corresponds to 1s to 4d transition in cobalt foil [72]. However, the pre-edge feature completely

disappeared for PtCo/C commercial and other samples prepared in this work, which is an indication of insertion of Co atom into the Pt lattices. As can be seen from Figure 4.7 close inspection of the XANES feature reveal that the intensities of the absorption hump from sample are higher than reference cobalt foil. This intensity increases in case of catalyst samples might be resulted from the nano-sized effects or due to the formation of higher oxidation states of Co such as Co-oxide species. Nevertheless, conclusions about this discrepancy can't be simply drawn from XANES data alone and plausible explanation and reason can only be given after understanding the Fourier transformed extended X-ray absorption fine structure (FT-EXAFS) of cobalt K-edge.
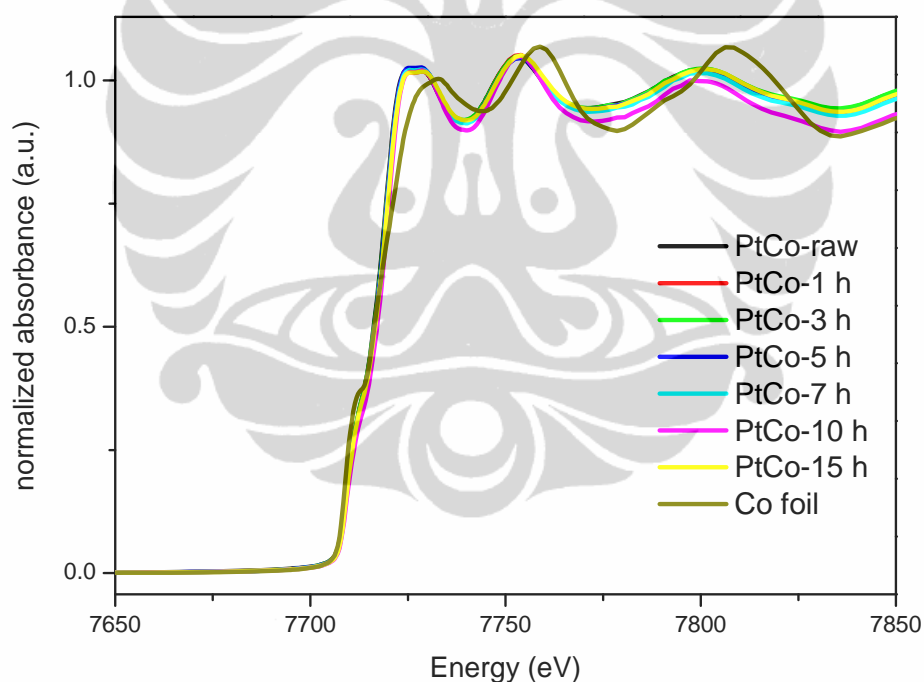

Figure 4.7. The XANES Spectra of the Co K-edge for Commercial and CO-treated PtCo/C Electrocatalyst and Reference Co Foil.

In order to gain structural information on the atomic level, EXAFS analysis has been performed. Figure 4.8 shows the Fourier transform (FT) magnitudes of experimental EXAFS data at Co K-edge for commercial and CO-treated PtCo/C

electrocatalysts. As can be seen from Figure 4.8, the FT modules of PtCo/C electrocatalyst exhibit a peak between 1.6 and 2.8 Å. The peak is related to the first coordination shell of Co-Co and Co-Pt, which is caused by the interference between the backscattering from Co to Co and Pt neighbors.
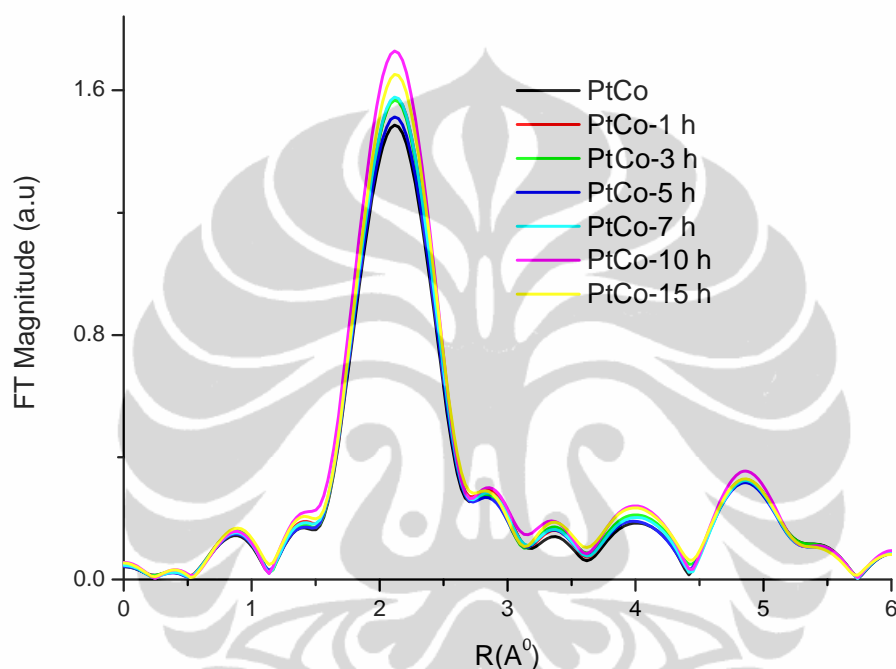
Figure 4.8. Fourier Transforms of Co K-edge EXAFS Spectra for Commercial and CO-treated PtCo/C Electrocatalyst

The electronic properties of PtCo/C nanoparticles were investigated by XANES analysis. Figure 4.9 represent the Pt L_{III}-edge XANES spectra for commercial and CO-treated PtCo/C electrocatalyst and reference Pt foil. The absorption at 11564 eV corresponds to $2p_{3/2} - 5d$ electronic transition of Pt metal and the magnitude of the absorption hump is termed as white line. The white line is attributed to the excitation of the $2p_{3/2}$ core electron to the unoccupied 5d states near the Fermi level, and its magnitude is directly related to the occupancy of the 5d electronic states [28, 69]. The white line intensity is a measure of occupancy of Pt 5d

electronic states. The intensity will be higher if the occupancy is lower. It reveals a very small reduction in the white line intensity in case of PtCo/C catalyst compared to the reference Pt foil. This is due to the alloying of Co with Pt metal leads to more occupied Pt 5d electronic state and more electronic hybrid states with Pt 5d electronic states.
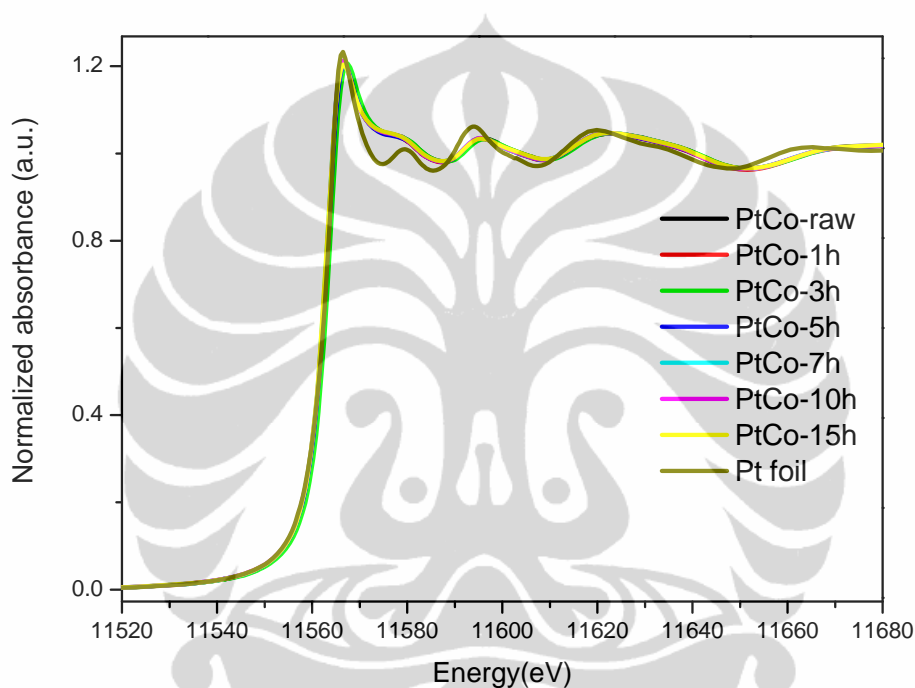
Figure 4.9. Pt L$_{III}$-edge Spectra for Commercial and
CO-treated PtCo/C Electrocatalyst

The corresponding Fourier transforms (FT) of k^2-weighted EXAFS oscillations at the Pt L$_{III}$-edge are shown in Figure 4.10. EXAFS measurement can provide valuable structural and chemical information on the neighborhood of the excited atom, particularly coordination numbers and bond distance [28]. Further, EXAFS spectra yield information on the number, type and distance of the backscattering atom surrounding the central absorbing atom and allow investigations

University of Indonesia

on the short range ordering and provide geometric information. As can be seen from Figure 4.10, comparison of the FT peak of commercial and CO-treated PtCo/C electrocatalyst nanoparticles appeared between 2 and 3 Å with the reference Pt FT peak show that Pt atoms are not the only constituents of the environment around Pt in the bimetallic nanoparticles. The peak centered at ca 2.5 Å in the FT spectra for these materials results from the coordinations related to the first Pt-Co and Pt-Pt coordination shell. The peak splitting in case of bimetallic nanoparticles indicates the presence of two types of backscattering atoms to the first shell coordination.

Figure 4.10. FT EXAFS Spectra at Pt L_{III}-edge of Commercial and
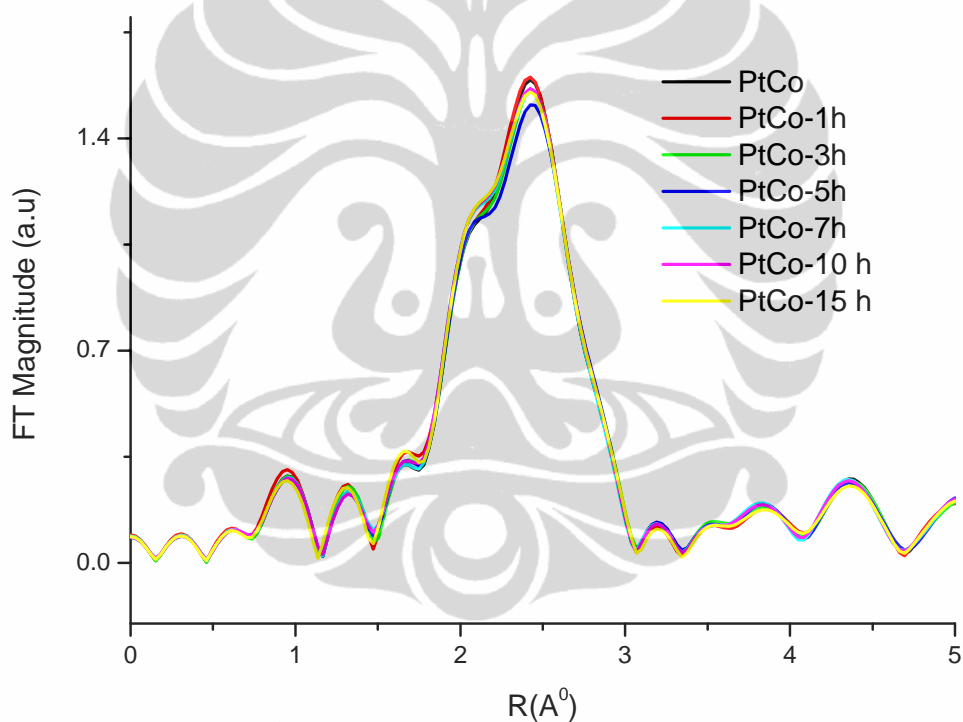CO-treated PtCo/C Electrocatalyst

It is of interest to estimate the alloy extent or atomic distribution of element in bimetallic NPs to get more detail about the structure and the composition. In this direction, we have analyzed the bimetallic NPs of type A-B by XAS. Firstly we

estimate the ratio of the coordination number of Pt around Co and also coordination number of Co around Pt to the total coordination number, and then we deduced the qualitative parameter, J_{Pt} and J_{Co} for the alloying extent in Pt-Co bimetallic NPs. These structural parameter are not only helpful to distinguish random and non random alloying Pt and Co in a Pt-Co cluster but also give information about the extent Pt and Co atomic distribution in nanoparticle [28, 69].

From EXAFS fitting at Pt L_{III}-edge and Co K-edge are obtained the coordination number as follows:

Table 4.5. Structural Coordination Number Parameter

Sample	N_{Pt-Co}	N_{Pt-Pt}	N_{Co-Co}	N_{Co-Pt}
PtCo/C commercial	3.00	5.65	4.38	2.90
PtCo/C- CO-treated 1 h	2.79	6.57	4.30	2.70
PtCo/C- CO-treated 3 h	2.85	6.08	4.02	2.76
PtCo/C- CO-treated 5 h	2.85	5.93	4.61	2.76
PtCo/C- CO-treated 7 h	2.93	5.63	5.79	2.84
PtCo/C- CO-treated 10 h	2.97	5.87	6.18	2.87
PtCo/C- CO-treated 15 h	2.57	5.99	6.20	2.49

The calculation of J_{Pt} and J_{Co} of PtCo/C bimetallic nanoparticle involves, obtaining the ratio of scattering atom Co coordination number around absorbing Pt atom (N_{Pt-Co}) to the total coordination number of absorbing platinum atoms ($\sum N_{Pt-i} = N_{Pt-Co} + N_{Pt-Pt}$) denoted as $P_{observed}$ ($P_{observed} = N_{Pt-Co}/\sum N_{Pt-i}$). The $P_{observed}$ provides information about the probability of Pt bonds with a Co atom and serves as an index to Pt atomic distribution in a Pt-Co cluster. Similarly, the ratio of the scattering atom Pt coordination number around absorbing Co atom (N_{Co-Pt}) to the total coordination number of absorbing cobalt atoms ($\sum N_{Co-i} = N_{Co-Pt} + N_{Co-Co}$) denoted as $R_{observed}$. ($R_{observed} = N_{Co-Pt}/\sum N_{Co-i}$). The parameter $R_{observed}$ provides information about the Co atomic distribution in a Pt-Co cluster. The ratio of $\sum N_{Pt-i}$ to $\sum N_{Co-i}$ ($Q = \sum N_{Pt-i} / \sum N_{Co-i}$) is also an important parameter to assess the structure of bimetallic NPs. If the Q value is higher than 1 then catalyst possesses a Pt rich in core Co rich in shell structure, and if the value is lower than 1 the reserve is true [28].

University of Indonesia

The coordination numbers and the alloying extent of Pt and Co estimated from the Pt L_{III}-edge and Co K-edge XAS structural parameters are listed in Table 4.5. As can be seen from Table 4.5, for PtCo/C commercial and PtCo/C catalyst subjected to CO treatment for 1, 3 and 5 h, the observed total coordination number parameter relationship of $\sum N_{Pt-i} > \sum N_{Co-i}$ and the alloying extent $J_{Pt} < J_{Co}$, the Q value > 1, indicate that Co atoms are mostly segregated to the surface of the nanoparticle and Pt atoms to the core resulting in a Pt rich in core Co rich in shell structure to the nanoparticles. In contrast, when the CO treatment times increased to 7, 10 and 15 h, the trend in the coordination numbers has changed. Now, the total coordination number parameter relationship show that $\sum N_{Pt-i} < \sum N_{Co-i}$ and alloying extent $J_{Pt} > J_{Co}$, the Q value < 1, indicate that Pt atoms are segregated to the surface of the nanoparticle and Co atoms to the core resulting in a Pt rich in shell Co rich in core structure.

Table 4.6. Alloying Extent and Atomic Distribution Parameters of Commercial and CO-treated PtCo/C Electrocatalysts

Sample	$\sum N_{Pt-i}$	$\sum N_{Co-i}$	P_{obs}	R_{obs}	J_{Pt}	J_{Co}	Q
PtCo/C commercial	8.65	7.28	0.3468	0.3984	70.51	78.40	1.188
PtCo/C- CO-treated 1 h	9.36	7.00	0.2981	0.3857	60.60	75.91	1.337
PtCo/C- CO-treated 3 h	8.93	6.78	0.3191	0.4071	64.88	80.12	1.317
PtCo/C- CO-treated 5 h	8.78	7.37	0.3246	0.3745	65.99	73.70	1.191
PtCo/C- CO-treated 7 h	8.56	8.63	0.3423	0.3291	69.59	64.77	0.992
PtCo/C- CO-treated 10 h	8.84	9.05	0.3360	0.3171	68.30	62.41	0.977
PtCo/C- CO-treated 15 h	8.56	8.69	0.3002	0.2865	61.04	56.39	0.985

From the XAS measurement, based on Hwang [27] it can be concluded that the experiment is related to the Case 3, which is $J_{Pt} < 100\%$ and $J_{Co} < 100\%$, then both Pt and Co atoms are not preferred to be alloyed, and it indicates that a higher extent of Pt/Co atoms prefer only to a lesser extent alloying between Pt and Co atoms. If $J_{Co} > J_{Pt}$, it appears that the core is rich in Pt atoms and shell is rich in Co atoms. On the contrary if $J_{Pt} > J_{Co}$ resulting in Co atoms are rich in the core and Pt atoms are rich in the shell.

University of Indonesia

The energy binding of CO for 1, 3 and 5 h is not strong enough to segregate the Pt atom into the surface. Consequently, only a few Pt migrates to the surface to displace Co. In contrast to CO treatment for 7, 10 and 15 h, the energy binding is more apt to segregate Pt into the surface and correspondingly displace Co to the core. Among these catalysts, the PtCo/C subjected to CO-treated 3 h owns higher J_{Pt} and J_{Co} values, indicating a higher extent of Pt and Co alloying, therefore it is predictable that catalytic performance toward ORR will be good. This is in relation with previously reported study [69] that Pt rich in core and Co rich in shell with the higher extent alloying showed the good catalytic activity toward ORR.

The surface of a bimetallic system can be very different from the bulk, it depends on the heat of segregation and the surface mixing energy. The chemical potential of the gas phase also influence the system since the strong bonding of adsorbates will result in a gain in energy of the system [25]. An adsorbate-induced to the system will control the surface segregation as shown in the Figure 4.11.
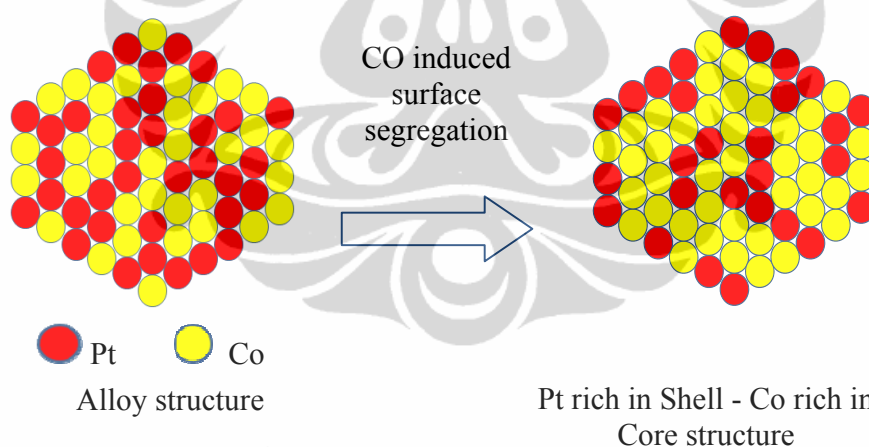
Figure 4.11. Structure Catalyst Changed by Induced Surface Segregation [107]

The adsorbate induced into the electrocatalyst leads to change in the catalyst structure. In general, catalytic performance is governed by a sequence of bond breaking and bond making processes that are carried out over the active metal surface. Individual bond breaking and forming steps are largely controlled by a balanced between the metal-adsorbate bond strength and the intramolecular bond

strength. Alloying two metals can alter their electronic structure as well as their geometric structure. It has been shown that the metal-adsorbate bond strength on the alloy surface can be very different from that on the pure metal surfaces and can therefore alter the mechanism of a reaction [108].

The composition of the surface of the bimetallic system can be very different from the bulk, depending on the segregation heat and the surface mixing energy. This statement is in accordance with Maillard et al [109] who proved the direct evidence of bulk Co segregation to the surface. They showed that the binding energy of oxygen onto Co atoms located on a Pt_3Co surface is greater than that on the monolayer Pt-skin which may provide sufficient driving force to overcome the segregation energy of Co atoms to the surface. It has been showed that surface structure is significantly modified under the influence of surface segregation [110].

This effect is additionally dependent upon the chemical potential of the gas phase, since the strong bonding of adsorbates will result in a gain in energy of the system. Consequently, for the bimetallic system enrichment at the surface of the component that binds a certain adsorbate more strongly may occur [25]. Recently, Mayrhofer et al [25] presented a novel preparation procedure of such core-shell nanoparticles with a platinum shell by using an adsorbate-induced surface segregation effect to modify an un-leached carbon supported Pt_3Co alloy high-surface area catalyst to increase the utilization of platinum in the particles. For this purpose the catalyst was subjected to a gas-phase treatment. The catalyst powder was placed into a rotary evaporator, which was then repeatedly evacuated and filled with CO to eliminate residual oxygen, and then the distiller was filled with ambient pressure of CO and heated to 200 ^{o}C for three hours. Because the adsorption enthalpy of CO on Pt is higher than on Co, Pt segregates to the surface of the nanoparticles and correspondingly displaces Co to the core.

The utilization of adsorbate-controlled surface segregation was done by Han et al [111]. It was proposed that adsorbed oxygen on Pt-Ru induces surface segregation of Ru due to the strong binding between Ru and O on the surface. Hwang et al [28] developed a controlled thermal-treatment strategy to alter the surface

University of Indonesia

population of Pt and Ru without varying the particle size of the initial PtRu/C NPs. It was reported that heat treatment in O_2 atmosphere can draw the Ru present in the core of the cluster to the surface, and heat treatment in a H_2 atmosphere led to the migration of core Pt to the shell region.

The core shell nanoparticles can be regarded as a kind of phase separation of an alloy into a core surrounded by the shell composed of a metal. This kind of structure will protect the dissolution of the transition metal [112], Co at the core is protected by Pt at the shell and the decay of the electroactivity may be inhibited.

4.2.2. Electrochemical Property of CO-treated PtCo/C Electrocatalyst

The cyclic voltammetry (CV) of PtCo/C electrocatalyst with various CO-treatment times recorded in N_2 saturated 0.5 M sulfuric acid electrolyte solution at scan rate of 10 mV/s is presented in Figure 4.12. The figure displays the feature of the hydrogen adsorption-desorption region between 0 and 0.35 V, followed by the double-layer potential region. At potentials > 0.7 V adsorption followed by oxide formation was observed. For the treated catalysts, the hydrogen adsorption-desorption region laid between the same potentials than commercial-PtCo/C, while the OH adsorption and the oxide formation commenced at potentials > 0.8 V. The formation of the Pt oxide layer is shifted towards more positive potentials for the bimetallic samples subjected to thermal treatments.

From Figure 4.12, it can be seen that the onset potential for Pt oxide formation in the positive going sweep and the oxide reduction in the negative going sweep and slightly shifted to more positive potential. This indicates that alloying inhibited the chemisorptions of oxygenated species such as OH_{ad} on the Pt sites at high potential (above 0.8 V) by the change in the Pt electronic structure induced by the addition of Co. This may be beneficial to the oxygen adsorption at lower potentials and correspondingly it will enhance the ORR activity. The enhanced ORR performance of PtCo is attributed its comparably higher extent Pt and Co alloying, number of Pt unfilled d-state created by alloying metal and convenient grain size.
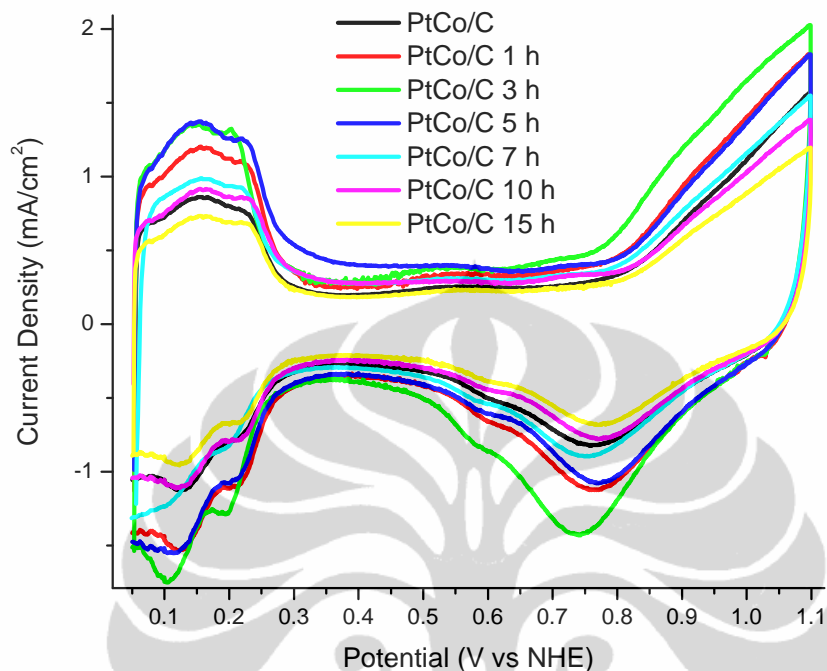
University of Indonesia

Figure 4.12. Cyclic Voltammogram for Commercial and
CO-treated PtCo/C Elecrocatalyst in N_2 Saturated 0.5 M H_2SO_4 Electrolyte
at a Scan Rate of 10 mV/s

Figure 4.13 shows the ORR activity of the catalyst under oxygen saturated 0.5 H_2SO_4 solutions at room temperature. From the figure, the ORR on the all catalysts are diffusion controlled when the potential is less than 0.7 V and is under a mixed control region of diffusion-kinetic from 0.7-0.85 V. In the Tafel region (higher than 0.85 V) and the mixed potential region, the ORR activities show a significant difference in their magnitude. It can be clearly seen that the PtCo/C CO-treated 1-5 h shifted to more positive potential indicates enhanced ORR activity while PtCo/C CO-treated 7-15 h shifted to less positive potential, indicates decreasing activity. In this case, PtCo/C subjected to CO treatment for 3 h shows the most shifted to positive potential, indicating the most active catalyst.toward ORR. This is in relation with the

University of Indonesia

data of the XAS, that PtCo/C CO-treated 3 h has the highest alloying extent; therefore it is predictable to have a good catalytic performance toward ORR [69].
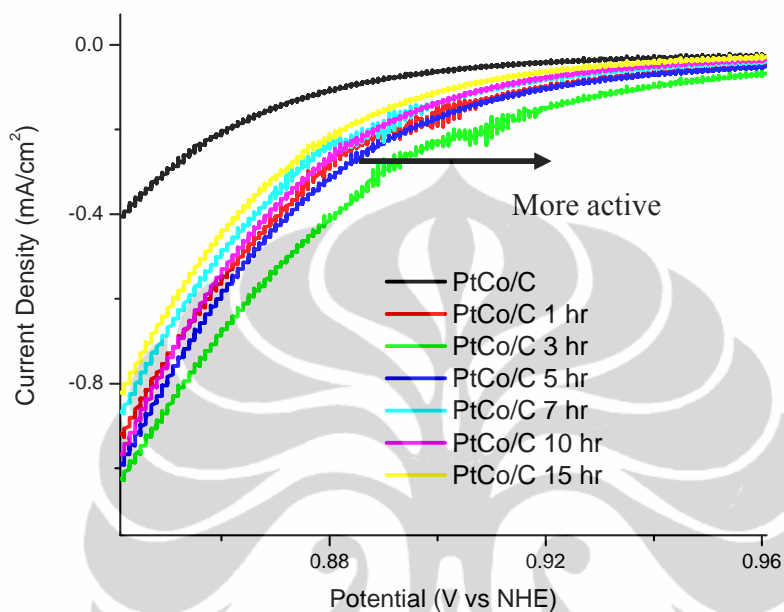

Figure 4.13. Linear Sweep Voltammogram Recorded at 1 mV/s for the ORR of Commercial and CO-treated PtCo/C Electrocatalysts

In term of stability, the electrocatalyst was measured through cyclic voltammetry until 2000 cycles. Figure 4.14 shows the electrochemical surface area as a function of the cycle number. The surface area was estimated by integrating the H_{UPD} peak and assuming the hydrogen adsorption-desorption process occurs on a polycrystalline Pt surface. During the first cycle, the surface area initially increase until it reaches a maximum value. As discussed previously, from the XAS measurement showed PtCo/C electrocatalyst subjected to CO treatment 1-5 h resulting the structure of Pt rich in core and Co rich in shell, PtCo/C electrocatalyst subjected to CO treatment 7-15 h resulting in the structure of Pt rich in shell Co rich in core.
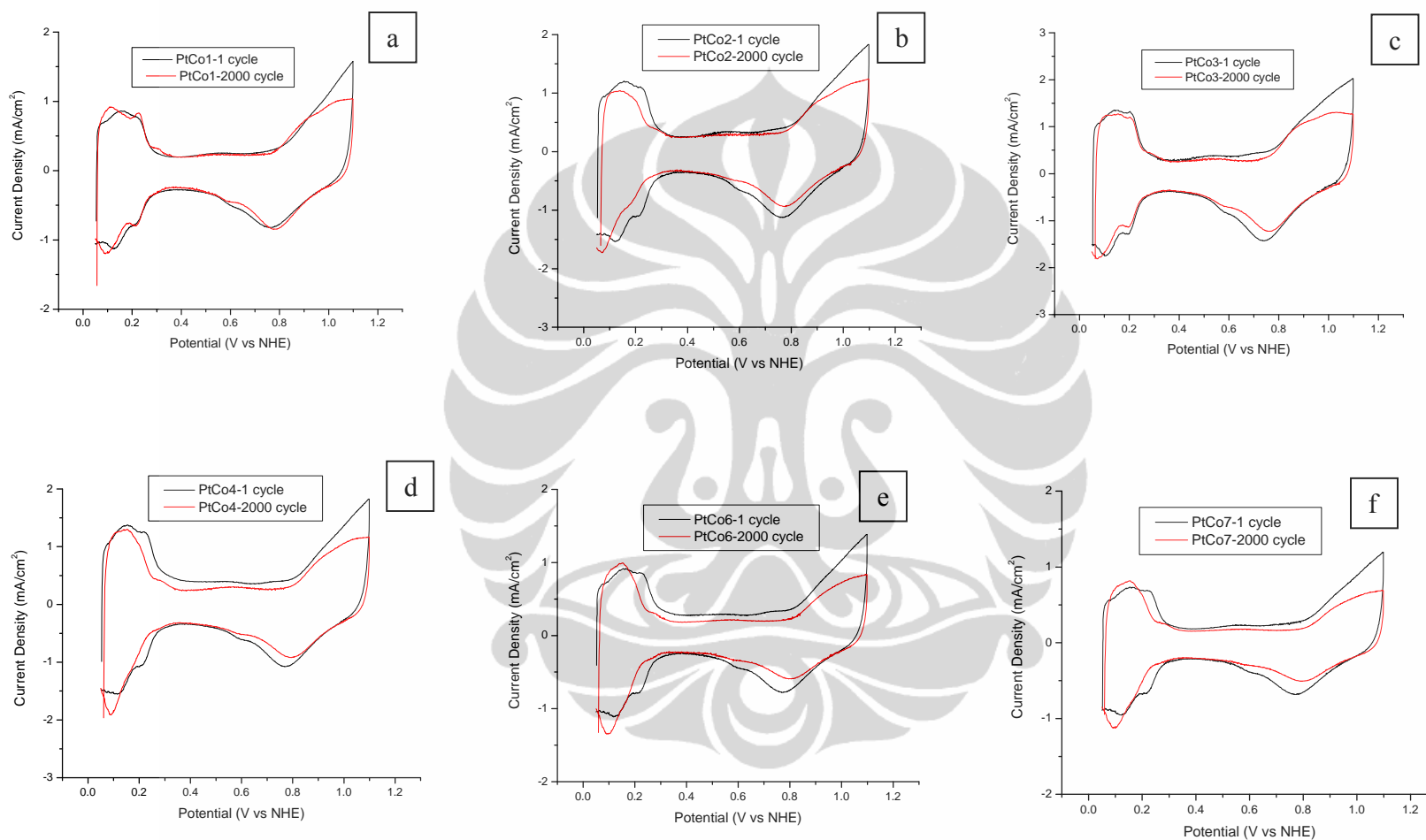
University of Indonesia

Figure 4.14. Cycle Voltammetry of PtCo/C Electrocatalyst as Function of Cycle Number

a) Commercial b) CO-treated 1h, c) CO-treated 3 h, d) CO-treated 5 h, e) CO-treated 10 h, f) CO-treated 15 h

As shown in Figure 4.14, PtCo/C commercial and CO treatment 1-5 (Figure 4.14 a-d) shows the specific surface area of 2000 cycles are lower than that of 1 cycle, indicates the catalyst is unstable due to the dissolution of Co could not be hindered. Pt in the core could not protect Co in the shell. In contrast, PtCo/C subjected to CO treatment 7-15 h (Figure 4.14 e-f) shows the specific surface area of 2000 cycles are higher than that of 1 cycle. The dissolution of Co could be inhibited by Pt in the shell. Pt in the shell could protect Co from dissolution, therefore the catalyst is stable.

In order to give clearly figure, the surface area of the catalyst was calculated and described in the Figure 4.15
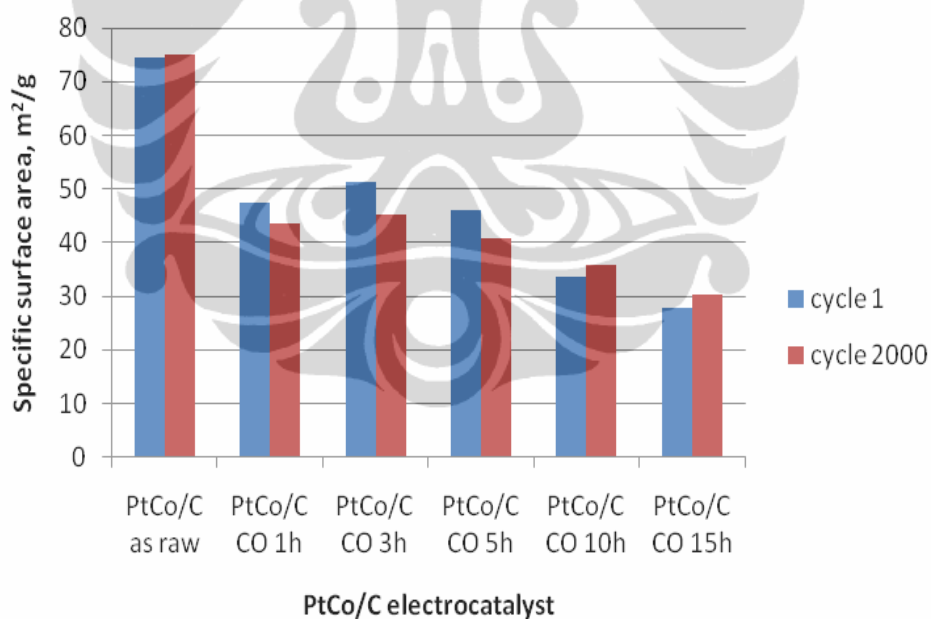

Figure 4.15. Specific Surface Area of CO-treated PtCo/C Electrocatalyst with 1 and 2000 Cycles

The enhancement of ORR activity upon alloying has been explained by Fernandez et al [88]. In his study, Fernandez proposed a simple thermodynamic

model based on data of bulk metal oxide. It is proposed that the incorporation of more active cobalt metals could facilitate the dissociate adsorption of O_2 and produce O_{ads} species, migrate from the cobalt side to the noble metal site. Therefore, it will cause less polarization and electroreduction. In term of this experiment, PtCo/C subjected to CO-treatment 3 h, which has higher alloying extent of Pt and Co, will enhance ORR performance and less polarization [113].

The mass activities for ORR on commercial and CO-treated Pt-Co/C electrocatalyst are compared in Figure 4.16. The mass activity can be taken as an index to assess the applicability of the catalyst toward ORR. The observed tendency in the mass activity values is consistent with our finding of alloying extent.
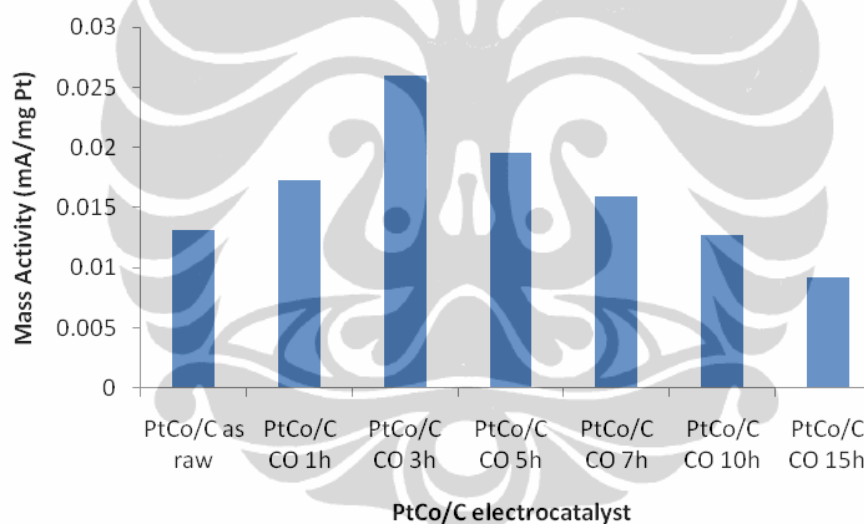
Figure 4.16. Mass Activity for Commercial and CO-treated PtCo/C Electrocatalyst

The observed variations in the ORR activity of CO-treated catalysts are in accordance with the specific surface area of the sample as listed in Figure 4.15. The electrochemical active surface area (EASA) was quantitatively determined by integrating the area under the hydrogen-adatoms desorption region after the background-subtraction of the charge. The catalyst with higher surface area will have higher activity. Catalysts subjected to CO-treatment for 7, 10 and 15 h leads to decrease in the surface area, and hence the activity is also decreased.

University of Indonesia

Figure 4.17. Surface Area of the Commercial and CO-treated PtCo/C Electrocatalysts

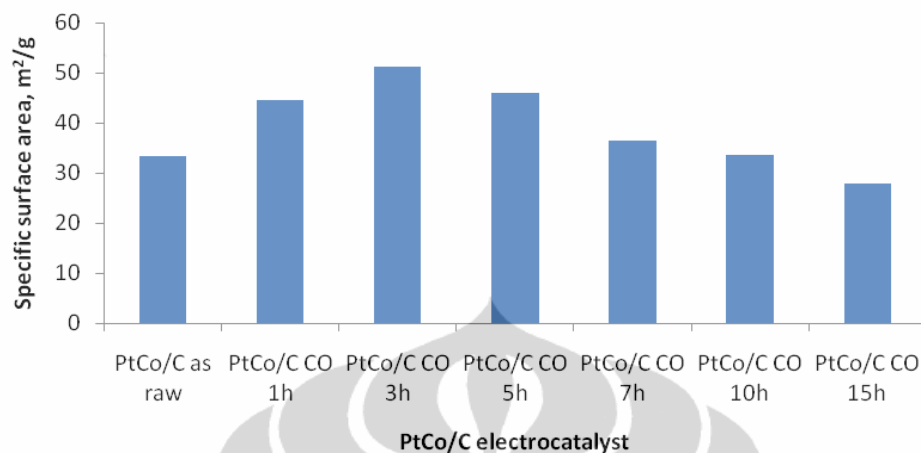From the Figure 4.16 and 4.17 PtCo/C subjected to CO-treatment 3 h showed the best activity toward ORR even though the structure of the catalyst is Pt rich in core Co rich in shell. Ideally the catalyst with the structure of Pt rich in shell and Co rich in core is the best structure for improving activity since Pt is an active metal located in the surface, where the reaction take place. However, improvement of activity by the addition of transition metal to Pt due to the lowering of Pt oxidation state, suppression of Pt oxide formation, formation of new electronic structure with higher Pt 5d orbital vacancies, decrease in the Pt-Pt distance and therefore more favorable adsorption of O_2 [72[.

4.2.3. Polarization Curve of Single Cell Performance on PtCo/C Electrocatalyst

In order to study the activity of catalyst, the PtCo/C electrocatalyst was applied in the single cell performance measurement. The measurement was conducted at Fuel Cell Laboratory, PUSPIPTEK Serpong.

The cyclic voltammetry (CV) is very useful to check the activity of an electrocatalyst. However, it is necessary to observe the performance of the same catalyst in a complete fuel cell. In this test, we measured the performance of single

University of Indonesia

cell using a commercial E-TEK Pt/C 40 wt% at anode side, and a commercial PREMETEK PtCo/C 20 wt %, PtCo/C CO treated 3 h, 7 h and 15 h respectively for the cathode side.

The Figure 4.18 presents the polarization curve of single cell PEM fuel cell performance using PtCo/C electrocatalyst.
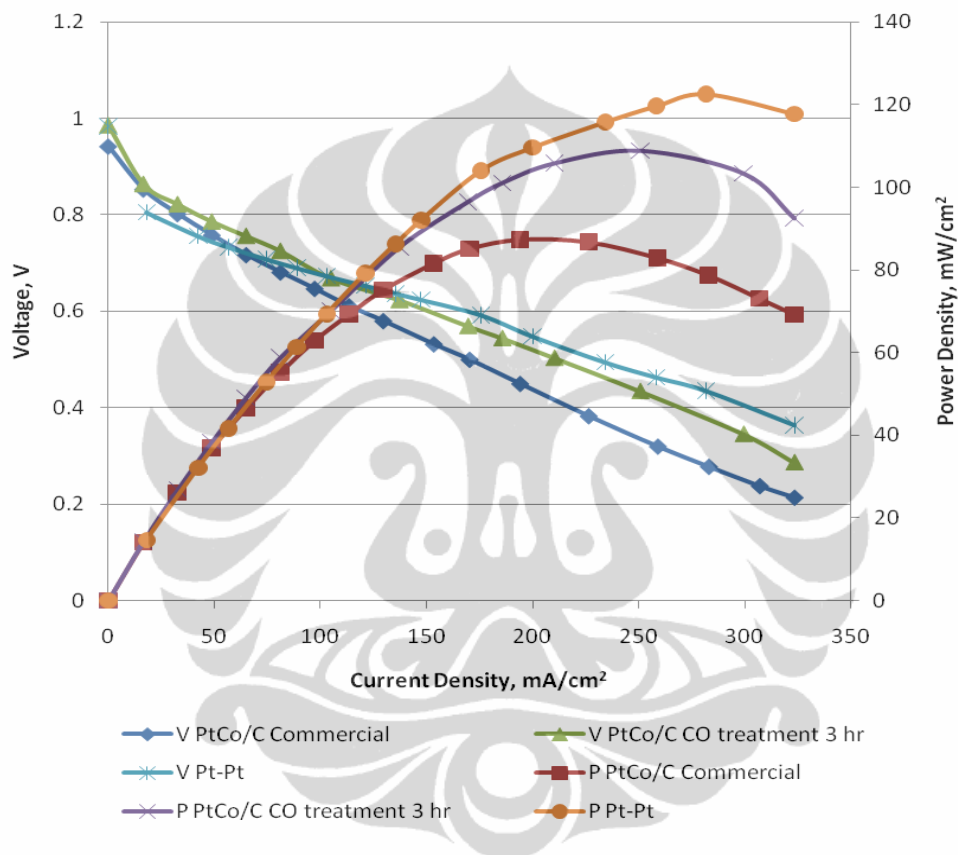
Figure 4.18. Comparison of Single Cell PEM Fuel Cell Performance
of Pt and PtCo/C Electrocatalyst

Based on the electrochemical analysis, that PtCo/C subjected to CO-treatment 3 h is the most active catalyst toward ORR, and also from the XAS data, which is the highest alloying extent, it is predicted that the PtCo/C could perform the highest energy output when applied on single cell measurement. The result of the single cell measurement is described in the following table:

University of Indonesia

Table 4.7. Single Cell Performance of PtCo/C Electrocatalyst

Sample (anode – cathode)	Open Circuit Potential (V)	Current Density (mA/cm^2)	Power Density (mW/cm^2)
Pt – Pt	0.983	281.697	122.538
Pt – PtCo/C commercial	0.942	210.303	88.327
Pt – PtCo/C CO-treated 3 h	0.986	250.747	108.824
Pt – PtCo/C CO-treated 7 h	0.971	169.859	69.982
Pt – PtCo/C CO-treated 15 h	0.937	153.535	65.560

Open circuit potential (OCP) of single cell PEM fuel cell over commercial PtCo/C electrocatalyst was about 0.942 V and OCP of PtCo/C CO-treated 3 h was 0.986. The OCP of PtCo/C CO-treated 3 h is slightly higher than the OCP over Pt/C (reference) catalyst wchis is about 0.983 V. These result is in a good agreement/confirmed to the result in a half cell testing concerning to the activity of the catalyst.

It is clearly can be seen from Table 4.7, that Pt-Co treated 3 h show the best performance of single cell measurement. This result is in good agreement with the specific surface area and mass activity of PtCo/C CO-treated 3 h that has a better activity toward ORR. It is found that catalyst treatment would increase the fuel cell performance of 20.49 % (Power density of PtCo/C commercial : 88.327 mW/cm^2, PtCo/C CO-treated 3 h : 108.327 mW/cm^2)

University of Indonesia

CHAPTER 5
CONCLUSION

Nitrogen and adsorbate-induced with CO has been successfully applied to treat the commercial PtCo/C electrocatalyst in order to study the effect of particle size and catalyst structures on its activity and stability.

Catalyst that is subjected to nitrogen treatment will result in increasing of particle size with increasing temperature treatment due to the sintering and agglomeration. Increasing particle size leads to an easily dissolved catalyst. Consequently, the catalyst activity is decreased. Electrochemical analysis shows that the catalyst is more Pt-like due to the dissolution of second metal, Co. It shows that the catalyst is unstable.

Catalysts treated with CO resulted in the same grain size. The XRD pattern shows that the appearance of Co related species after CO treatment indicates the presence of segregation. Catalysts treated for 1, 3 and 5 hours lead to higher populations of Pt on the core and Co was moved to the surface, resulting in a Pt rich in core Co rich in shell. In contrast, catalysts treated for 7, 10 and 15 hours lead to higher populations of Pt on the shell and Co on the core, resulting in a Pt rich in shell Co rich in core. The electrochemical analysis shows that PtCo/C with CO-treatment is more active than commercial PtCo/C for the ORR and it is found that PtCo/C subjected to CO treatment for 3 hours electrocatalyst has the highest mass activity, therefore performs as the best catalytic activity toward ORR. XAS measurement shows that PtCo/C subjected to CO treatment for 3 hours electrocatalyst has a higher alloying extent, therefore has a good activity performance toward ORR.

Pt located in the shell is able to protect Co in the core from dissolution; therefore the catalyst would be stable. PtCo/C subjected to CO treatment for 1-5 hours electrocatalyst resulting in unstable catalyst due to Pt in the core is unable of protecting Co in the shell from dissolution. In contrast, PtCo/C subjected to CO

81 **University of Indonesia**

treatment for 7-15 hours electrocatalyst resulting in stable catalyst due to Pt in the shell is capable of protecting Co from dissolution.

Catalyst treatment would increase the fuel cell performance by 20.49 % (Power density of commercial PtCo/C electrocatalyst : 88.34 mW/cm^2, PtCo/C subjected to CO treatment for 3 hours electrocatalyst : 108.82 mW/cm^2).

University of Indonesia

REFERENCES

1. Zhang, L.; Zhang, J.; Wilkinson, D.P.; Wang, H, J. Power Sources. **2006,** 156, 171-182

2. Liu, H.; Song, C.; Zhang, L.; Zhang, J.; Wang, H.; Wilkinson, D.P, J. Power Sources. **2006**, 155, 95-110

3. Lee, K.; Zhang, J.; Wang, H.; Wilkinson, D.P, J. Appl. Electrochem. **2006,** 36, 507-522

4. Bashyam, R.; Zelenay, P, Nature. **2006**, 443, 63-66

5. Guha, A.; Lu, W.; Zawodzinski, T.A.; Schiraldi, D.A, Carbon. **2007**, 45, 1506-1517

6. Mukerjee, S.; Srinivasan, S in Vielstich, W.; Lamm, A.; Gasteiger, H.A. (Eds) Handbook of Fuel Cells : Fundamentals, Technology and Applications, vol. 2. Electrocatalysis, Wiley, Chicester, **2003**, p. 502-519

7. Gattrell, M.; MacDougall, B in Vielstich, W.; Lamm, A.; Gasteiger, H.A. (Eds) Handbook of Fuel Cells : Fundamentals, Technology and Applications, vol. 2. Electrocatalysis, Wiley, Chicester, **2003**, p. 443-464

8. He, T.; Kreidler, E.; Xiong, L.; Luo, J.;. Zhong, C.J, J. Electrochem. Soc. **2006**, 153, A1637-A1643

9. Wang, B, J. Power Sources. **2005**, 152, 1-15

10. Gottesfeld, S.; Zawodzinski, T.A. in Alkire, R.C.; Gerischer, H.; Kolb, D.M.; Tobias, C.W (Eds) Advances in Electrochemical Science and Engineering, vol. 5, 1st ed, Wiley-VCH, Weinheim, **1997**, p.195

11. Zignani, S.C.; Antolini, E.; Gonzalez, E.R, J. Power Sources. **2008**, 182, 83-90

12. Gasteiger, H.A.; Kocha, S.S.; Sompalli, B.; Wagner, F.T, Appl. Catal. B. **2005**, 56(1-2), 9-35

13. Paulus, U.A.; Wokaun, A.; Scherer, G.G.; Schimdt, T.J.; Stamenkovic, V.; Radmilovic, V.; Markovic, N.M.; Ross, P.N, J. Phys. Chem B. **2002**, 106 (16), 4181-4191

14. Paulus, U.A.; Wokaun, A.; Scherer, G.G.; Schmidt, T.J.; Stamenkovic, V.; Markovic, N.M.; Ross, P.N, Electrochimica Acta. **2002**, 47 (22-23), 3787-3798

15. Travitsky, N.; Ripenbein, T.; Golodnitsky, D.; Rosenberg, Y.; Burshtein, L.; Peled, E, J. Power Sources. **2006**, 161(2), 782-789

16. Mukerjee, S.; Srinivasan, S.; Soriaga, M.P.; McBreen, J, J. Electrochem. Soc. **1995**, 142(5), 1409-1422

17. Watanabe, M.; Tsurumi, K.; Mizukami, T.; Nakamura, T.; Stonehart, P, J. Electrochem. Soc. **1994**, 141(10), 2659-2668

18. Bezerra, C.W.B.; Zhang, L.; Liu, H.; Lee, K.; Marques, A.L.B.; Marques, E.P.; Wang, H.; Zhang, J, J. Power Sources. **2007**, 173, 891-908

19. Coloma, F.; Escribano, A.S.; Fierro, J.L.G.; Rodriguez-Reinoso, F, Langmuir. **1994**, 10, 750-755

20. Tian, J.H.; Wang, F.B.; Shan, Z.Q.; Wang, R.J.; Zhang, J.Y, J. Appl. Electrochem. **2004**, 34, 461-467

21. Hinds, G, NPL Report, United Kingdom, **2005**, p.10-12

22. Kang, M.; Bae, Y.S.; Lee, C.H, Carbon. **2005**, 43, 1512-1516

23. Mazurek, M.; Benker, N.; Roth, C.; Fuess, H, Fuel Cells. **2006**, 6, 208-213

24. Cheng, H.; Yan, W.; Scott, K, Fuel Cells. **2007**, 7, 16-20

25. Mayrhofer, K.J.J.; Juhart, V.; Hartl, K.; Hanzlik, M.; Arenz, M, Angew. Chem. Int. Ed, **2009**, 48, 3529-3531

26. Chen, C.H.; Sarma, L.S.; Chen, J.M.; Shih, S.C.; Wang, G.R.; Liu, D.G.; Tang, M.T.; Lee, J.F.; Hwang, B.J, J. ACS Nano. **2007**, 1, 114

27. Hwang, B.J.; Sarma, L.S.; Chen, J.M.; Chen, C.H.; Shih, S.C.; Wang, G.R.; Liu, D.G.; Lee, J.F.; Tang, M.T, J. Am. Chem. Soc. **2005**, 127, 11140-11145

28. Hwang, B.J.; Sarma, L.S.; Wang, G.R.; Chen, C.H.; Liu, D.G.; Sheu, H.S.; Lee, J.F, Chem. Eur. J. **2007**, 13, 6255-6264

29. Kordesch, K.; Simader, G. Fuel Cell and Their Application, VCH, **1996**

30. Ledjeff, K. Brennstoffzellen : Entwicklung-Technologie-Anwendung, 1st ed, **1995**. CF. Mulller, Heidelberg

31. Holland, B.J.; Zhu, J.G.; Jamet, L. Fuel Cell Technology and Application

32. Ying, Q, **(2006)** M.Sc Thesis, Department of Chemistry, University of the Western Cape

33. Hirschenhofer, J.H.; Stauffer, D.B.; Engliman, R.R.; Klett, I.G. Fuel Cell Handbook – Fuel Cell Description **(1998)**

34. Easton, E.B **(2003)** Publish Dissertation, [online], available : http://www.fuelcon.de/download/literatur/Lit0082.pdf

35. Crow, D.R, Principles and Application of Electrochemistry, 4th ed, London, New York : Blackie, **1994**

36. Hoogers, G. Fuel Cell Technology Handbook, 1st ed, CRC press, **2002**

37. Carrette, L.; Friedrich, K.A.; Stimming, U. Fuel Cells – Fundamentals and Applications, Fuel Cells, **2001**, 1(1), 5-39

38. Kinoshita, K.; McLarnon, F.R.; Cairns, E.J. Fuel Cells – A Handbook, 1988, U.S. Department of Energy, Morgantown, West Virginia

39. Wedler, G. Lehrbuch der Physikalishen Chemie, 3rd ed. **1987**, VCH, Weinheim

40. Hamann, C.H.; Hamnett, A.; Vielstich, W. Electrochemistry, 1st ed. **1998**, Wiley-VCH, Weinheim

41. Catalyst, [2009], [Online], available : http://www.princeton.edu/

42. Hamann, C.H.; Hamnett, A.; Vielstich, W, Electrochemistry 1st ed, **1998**, Wiley-VCH, Weinheim

43. Wroblowa, H.S.; Pan, Y.C.; Razumney, G, Journal of Electroanalytical Chemistry. **1976**, 66, 195

44. Bagotskii, V.S.; Tarasevich, M.R.; Filinovskii, V.Y, Electrokhimiya. **1969**, 5, 1218

45. Yeager, E, Journal of Molecular Catalysis. **1986**, 38, 5

46. Min, M.K.; Cho, J.; Cho, K.; Kim, H, Electrochimica Acta. **2000**, 45, 4211-4217

47. Xiao, L.; Zhuang, L.; Liu, Y.; Lu, J, J. American Chemical Society. **2008**, 131, 602-608

48. Arico, A.S.; Shukla, A.K.; Kim, H.; Park, S.; Min, M.; Antonucci, V, Applied Surface Science. **2001**, 172, 33-40

49. Takako, T,; Hiroshi, I.; Hiroyuki, U.; Masahiro, W, J. Electrochem. Soc. **1999**, 146, 3750-3756

50. Wang, L.L.; Johnson, D.D, J. American Chemical Society. **2007**, 129, 3658-3664

51. Zhang, J.; Sasaki, K.; Sutter E.; Adzic, R.R, Science. **2007**, 315, 220-222

52. Ye, H.; Crooks, R.M, J. American Chemical Society. **2005**, 127, 4930-4934

53. Yong, T.K.; Kazuyoshi, O.; Koichi, H.; Tomoya, U.; Masaki, T.; Hiroyoshi, S.; Tadaoki, M, Angewandte Chemie International Edition. **2006**, 45, 407-411

54. Stamenkovic, V.R.; Mun, B.S.; Arenz, M.; Mayrhofer, K.J.J.; Lucas, C.A.; Wang, G.; Ross, P.N.; Markovic, N.M, Nature Matter. **2007**, 6, 241-247

55. Stamenkovic, V.R.; Mun, B.S.; Mayrhofer, K.J.J.; Ross, P.N.; Markovic, N.M, J. American Chemical Society. **2006**, 128, 8813-8819

56. Stamenkovic, V.R.; Fowler, B.; Mun, B.S.; Wang, G.; Ross, P.N.; Lucas, C.A.; Markovic, N.M, Science. **2007**, 315, 493-497

57. Chen, S.; Ferreira, P.J.; Sheng, W.; Yabuuchi, N.; Allard, L.F.; Shao, H.Y, J. American Chemical Society. **2008**, 130, 13818-13819

58. Zhang, J.V.; Xu, Y.; Mavrikakis, M.; Adzic, R.R, Angew. Chem. Int. Ed. **2005**, 44, 2

59. Zhang, J.; Vukmirovic, M.B.; Sasaki, K.; Nilekar, A.U.; Mavrikakis, M.; Adzic, R.R, J. American Chemical Society. **2005**, 127, 12480-12481

60. Koh, S.; Strasser, P, J. American Chemical Society. **2007**, 129, 12624-12625

61. Ratndeep, S.; Prasanna, M.; Nathan, H.; Strasser, P, Angewandte Chemie International Edition. **2007**, 46, 8988-8991

62. Stamenkovic, V.; Schmidt, T.J.; Ross, P.N.; Markovic, N.M, J. Physical Chemistry B. **2002**, 106, 11970

63. Toda, T.; Igarashi, H.; Watanabe, M, J. Electrochem. Soc. **1998**, 145, 4185

64. Toda, T.; Igarashi, H.; Uchida, H.; Watanabe, M. J. Electrochem. Soc, **1999**, 146, 3750-3756

65. Beard, B.C.; Ross, J.P.N, J. Electrochem. Soc. **1990**, 137, 3368-3374

66. Shukla, A.K.; Neergat, M.; Bera, P.; Jayaram, V.; Hedge, M.S, J. Electroanalytical Chemistry. **2001**, 504, 111

67. Duong, H.T.; Rigsby, M.A.; Zhou, W.P.; Wieckowski, A, J. Phys. Chem. C. **2007**, 111, 13460-13465

68. Zhang, J.; Lima F.H.B.; Shao, M.H.; Sasaki, K.; Wang, J.X.; Hanson J.; Adzic, R.R, J. Phys. Chem B. **2005**, 109, 22701

69. Lai, F.J.; Sarma, L.S.; Chou, H.L.; Liu, D.G.; Hsieh, C.A.; Lee, J.F.; Hwang, B.J, J. Phys. Chem. C. **2009**, 113, 12674-12681

70. Jayasayee, K.; Dam, V.A.T.; Verhoeven, T.; Celebi, T.; DeBruijn F.A, J. Phys. Chem. C. **2009**, 113, 20371-20380

71. Wang, J.X; Markovic, N.M.; Adzic, R.R, J. Phys. Chem. B. **2004**, 108(13), 4127-4133

72. Hwang, B.J.; Kumar, S.M.S.; Chen, C.H.; Monalisa, Cheng, M.Y.; Liu, D.G.; Lee, J.F, J. Phys. Chem. C., **2007,** 111(42), 15267-15276

73. Mukerjee, S.; Srinivasan, S.; Soriaga, M.P.; McBreen, J, J. Phys. Chem. **1995,** 99(13), 4577-4589

74. Stamenkovic, V.; Schmidt, T.J.; Ross, P.N.; Markovic, N.M, J. Electroanal. Chem. **2003**, 554-555, 105-116

75. Drillet, J.F.; Ee, A.; Friedemann, J.; Kotz, R.; Schnyder, B.; Schmidt. V.M, Electrochim. Acta., **2002,** 47(12), 1983-1988

76. Neergat, M.;.Shukla, A.K.; Gandhi, K.S, J. Appl. Electrochem., **2001**, 31(4), 373-378

77. Paffett, M.T.; Beery, J.G.; Gottesfeld, S, J. Electrochem. Soc. **1988**, 135(6), 1431-1436

78. Antolini, E.; Passos, R.R.; Ticianelli, E.A, Electrochim. Acta. **2002,** 48(3), 263-270

79. Saejeng, Y.; Tantavichet, N, J. Appl. Electrochem. **2009**, 39 (1), 123-134

80. Antolini, E.; Salgado, J.R.C.; Gonzales, E.R, J. Power Sources. **2006**, 160, 957-968

81. Yu, P.; Pemberton, M.; Plasse, P, J. Power Sources. **2005**, 144, 11

82. Mercado, H.R.C.; Popov, B.N, J. Power Sources. **2006**, 155, 253-263

83. Cambanis, G.; Chadwick,D, Appl. Catal. **1986**, 25, 191-198

84. Santos, L.G.R.A.; Freitas, K.S.; Ticianelli, E.A, Electrochimica Acta, **2009**, 54, 5246-5251

85. Santiago, E.I.; Varanda, L.C.; Villullas, H.M. J. Phys. Chem. C. **2007**, 111, 3146-3151

86. Salgado, J.R.C.; Antolini, E.; Gonzales, E.R, J. Phys. Chem. B. **2004**, 108, 17767-17774

87. Xiong, L.; Kannan, A.M.; Manthiram, A, Electrochem. Commun. **2002**, 4, 898-903

88. Fernandez, P.H.; Rojas, S.; Ocon, P.; de la Fuente, J.L.G.;. Terreros, P.; Pena, M.A.; Garcia-Fierro, J.L, Applied Catalysis B : Environmental. **2007**, 77, 19-28

89. Schulenburg, H.; Muller, E.; Khelashvili, G.; Roser, T.; Bonnemann, H.; Wokaun, A.; Scherer, G.g, J. Phys. Chem. C. **2009**, 113, 4069-4077

90. Prutton, M, Introduction to surface Physics, New York; Oxford university Press, 1994

91. Gauthier, Y.; Joly, Y.; Baudoing, R.; Rundgren, J, Physical Review B. **1985**, Vol 31, 6216-6218

92. Gauthier, Y.; Bauoding, R, Physical Review B. **1987**, vol. 35, 7867-7878

93. Ruban, A.V.; Skriver, H.L.; Norskov, J.K, Physical Review B. **1999**, Vol. 59, 15990-16000

94. Nilekar, A.U.; Mavrikakis, M, Surface Science. **2009**, Vol 603, 91-96

95. Ma, Y.; Balbuena, P.B, Surface Science. **2008**, Vol 602, 107-113

96. Tseng, C.J.; Lo, S.T.; Lo, S.S.; Chu, P.P, Mater. Chem. Phys. **2006**, 100, 385-390

97. Xiong, L.; Manthiram, A, J. Electrochem. Soc. **2005**, 152, A697-703

98. Beard, B.C.; Ross Jr, P.N, J. Electrochem. Soc. **1986**, 133, 1839-1845

99. Russell, A.E.; Rose, A, Chem. Rev. **2004**, 104, 4613-4635

100. Lai, F.J, Structural Characterization of Bimetalic Nanoparticles and Their Application in direct Methanol Fuel Cells, Dissertation, National Taiwan University of Science and Technology, **2009**

101. Toshima, N.; Yonezawa, T, New J. Chem. **1998**, 22, 1179-1201

102. Stern, E.A.; Newville, M.; Ravel, B.; Yacoby, Y.; Haskel, D. Physica B: Physics of Condensed Matter. **1995**, 208-209, 117-120

103. Zabinsky, S.I.; Rehr, J.J.; Ankudinov, A.; Albers, R.C.; Eller, M, J. Phys. Rev. B. **1995**, 52(4), 2995-3009

104. Paulus, U.A, Electrocatalysis for Polymer Electrolyte Fuel Cells : Metal Alloys and Model System, Dissertation, Swiss Federal Institute of Technology Zurich, **2002**

105. Markovic, N.M.; Gasteiger, H.A.; Ross, P.N, J. Phys. Chem. **2002**, 99, 3411-3415

106. Bard, A.J.F, Electrochemical Methods – Fundamentals and Applications, 2nd ed, **2001**

107. Budiman, A.H.; Dewi, E.L.; Purwanto, W.W.; Dalimi, R.; Hwang, B.J, Indonesian Journal of Materials Science. **2010**, vol. 11, No. 3, 145-149

108. Ge, Q.; Desai, S.; Neurock, M.; Kourtakis, K, J. Phys. Chem. B. **2001**, 105(39), 9533-9536

109. Maillard, F.; Dubau, L.; Durst, J.; Chatenet, M.; Andre, J.; Rossinot, E, Electrochem. Com. **2010**, 12(9), 1161-1164

110. Ma, Y.; Balbuena, P.B, Surface Science. **2009**, 603(2), 349-353

111. Han, B.C.; Van Der Ven, A.; Ceder, G.; Hwang, B.J,. Phys. Rev. B: Condensed Matter and Material Physics. **2005**, 72(20), 1-9

112. Lee, M.H.; Wang, P.S.; Do, J.S, J. Solid State Electrochem. **2008**, 12, 879-884

113. Hwang, B.J.; Senthil Kumar, S.M.; Chen, C.H.; Chang, R.W.; Liu, D.G.; Lee, J.F, J. Phys. Chem C. **2008**, 112, 2370-2377

APPENDIX

CURRICULUM VITAE

I. Personal Identity

Name	:	Abdul Hamid Budiman
Place, Date of Birth	:	Pemalang, November 1st , 1970
Occupation	:	Researcher on the Field of Renewable Energy
Organization	:	Agency for the Assessment and Application of Technology
Department	:	Center for Energy Conversion and Conservation Technology
Address	:	
a. Office	:	BPPT II Building 20th Floor
		Jl. MH. Thamrin No. 8
		Jakarta 10340
		Indonesia
		Phone. (021) 3169754
		Fax. (021) 3169765
b. Home	:	Jl. W.R. Supratman No. 56 RT. 002 RW. 004
		Kampung Utan - Ciputat
		Tangerang 15412
		Indonesia
		Phone. (021) 7410004
		HP. 08128631135
Email	:	hamidbudiman@yahoo.com
Sex	:	Male
Marital Status	:	Married
Nationality	:	Indonesian

II. Educational Background

1. Elementery School : SD Negeri Kebondalem 03 Pemalang, 1983
2. Junior High School : SMP Negeri 02 Pemalang, 1986
3. Senior High School : SMA negeri 01 Pemalang, 1989
4. Bachelor : Chemical engineering Department, UPN Veteran Yogyakarta, 1995
5. Master : Sustainable Energy System and Mangement, University of Flensburg Germany, 2002

III. Working Experiences

1998 – now : Center for Energy Conversion and Conservation Technology, Agency for the Assessment and Application of Technology (BPPT)
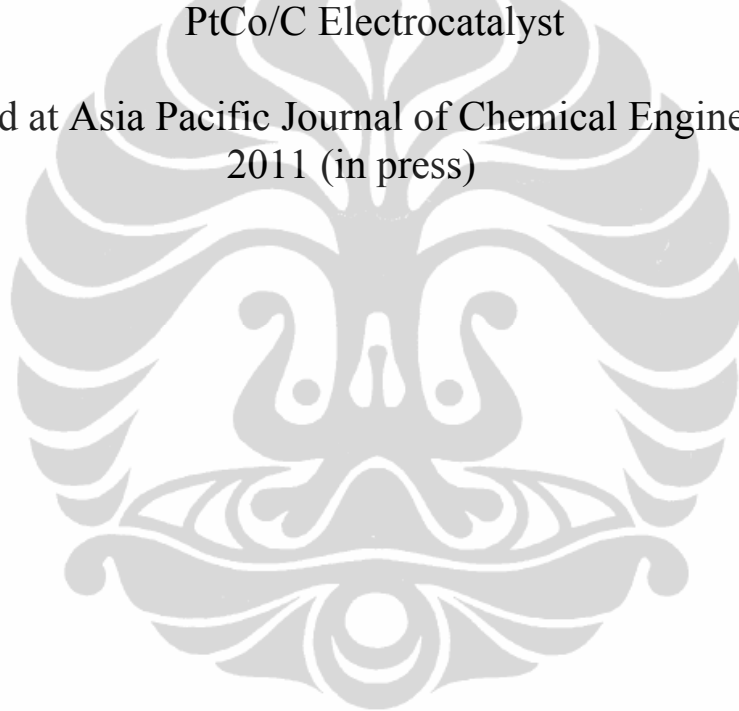
IV. Publications

1. Understanding Adsorbate-Induced Surface Segregation in PtCo/C Electrocatalyst.
   Asia Pacific Journal of Chemical Engineering, **2011** (in press)

2. Activity Enhancement of Carbon-Supported PtCo Electrocatalyst through Controlled Heat-Treatment for Proton Exchange Membrane Fuel Cell Applications.
   International Journal of Chemical Engineering Research, ISSN 0975-6422, Volume 3, No. 2, **2011**, 125-133

3. Atomic Distribution of PtCo/C Nanoparticles as Investigated by X-ray Absorption Spectroscopy.
   Indonesian Journal of Material Science, special Edition on Materials for Energy and Device, **2010**, 35-39

4. Effect of PtCo/C Treatment on Performance of Single Cell PEM Fuel Cell.
   Indonesian Journal of Materials Science, Vol. 11, No. 3, **2010**, 145-149

5. Effect of Heat Treatment of Pt-Co/C Electrocatalyst on Their Activity and Stability.
   Proceeding of 2nd International Conference on Fuel Cells and Hydrogen Technology, ISBN 978-602-95555-1-6, **2009**, 132-137

6. Material Combination for Cathode PEMFC Electrocatalyst Development : A Review.
   International Conference on Advance and Sustainable Polymer, **2008**

PUBLISHED PAPER

Paper 1 :
Understanding Adsorbate-Induced Surface Segregation in
PtCo/C Electrocatalyst

Accepted at Asia Pacific Journal of Chemical Engineering,
2011 (in press)

Understanding Adsorbate-Induced Surface Segregation in PtCo/C Electrocatalyst

Abdul Hamid Budiman[1], Widodo Wahyu Purwanto[1*], Eniya Listiani Dewi[2], Rinaldy Dalimi[3], Bing Joe Hwang[4]

1) Chemical Engineering Department, University of Indonesia, Depok, Indonesia
2) Centre of Material Technology, Agency for the Assessment and Application of Technology, Jakarta, Indonesia
3) Electrical Engineering Department, University of Indonesia, Depok, Indonesia
4) Chemical Engineering Department, National Taiwan University of Science and Technology, Taipei, Taiwan ROC

Abstract

The x-ray diffraction (XRD) was used to study the effect of treatment on particle size and catalyst structure of PtCo/C electrocatalysts. The XRD showed the grain sizes of N_2-treated electrocatalysts increase with temperature treatment, while those treated with CO remain the same. The x-ray absorption spectroscopy (XAS) was used to study the changes in atomic distribution, extent of alloying as well as the surface population of PtCo/C nanoparticles. The XAS revealed that the time of CO treatments influence the surface population due to phase segregation. Catalysts treatment for 1, 3 and 5 h lead to higher population of Pt on the core and Co on the surface resulting in Pt rich in core – Co rich in shell. In contrast, CO treatments for 7, 10 and 15 h lead to higher population of Pt on the shell and Co on the core resulting in Pt rich in shell – Co rich in core. The electrochemical results showed that PtCo/C CO-treatment is more active than commercial PtCo/C for the ORR and it is found that PtCo/C CO-treatment 3 h has the highest catalytic activity; because it has higher J_{Pt} and J_{Co} values, indicating a higher extent of Pt and Co alloying.

Keywords : XRD, XAS, phase segregation, coordination number, alloying extent

1. Introduction

It has been reported that bimetallic nanoparticles (NPs) is a promising candidate materials for oxygen reduction reaction (ORR) electrocatalyst. In recent years, many efforts to develop an alternative catalyst to Pt focused primarily on Pt based bimetallic alloys, in which platinum is partially replaced by other less expensive metals.[1-2] Numerous studies have highlighted the alloying of Pt with transitional metal such as Co,[3-4] Ni,[3-7] Fe,[8] Mn,[8] Cr,[9-11] and V[12] as a promising approach toward improving ORR electrocatalyst in acidic solutions.

Pt is the most common electrode catalyst and presents the best catalytic activity for ORR among all pure metals and when supported on a conductive carbon serves as state of the art electrocatalyst in low temperature fuel cell air cathodes.[13] However, due to the high cost and limited supply of Pt and also due to kinetic limitations of ORR, the development of more active and less expensive oxygen reduction electrocatalyst than pure Pt has been the subject of extensive research for a number of decades.[1-[2]

Alternatively, it has been shown that the activity and stability of the catalyst can be improved by alloying Pt with some transition metals. Among these Pt alloys, Pt-Co nanomaterials have been widely studied as promising alternative catalyst for proton exchange membrane fuel cell (PEMFC) applications. It was reported that Pt alloyed with Co on the carbon support yields better catalytic activity than pure Pt, where Pt:Co ratios of 1:1 to 3:1 are most studied.[5,14-16] Among these Pt catalyst, the intermetallic Pt_3Co solid solution were extensively studied.[2] A number of explanations for the improvement in activity by the addition of transition metals to Pt have been ascribed, including the lowering of the Pt oxidation state,[4] the suppression of Pt oxide formation,[4,17] the formation of new electronic structure with higher Pt 5d orbital vacancies,[9] a decrease in the Pt-Pt distance and therefore a more favorable adsorption of O_2,[9] and the formation of a catalytic and thin Pt skin on the surface of the alloy.[18-20]

Many researchers have demonstrated that the activity of electrocatalysts toward ORR is strongly dependent on many factors, such as particle size and distribution,[9,21-22] the catalyst's morphology[23] and composition, particularly its surface composition, the oxidation state of Pt and the second metal atom,[4] and the surface structure of the catalyst.[19] One of the major approaches to improve the activity and stability of Pt based catalysts is to optimize the catalyst synthesis procedure. It is recognized that the electrocatalyst performance is strongly dependent on the preparation procedures, including the addition of metal and its precursor, the support type and supported strategy, and the heat treatment strategy.[24]

The improvement of catalytic activities can be attributed to the modification of the geometric and electronic properties in the alloys.[25] Surface segregation was found closely related to the activity improvement. For example, Stamenkovic et al[26] compared the kinetics of the ORR on bilk alloy of Pt_3Co and the Pt-skin structure produced by Pt segregating on topmost layer of the annealed surface. The ORR was uniquely active on Pt-skin surface and the rate of reaction is four times than for pure Pt catalyst.

The effect of phase segregation on the catalytic properties of NPs is of considerable practical interest, but not completely understood at this time.[27] It is believed that phase segregation is partially responsible for catalytic activity enhancement or degradation under certain treatment conditions, phenomenon referred to as "synergistic effect" or "burning effect".[27]

Recently, a novel preparation procedure has demonstrated for PtCo with a core shell structure using an adsorbate-induced surface segregation by Mayrhofer et al.[28] Motivated by this study, herein we focused on adsorbate-induced surface

segregation in PtCo/C electrocatalyst obtained by treating the catalyst using CO. The X-ray absorption spectroscopy (XAS) technique is used to understand the structural properties such as atomic distribution and alloying extent of the catalyst. Electrochemical measurement was applied to determine the activity of the catalyst.

2. Experimental Section
Thermal treatment of PtCo/C Electrocatalyst

A commercial E-TEK PtCo/C (30 wt% Pt) catalyst was used for the nitrogen treatment studies. To obtain a reliable comparison, sample from the same batch with homogenous mixing were used. First, the as received catalyst powder was pre-treated by flowing H_2 for 2 h at 300 ^{o}C. The sample then was allowed to cool temperature under N_2 atmosphere. In the case of N_2 thermal treatment experiments, pure N_2 gas was introduced into the sample chamber with a flow rate of 60 mL min-1 for about 2 h at various temperature i.e. 300, 400, 500, 600 and 700 ^{o}C. Again, the catalyst was allowed to cool temperature under N_2 atmosphere. H_2 was flowed to clean any existing impurities and to eliminate the oxide contribution.

In the case of CO thermal treatment, a commercial PREMETEK PtCo/C (20 wt% Pt) was used. First, catalyst was purged by flowing H_2 at 300 ^{o}C for 2 h. The sample then was allowed to reduced to 200 ^{o}C then purged by flowing 20% CO at various time i.e. 1, 3, 5, 7. 10 and 15 h. Later, the sample was allowed to cool temperature. H_2 was flowed to clean the impurities if present any and to eliminate the oxide contribution.

Description of the sample code is described as follow :

Table 1. Description of the catalyst samples

No. of sample	Description
(1)	PtCo/C commercial (E-TEK)
(2)	PtCo/C - N_2 treatment 300 ^{o}C
(3)	PtCo/C - N_2 treatment 400 ^{o}C
(4)	PtCo/C - N_2 treatment 500 ^{o}C
(5)	PtCo/C - N_2 treatment 600 ^{o}C
(6)	PtCo/C - N_2 treatment 700 ^{o}C
(7)	PtCo/C commercial (PREMETEK)
(8)	PtCo/C - CO treatment 1 h
(9)	PtCo/C - CO treatment 3 h
(10)	PtCo/C - CO treatment 5 h
(11)	PtCo/C - CO treatment 7 h
(12)	PtCo/C - CO treatment 10 h
(13)	PtCo/C - CO treatment 15 h

2.2. XRD measurement

X-ray diffractograms of the electrocatalyst were obtained with a universal Rigaku diffractometer operating with a Cu Kα radiation ($\lambda = 0.15406$ nm) generated at 40 kV and 100 mA. Scan were done at 0.05 deg s^{-1} for 2θ values between 20 and 90°. An average value of the lattice parameter was obtained from the Pt (111), (200), (220) and (311) peaks. The crystalline sizes were obtained from the Pt (220) reflection using Scherrer's equation.

2.3. TEM measurement

Transmission electron microscopy (TEM) and electron diffraction measurements were carried out on Phillips TEM. High angle annular dark field scanning transmission electron microscopy images were obtained with Tecnai G2 F20 operated at 300 kV. Sample were prepared by sonicating a small amount of the catalyst NPs in ethanol. A drop of this slurry was deposited onto a holey carbon-copper grid followed by drying in the oven.

2.4. XAS measurement

The X-ray absorption spectra were recorded at the beamline 17C1, National Synchrotron Radiation Research Centre, Hsinchu, Taiwan. The electron storage ring was operated at 1.5 GeV with a current of 300 mA. A Si (111) double crystal monochromator was employed for the energy selection with a resolution $\Delta E/E$ better than 2 x 10^{-4} at both the Pt L$_{III}$-edge (11564 eV) and the Co K-edge (7709 eV). All of the experiments on bimetallic nanoparticles were conducted on homemade cells fabricated with stainless steel for an XAS powder study. Prior to the XAS measurements, samples were reduced with 10% H$_2$ for 1 h at 300 ^{0}C to remove any oxidized species remaining on the catalyst surface. The total amount of the sample was adjusted to reach the optimum absorption thickness ($\Delta \mu x = 1.0$, $\Delta \mu$ is the absorption edge, x is the thickness of the sample) so that the proper edge jump step could be achieved during measurements. All of the spectra were recorded at room temperature in a transmission mode. Higher harmonics were eliminated by detuning the double crystal Si(111) monochromator. A series of three gas filled ionization chambers were used to measure the intensities of the incident beam (I$_0$), the beam transmitted by the sample (I$_t$) and the beam subsequently transmitted by the reference foil (I$_r$). The third ion chamber was used in conjunction with the reference sample, which was a Pt foil for Pt L$_{III}$-edge measurements and a Co foil for the Co K-edge measurements. The control of parameters for EXAFS measurements, data collection modes, and calculation of errors were all carried out according to the guidelines set by the International XAFS Society Standards and Criteria Committee.

EXAFS Data Analysis. The XAS experimental data were treated by utilizing the standard procedures. The EXAFS function, χ , was obtained by subtracting the post edge background from the overall absorption and then normalized with respect

to the edge jump step. The normalized $\chi(E)$ was transformed from energy space to k-space, where "k" is the photoelectron wave vector. The $\chi(k)$ data were multiplied by k^2 to compensate for the damping of EXAFS oscillations in the high k-region. Subsequently, k^2 weighted $\chi(k)$ data in k-space ranging from 3.53 to 13.95 Å^{-1} for the Pt L $_{III}$-edge and from 3.53 to 10.36 Å^{-1} for the Co K-edge were Fourier transformed (FT) into r-space to separate the EXAFS contribution from the different coordination shells. A non linear least squares algorithm was applied to the curve fitting of an EXAFS in the r-space between 1.8 and 3.2 Å for both Pt and Co depending on the bond to be fitted. The PtCo reference file was determined by a theoretical calculation. Reference phase and amplitude for the Pt-Pt absorber scatter pairs were obtained from a Pt foil. For the Co-Co and Co-O absorber scatter pairs, the phase and amplitude were obtained from the reference Co foil and CoO, respectively. All of the computer programs were implemented in the UWXAFS 3.0 package,[29] with the backscattering amplitude and the phase shift for the specific atom pairs being theoretically calculated by using the Feff7 code.[30] From these analysis, structural parameters such as coordination numbers (N), bond distance (R), Debye-Waller factor ($\Delta\sigma_j^2$) and inner potential shift (ΔE_0) have been calculated. For the amplitude reduction factor, S_0^2, values for the Pt and Co were obtained by analyzing the Pt and Co foil reference samples respectively, and by fixing the coordination number in the FEFFIT input file.

2.5. Electrode Preparation and Electrochemical Measurements

Analytical grade Millipore water (18 MΩ) and sulfuric acid (ACROS) were used in this study. All of the experiments were carried out at ambient temperature of $25 \pm 1^\circ$C. A conventional three electrode electrochemical cell was used for the CV measurements, with a high surface area Pt counter electrode and the saturated calomel electrode (SCE) as a reference electrode powered by a Solartron 1480 potentiostat/galvanostat. However, all potentials reported herein are referenced to the NHE. The working electrode was made of the carbon supported PtCo catalyst immobilized on a GCE surface (0.1964 cm^2). The procedure for the electrode fabrication involves, first, preparation of a clear suspension by sonicating a known amount of PtCo/C catalyst powder dispersed in 0.5% Nafion, second, placing an aliquot of this suspension (7 μL) on the GCE disk, and, third, air drying about 5 minutes at room temperature and then at 80° C to yield a uniform thin film of the catalyst. CV experiments were performed in 0.5 M H_2SO_4 solution at a scan rate of 10 mV/s. N_2 gas was purged for nearly 30 minutes before starting the experiment, and stable voltammogram recorded after two cycles were taken into account for all the CV experiments. Linear sweep voltammetry was performed in the potential range from 0.856 to -0.244 V in 0.5 M H_2SO_4 solution with a scan rate of 1 mV/s and rotation of 1600 rpm.

3. Result and Discussion

Figure 1 shows the x-ray diffraction pattern of the commercial PtCo/C electrocatalyst and the Pt-Co/C catalyst subjected to nitrogen treatment at various temperatures (Figure 1.a) and the Pt-Co/C electrocatalyst subjected to carbon monoxide treatment at various times (Figure 1.b). In all of the catalysts the peak located at about 24.8^o is attributed to the (002) plane of hexagonal structure of the Vulcan XC 72 carbon.[31]
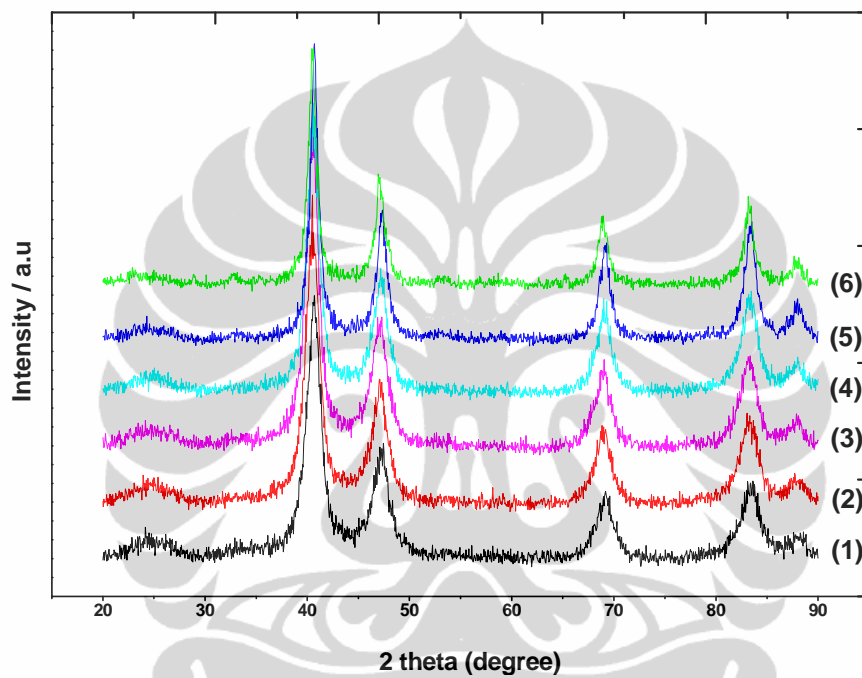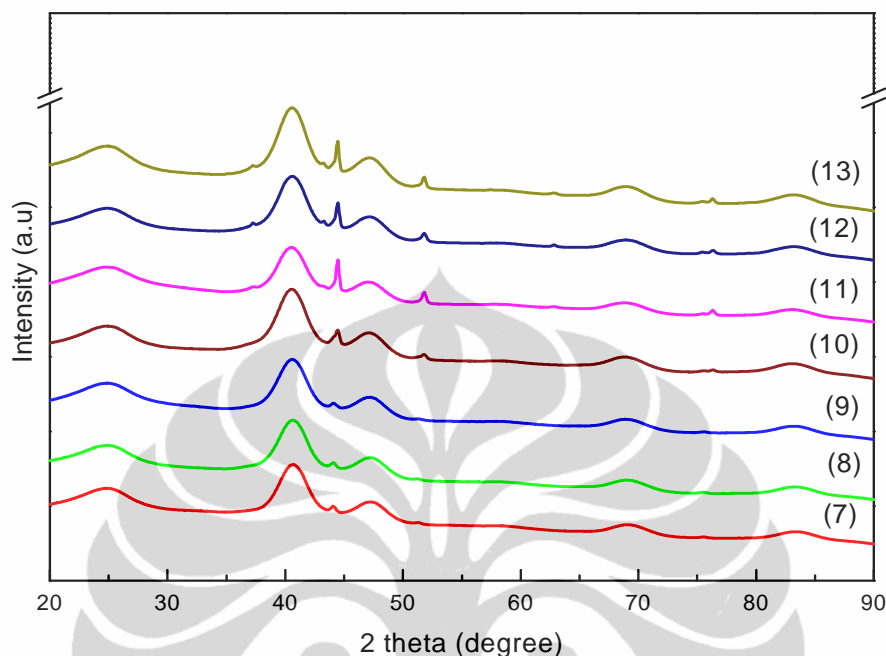
Figure 1. XRD diffractograms of commercial and (a) N_2-treated (b) CO-treated PtCo/C electrocatalysts

As observed in Figure 1(a) all the catalysts exhibit the main characteristic peaks of the face centered cubic (fcc) crystalline Pt with the peak position of the planes (111), (200), (220), (311) and (222) planes are at 2θ of ca. 40.25^o, 46.82^o, 68.36^o, 82.42^o and 86.96^o respectively (JCPDS No. 87-0647). In this pattern shows there is no super lattice reflection, which indicates the formation of only disordered solid solution. It is noted that no individual peaks of Co were detected, no peaks for pure Co or its oxides was found which indicates Co might be fully incorporated into the Pt crystal to form an alloy since the ICP data confirms an existence of cobalt in the alloy. This presence can not be discarded because may be they present in a small amount or even in amorphous form.[32]

As indicated in Figure 1(b) all the catalysts exhibit the main characteristic peaks of the face centered cubic (fcc) crystalline Pt with the peak position of the planes (111), (200), (220), and (311) planes are at 2θ of ca. 40.25^o, 46.82^o, 68.36^o and 82.42^o respectively (JCPDS No. 87-0647).

From the figure, it is also clearly observed that for sample numbers 10, 11, 12 and 13 which are subjected to CO treatment for 5, 7, 10, 15 h respectively show diffraction peaks namely (400), (331) and (531) plane characteristic to Co related species (JCPDS No. 01-1259). The appearance of Co related species after carbon monoxide treatment indicates the presence of segregation in CO-treated catalysts.

Although the commonly available x-ray powder diffraction technique is capable to predict the atoms arrangement preferably in single crystals or poly crystals with sufficient long range order, but it lacks of providing information about the structural parameters required to understand the atomic distribution in bimetallic nanoparticle. Therefore, information about the alloy structure related to nanoparticle where short range order exists is incomplete from XRD results.[33] Since XRD is very sensitive to grain size, the larger grain would produce the narrow diffraction peaks. Thus, the broad diffraction peaks appearing for the present catalyst suggest that the grain size is small.

The lattice parameter and particle size of the Pt-Co/C catalyst were calculated using Scherrer's equation and are summarized in Table 2. It is clearly shown that the grain size of the particle for N_2-treated Pt-Co/C electrocatalyst increased correspondingly with the increase of the temperature treatment due to agglomeration. This is in a good agreement with Makoto et al.[34] From the TEM measurement, it is showed that particle size distribution of commercial E-TEK PtCo/C is uniform, with the grain size of 4.6 nm.[2] The average grain size is 7.12 nm, which is greater than the Pt/C catalyst of 2.5 nm.

Table 2. Grain size calculation from XRD data for commercial, N_2-treated and CO-treated PtCo/C electrocatalyst

No. of sample	Grain size nm	Lattice Parameter Å
N_2 treatment		
(1)	5.532	3.838
(2)	5.534	3.848
(3)	6.146	3.851
(4)	6.543	3.845
(5)	9.361	3.834
(6)	9.594	3.852
CO treatment		
(7)	3.052	3.822
(8)	3.018	3.842
(9)	2.909	3.845
(10)	2.935	3.841
(11)	3.073	3.838
(12)	2.984	3.802
(13)	3.055	3.828

The lattice parameter of platinum in the Pt-Co/C catalyst is 0.385 nm, which is smaller than a Pt/C catalyst of 0.392.[35] The decrease in the lattice parameter of the Pt-Co/C alloy reflects the introduction of Co into the alloyed state and indicates that the addition of Co in the Pt crystal reduces spacing of Pt-Pt atoms, which is considered to be a mechanism for enhancement of activity. From XAS measurement,

the atomic composition of the PtCo/C commercial from E-TEK is about 72:28 for Pt and Co respectively, which is very close to the nominal value (3:1).

Transmission electron microscopy (TEM) images of PtCo/C subjected to N_2-treatment are shown in Figure 2. From the figure, it is clearly observed that the dispersion of the catalyst is uniform throughout the region. Particle size of N_2-treated PtCo/C at 600 ^oC is greater than that at 300 ^oC, which agrees with the XRD result.
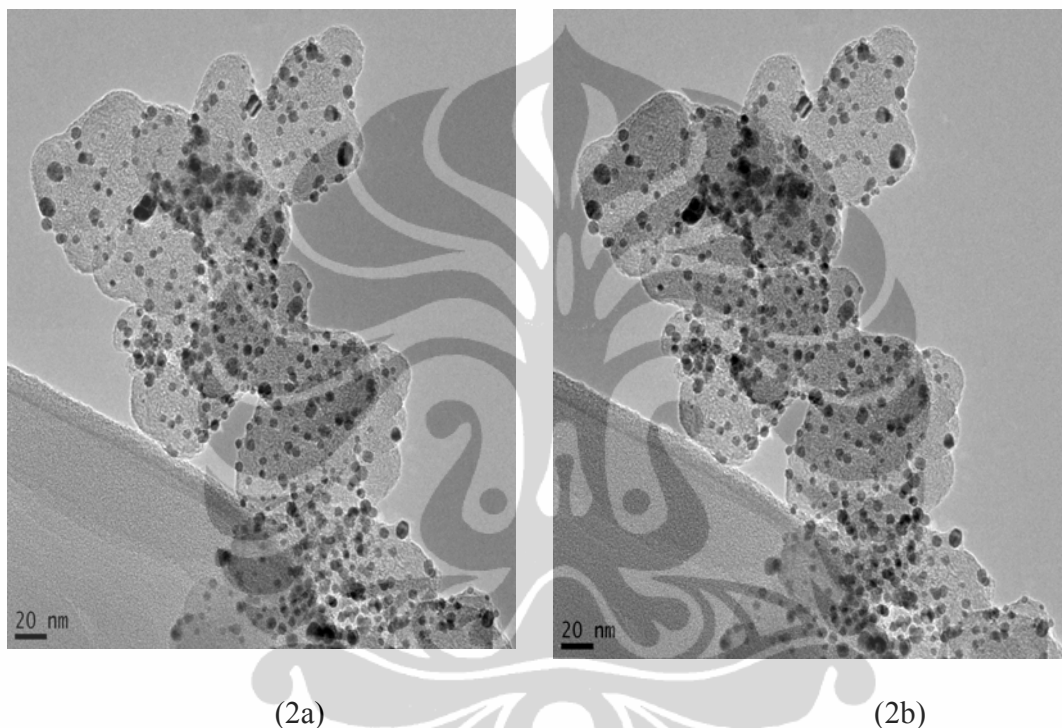

(2a)   (2b)

Figure 2. TEM images of the N_2-treated PtCo/C (a) 300^oC (b) 600^oC

The grain size of all catalysts subjected to CO-treatment is almost same. The particle size changes smoothly and the treatment leads to change the catalyst structure due to the phase segregation as illustrated in Figure 3. From XAS, it was found that the atomic composition of PtCo/C commercial from PREMETEK is about 49:51 for Pt and Co respectively, which is very close to nominal value (1:1).
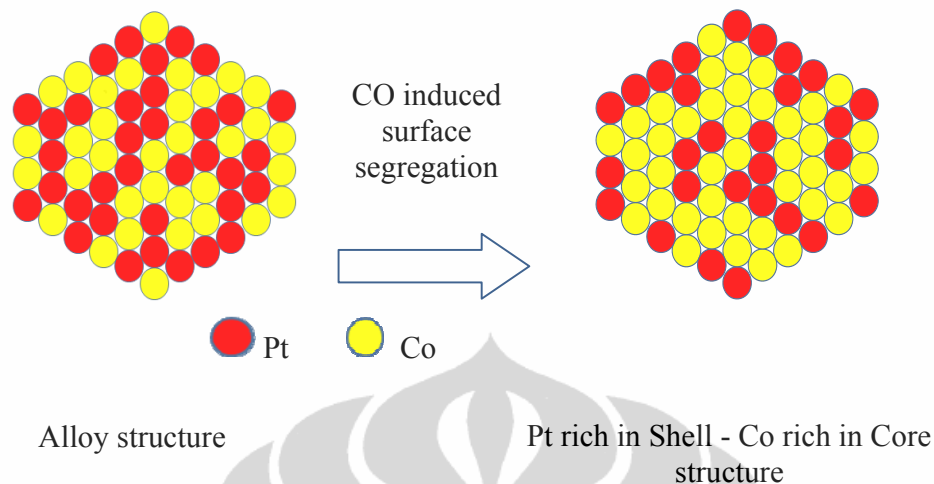
Figure 3. Catalyst structure was changed by induced surface segregation.

The adsorbate induced into the electrocatalyst leads to change in the catalyst structure. In general, catalytic performance is governed by a sequence of bond breaking and bond making processes that are carried out over the active metal surface. Individual bond breaking and forming steps are largely controlled by a balanced between the metal-adsorbate bond strength and the intramolecular bond strength. Alloying two metals can alter their electronic structure as well as their geometric structure. It has been shown that the metal-adsorbate bond streng on the alloy surface can be very different from that on the pure metal surfaces and can therefore alter the mechanism of a reaction.[36]

The composition of the surface of the bimetallic system can be very different from the bulk, depending on the segregation heat and the surface mixing energy. This statement is in agreement with Maillard et al[37] who proved the direct evidence of bulk Co segregation to the surface. They showed that the binding energy of oxygen onto Co atoms located on a Pt_3Co surface is greater than that on the monolayer Pt-skin which may provide sufficient driving force to overcome the segregation energy of Co atoms to the surface. It has been showed that surface structure is significantly modified under the influence of surface segregation.[25]

This effect is additionally dependent upon the chemical potential of the gas phase, since the strong bonding of adsorbates will result in a gain in energy of the system. Consequently, for the bimetallic system an enrichment at the surface of the component that binds a certain adsorbate more strongly may occur[28] Recently, Mayrhofer et al[28] presented a novel preparation procedure of such core-shell nanoparticles with a platinum shell by using an adsorbate-induced surface segregation effect to modify an un-leached carbon supported Pt_3Co alloy high-surface area catalyst to increase the utilization of platinum in the particles. For this purpose the catalyst was subjected to a gas-phase treatment. The catalyst powder was placed into a rotary evaporator, which was then repeatedly evacuated and filled with CO to eliminate residual oxygen, then the distiller was filled with ambient pressure of CO

and heated to 200 °C for three hours. Because the adsorption enthalpy of CO on Pt is higher than on Co, Pt segregates to the surface of the nanoparticles and correspondingly displaces Co to the core.

The utilization of adsorbate-controlled surface segregation was done by Han et al.[38] It was proposed that adsorbed oxygen on Pt-Ru induces surface segregation of Ru due to the strong binding between Ru and O on the surface. Hwang et al[39] developed a controlled thermal-treatment strategy to alter the surface population of Pt and Ru without varying the particle size of the initial PtRu/C NPs. It was reported that heat treatment in O_2 atmosphere can draw the Ru present in the core of the cluster to the surface, and heat treatment in a H_2 atmosphere led to the migration of core Pt to the shell region.
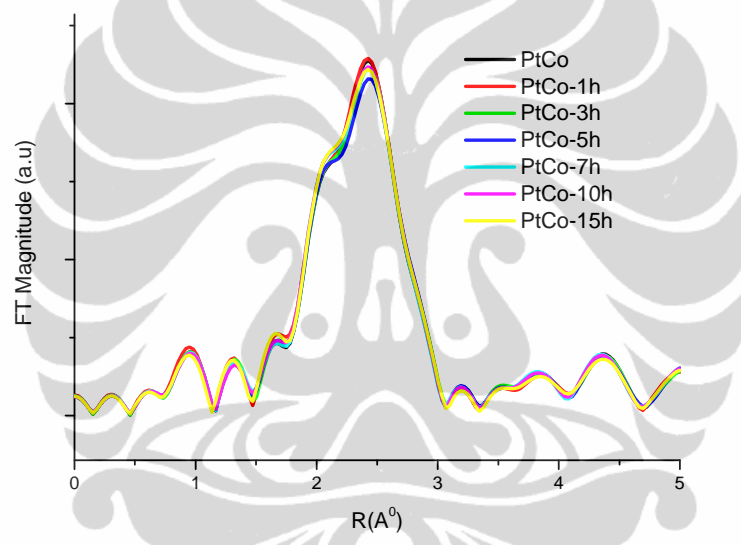
Figure 4.a. FT EXAFS spectra at Pt L_{III}-edge of commercial and CO-treated PtCo/C electrocatalyst
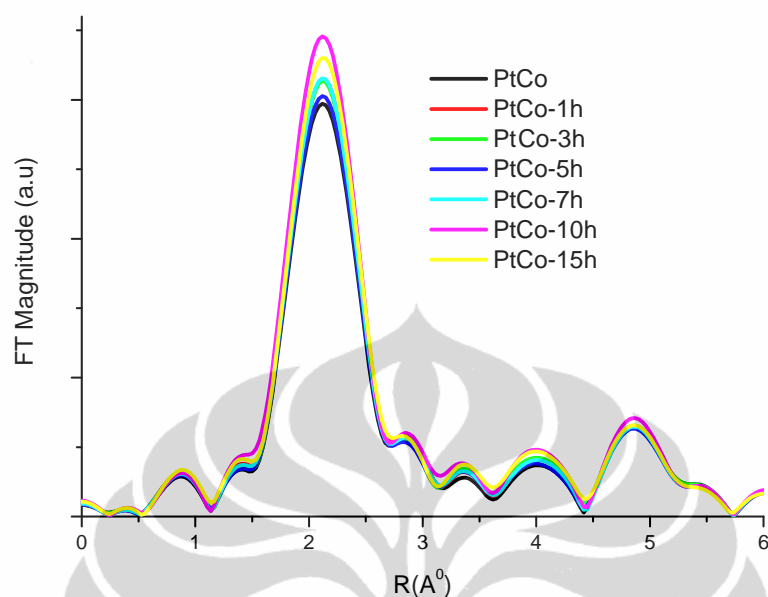
Figure 4.b. FT EXAFS spectra at Co K-edge of commercial and CO-treated PtCo/C electrocatalyst

As seen in the FT-EXAFS spectra at Pt L_{III}-edge (Figure 4.a), a strong peak appeared between 2 and 3Å with the reference Pt FT peak showing that Pt atoms are not the only constituents of the environment around Pt in the bimetallic nanoparticles. The peak splitting in the case of bimetallic nanoparticles indicates the presence of two types of backscattering atoms in the first shell coordination. The intensity of the peak resulting from Pt-Pt and Pt-Co interactions is increased with an increase in the time of treatment. The increased FT intensity implies a higher contribution of Pt coordination in the core region. These results suggest that a considerable number of Co atoms in the sample number 7-10 moved to the surface, thereby giving a predominant population of Pt in the core region. The FT-EXAFS spectra at the Co K-edge (Figure 4.b) also exhibit a peak in the R range of 2-3Å due to the first shell metal-metal bonding involving Co-Pt and Co-Co correlations. The peak is related to the first coordination shell of Co-Co and Co-Pt, which is caused by the interference between the back scattering from Co to Co and Pt neighbors. In this case, the intensity of the peak related to the Co-Co first coordination shell splitting is higher for the sample number 11-13. This finding indicates that Pt atoms present in the core are brought to the surface; and as a result, a higher population of Co atoms is present in the core region.

The atomic structures of catalysts are derived from experimentally obtained XAS structural parameters and the alloying extent of Pt (J_{Pt}) as well as cobalt (J_{Co}). As can be seen in Table 3, for the PtCo/C catalyst subjected to CO treatments for 1, 3 and 5 h (sample number 8, 9 and 10), the observed total coordination number

parameter relationship of $\sum N_{Pt-i} > \sum N_{Co-i}$ and the alloying extent $J_{Pt} < J_{Co}$ indicates that Co atoms are mostly segregated to the surface of the nanoparticle and Pt atoms to the core, resulting in a Pt rich in core and a Co rich in shell structure. In contrast, when the time for CO treatment increases to 7, 10 and 15 h the trend in the coordination number changes. The total coordination number parameter relationship of $\sum N_{Pt-i} < \sum N_{Co-i}$ and alloying extent $J_{Pt} > J_{Co}$ indicate that Pt atoms are segregated to the surface of the nanoparticle and Co atoms to the core, resulting in a Pt rich in shell and a Co rich in core structure.

Table 3. Coordination number and alloying extent of CO-treated PtCo/C electrocatalyst

No. of sample	Time of CO treatment	$\sum N_{Pt-i}$	$\sum N_{Co-i}$	J_{Pt}	J_{Co}
(7)	0 h	8.65	7.28	70.51	78.40
(8)	1 h	9.36	7.00	60.60	75.91
(9)	3 h	8.93	6.78	64.88	80.12
(10)	5 h	8.78	7.37	65.99	73.70
(11)	7 h	8.56	8.63	69.59	64.77
(12)	10 h	8.84	9.05	68.30	62.41
(13)	15 h	8.56	8.69	61.04	56.39

The energy binding of CO for 1, 3 and 5 h is not strong enough to segregate the Pt atom into the surface. Consequently, only a few Pt migrates to the surface to displace Co. In contrast to CO treatment for 7, 10 and 15 h, the energy binding is more apt to segregate Pt into the surface and correspondingly displace Co to the core. Among these catalysts, the sample number 9 owns higher J_{Pt} and J_{Co} values, indicating a higher extent of Pt and Co alloying, therefore it is predictable that catalytic performance toward ORR will be good.

The core/shell nanoparticles can be regarded as a kind of phase separation of an alloy into a core surrounded by the shell composed of a metal. This kind of structure will protect the dissolution of the transition metal.[40] When Co at the core is protected by Pt at the shell, the decay of the electroactivity may be inhibited.

N_2-treated PtCo/C electrocatalyst results in the base voltammogram become more Pt like, which is probably indicative of leaching of Co from the surface. This phenomenon is in agreement with Antolini et al who reported that the metal particle size of the Pt alloy influences the dissolution of the base metal in an acid environment.[41] The higher temperature treatment will affect the particle agglomeration, causing it to lose the active surface area.
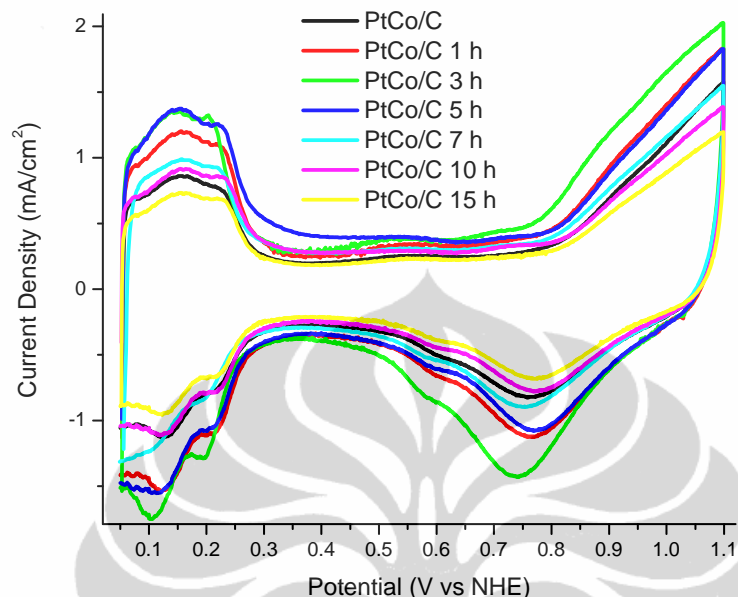
Figure 5. Cyclic voltammogram for commercial and CO-treated PtCo/C
electrocatalyst in N_2 saturated 0.5 M sulfuric acid electrolyte solution at scan rate of
10 mV/s

The cyclic voltammetry (CV) of PtCo/C electrocatalyst with various CO-treatment times are recorded in N_2 saturated 0.5 M sulfuric acid electrolyte solution at scan rate of 10 mV/s is presented in Figure 5. The figure displays the feature of the hydrogen adsorption-desorption region between 0 and 0.35 V, followed by the double-layer potential region. At potentials > 0.7 V adsorption followed by oxide formation was observed. For the treated catalysts, the hydrogen adsorption-desorption region laid between the same potentials than commercial-PtCo/C, while the OH adsorption and the oxide formation commenced at potentials > 0.8 V. The formation of the Pt oxide layer is shifted towards more positive potentials for the bimetallic samples subjected to thermal treatments.

Cyclic voltammetry of a CO-treated Pt-Co/C electrocatalyst indicated that alloying inhibited the chemisorptions of oxygenated species such as OH_{ad} on the Pt sites at high potential (above 0.8 V) due to the change in the Pt electronic structure induced by the addition of Co. This may be beneficial to the oxygen adsorption at low potential and it will enhance ORR activity. The enhanced ORR performance of PtCo is attributed to its comparably higher extent of Pt and Co alloying, number of Pt unfilled d state created by alloying metal and convenient grain size.

Figure 6 shows the ORR activity of the catalyst under oxygen saturated 0.5 H_2SO_4 solution at room temperature. From the figure, the ORR on the all catalysts are diffusion controlled when the potential is less than 0.7 V and is under a mixed control region of diffusion-kinetic from 0.7-0.85 V. In the Tafel region (higher than 0.85 V)

and the mixed potential region, the ORR activities show a significant difference in their magnitude. It can be seen clearly that the samples number 7-10 shows the enhanced ORR activity while sample number 11-13 displays poor activity.
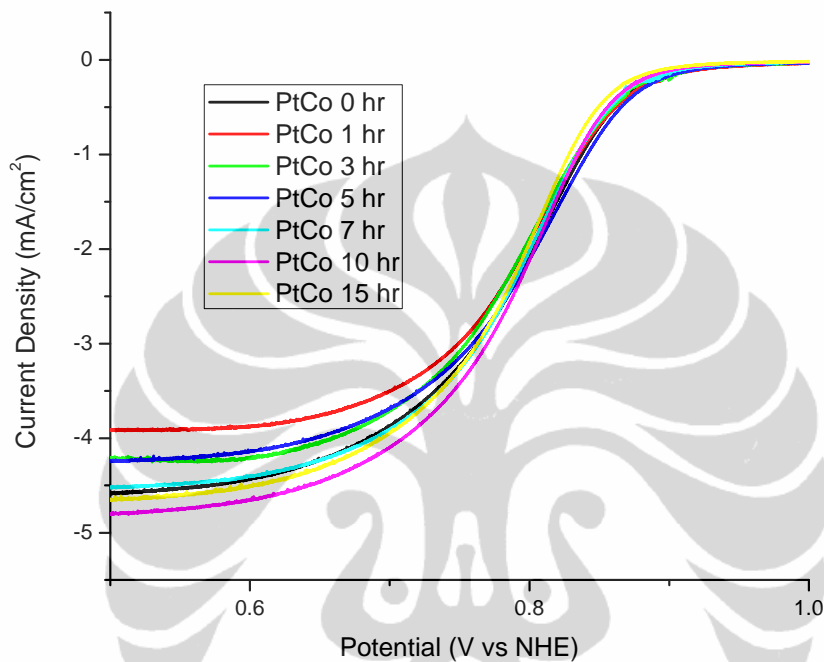

Figure 6. Linear sweep voltammogram recorded at 1 mV/s for the ORR of commercial and CO-treated PtCo/C electrocatalysts

4. Conclusion

XRD and XAS were used to study the effect of treatment on the particle size and structure of the catalyst. The grain size of N_2-treated PtCo/C increased with temperature of treatment due to agglomeration. TEM images show the size distribution of particles is uniform and the particle size is greater as the temperature of treatment increased. Catalysts treated with CO resulted in the same grain size. The XRD pattern showed that the appearance of Co related species after CO treatment indicates the presence of segregation in CO treated catalysts.

Catalysts treated for 1, 3 and 5 h lead to higher populations of Pt on the core and Co was moved to the surface, resulting in a Pt rich in core and a Co rich in shell. Catalysts treated for 7, 10 and 15 h lead to higher populations of Pt on the shell and of Co on the core, resulting in a Pt rich in shell and a Co rich in core. Nanoparticles consisting of a Pt shell around PtCo core were formed by utilizing an adsorbate-

induced surface segregation effect resulting in an active catalyst with a low amount of noble metal.

The electrochemical results showed that PtCo/C CO-treatment is more active than commercial PtCo/C for the ORR and it is found that sample number 9 (PtCo/C CO-treatment 3 h) has the highest catalytic activity; because it has higher J_{Pt} and J_{Co} values, indicating a higher extent of Pt and Co alloying.

Acknowledgements
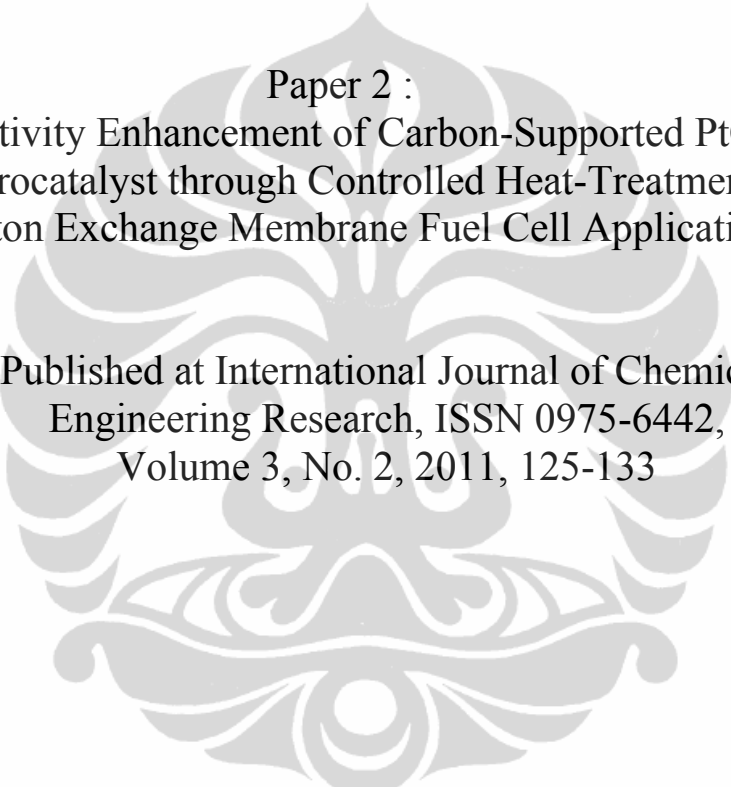
References

[1] J.X. Wang, N.M. Markovic, R.R. Adzic. J. Phys. Chem. B., **2004**; 108(13), 4127-4133.

[2] B.J. Hwang, S.M.S. Kumar, C.H. Chen, Monalisa, M.Y. Cheng, D.G. Liu, J.F. Lee. J. Phys. Chem. C., **2007**; 111(42), 15267-15276.

[3] S. Mukerjee, S. Srinivasan, M.P. Soriaga, J. McBreen. J. Phys. Chem., **1995**; 99(13), 4577-4589.

[4] A.S. Arico, A.K. Shukla, H. Kim, S. Park, M. Min, V. Antonucci. Appl. Surf. Sci., **2001**; 172(1-2), 33-40.

[5] U.A. Paulus, A. Wokaun, G.G. Scherer, T.J. Schmidt, V. Stamenkovic, V. Radmilovic, N.M. Markovic, P.N. Ross. J. Phys. Chem. B., **2002**; 106(16), 4181-4191.

[6] V. Stamenkovic, T.J. Schmidt, P.N. Ross, N.M. Markovic. J. Electroanal. Chem., **2003;** 554-555, 105-116.

[7] J.F. Drillet, A. Ee, J. Friedemann, R. Kotz, B. Schnyder, V.M. Schmidt. Electrochim. Acta., **2002**; 47(12), 1983-1988.

[8] S. Mukerjee, S. Srinivasan, M.P. Soriaga. J. Electrochem. Soc., **1995**; 142(5), 1409-1422.

[9] M.K. Min, J. Cho, K. Cho, H. Kim., Electrochim. Acta., **2000**; 45(25-26), 4211-4217.

[10] M. Neergat, A.K. Shukla, K.S. Gandhi. J. Appl. Electrochem., **2001**; 31(4), 373-378.

[11] M.T. Paffett, J.G. Beery, S. Gottesfeld. J. Electrochem. Soc., **1988**; 135(6), 1431-1436.

[12] E. Antolini, R.R. Passos, E.A. Ticianelli. Electrochim. Acta., **2002**; 48(3), 263-270.

[13] S. Gottesfeld, T.A. Zawodzinski, in : R.C. Alkire, H. Gerischer, D.M. Kolb, C.W. Tobias (Eds). Advances in Electrochemical Science and Engineering, Vol 5, 1st ed, Wiley-VCH, Weinheim, **1997**; 195

[14] H.A. Gasteiger, S.S. Kocha, B. Sompalli, F.T. Wagner. Appl. Catal, B., **2005;** 56(1-2), 9-35.

[15] U.A. Paulus, A. Wokaun, G.G. Scherer, T.J. Schmidt, V. Stamenkovic, N.M. Markovic, P.N. Ross. Electrochim. Acta., **2002**; 47(22-23), 3787-3798.

[16] N. Travitsky, T. Ripenbein, D. Golodnitsky, Y. Rosenberg, L. Burshtein, E. Peled. J. Power Sources., **2006;** 161(2), 782-789.

[17] A.K. Shukla, M. Neergat, P. Bera, V. Jayaram, M.S. Hegde. J. Electroanal. Chem., **2001**; 504(1), 111-119.

[18] T. Toda, H. Igarashi, M. Watanabe. J. Electrochem. Soc., **1998**; 145(12), 4185-4188.

[19] T. Toda, H. Igarashi, H. Uchida, M. Watanabe. J. Electrochem. Soc., **1999;** 146(10), 3750-3756.

[20] V. Stamenkovic, T.J. Schmidt, P.N. Ross, N.M. Markovic. J. Phys. Chem B., **2002;** 106(46), 11970-11979.

[21] J.T. Hwang, J.S. Chung. Electrochim. Acta., **1993**; 38(18), 2715-2723.

[22] B.C. Beard, P.N. Ross. J. Electrochem. Soc., **1990**; 137(11), 3368-3374.

[23] L. Xiao, L. Zhuang, Y. Liu, J. Lu, H.D. Abrufia. J. Am. Chem. Soc., **2009**; 131(2), 602-608.

[24] C.W.B. Bezerra, L. Zhang, H. Liu, K. Lee, A.L.B. Marques, E.P. Marques, H. Wang, J. Zhang. J. of Power Sources., **2007;** 173(2), 891-908.

[25] Y. Ma, P.B. Balbuena. Surface Science., **2009**; 603(2), 349-353.

[26] V.R. Stamenkovic, B.S. Mun, K.J.J. Mayrhofer, P.N. Ross, N.M. Markovic. J. Am, Chem. Soc., **2006**; 128(27), 8813-8819.

[27] O. Malis, M. Radu, D. Mott, B. Wanjala, J. Luo, C.J. Zhong. Nanotechnology., **2009;** 20(24), Art. No. 245708, 1-4.

[28] K.J.J Mayrhofer, V. Juhart, K. Hartl, M. Hanzlik, M. Arenz. Angew. Chem. Int. Ed., **2009;** 48(19), 3529-3531.

[29] E.A. Stern, M. Newville, B. Ravel, Y. Yacoby, D. Haskel. Physica B: Physics of Condensed Matter 208-209., **1995;** 117-120.

[30] S.I. Zabinsky, J.J. Rehr, A. Ankudinov, R.C. Albers, M. Eller. J. Phys. Rev. B., **1995;** 52(4), 2995-3009.

[31] L. Xiong, A.M. Kannan, A. Manthiram. Electrochemistry Communications., **2002;** 4(11), 898-903.

[32] S.C. Zignani, E. Antolini, E.R. Gonzalez. J. of Power Sources., **2008;** 182(1), 83-90.

[33] F.J. Lai, L.S. Sarma, H.L. Chou, D.G. Liu, C.A. Hsieh, J.F. Lee, B.J. Hwang. J. Phys. Chem. C., **2009;** 113(29), 12674-12681.

[34] M. Yuasa, A. Yamaguchi, H. Itsuki, K. Tanaka, M. Yamamoto, K. Oyaizu. Chem. Mater., **2005**; 17(17), 4278-4281.

[35] P. Yu, M. Pemberton, P. Plasse. J. of Power Sources., **2005;** 144(1), 11-20.

[36] Q. Ge, S. Desai, M. Neurock, K. Kourtakis. J. Phys. Chem. B., **2001;** 105(39), 9533-9536.

[37] F. Maillard, L. Dubau, J. Durst, M. Chatenet, J. Andre, E. Rossinot. Electrochem. Com., **2010**; 12(9), 1161-1164.

[38] B.C. Han, A.Van Der Ven, G. Ceder, B.J. Hwang. Phys. Rev. B: Condensed Matter and Material Physics., **2005**; 72(20), 1-9.

[39] B.J. Hwang, L.S. Sarma, G.R. Wang, C.H. Chen, D.G. Liu, H.S. Sheu, J.F. Lee. Chem. Eur. J., **2007**; 13(21), 6255-6264.

[40] M.H. Lee, P.S. Wang, J.S. Do. J. Solid State Electrochem., **2008;** 12(7-8), 879-884.

[41] E. Antolini, J.R.C. Salgado, E.R. Gonzalez. J. Power Sources., **2006;** 160(2), 957-968.

Paper 2 :
Activity Enhancement of Carbon-Supported PtCo
Electrocatalyst through Controlled Heat-Treatment for
Proton Exchange Membrane Fuel Cell Applications

Activity Enhancement of Carbon-Supported PtCo Electrocatalyst through Controlled Heat-Treatment for Proton Exchange Membrane Fuel Cell Applications

Abdul Hamid Budiman[1], Widodo Wahyu Purwanto[1], Eniya Listiani Dewi[2], Rinaldy Dalimi[3], Bing Joe Hwang[4]

1. Chemical Engineering Department, University of Indonesia
2. Center for Material Technology, Agency for the Assessment and Application of Technology
3. Electrical Engineering Department, University of Indonesia
4. Chemical Engineering Department, National Taiwan University of Science and Technology

Abstract

Controlled heat-treatment on a commercial carbon-supported PtCo (PtCo/C) electrocatalyst is systematically carried out to enhance the catalyst activity towards the molecular oxygen reduction reaction (ORR). The strategy involves treating the PtCo/C catalyst in a controlled way with carbon monoxide (CO) for various times at a specified temperature. XRD results show that no particle size variation in heat-treated PtCo/C at various times (3 h, 7 h and 15 h) when compared to as-received PtCo/C catalyst. Heat-treatment for 3 h changes the alloy type structure of as-received PtCo/C to a core-shell structure. However, further heat-treatment at 7 h and 15 h leads to phase separation in the catalyst. Under operating single cell H_2-fed proton exchange membrane fuel cell, among all other heat treated catalyst the 3 h heat-treated PtCo/C catalyst exhibits best performance with efficiency of about 80.15%. Heat-induced variations in surface population of the catalysts as well as structural changes may collectively help in increasing their activities toward the ORR

1. Introduction

Development of new materials that can solve challenging problems in the areas of clean energy production and conversion is extremely important in realizing the clean environment. Proton exchange membrane fuel cells (PEMFCs) either H_2 or CH_3OH fed have received great attention as promising power sources especially automotive and portable applications.[1-4] Nanosized Pt is known to catalyze the molecular oxygen reduction (ORR) and serve as a state-of-the art electrocatalyst in a low temperature PEMFC air cathode.[5-9] However, kinetic limitations of the ORR leads to cathodic overpotential losses amount to 0.3-0.4 V under typical PEMFC

operating conditions. In addition, Pt is expensive and the world's supply is limited. Therefore, the development of more active and less expensive ORR electrocatalysts than pure Pt has been the subject of extensive research for a number of decades which has favored the use of suitable Pt alloys.[7-9]

Numerous studies have highlighted the alloying of Pt with transition metals such as Co, Ni, Fe, Mn, Cr and V as a promising approach to increase ORR activity.[7,10] Alloying Pt with transition metals is believed to offer greater stability and facilitate desorption of oxygen species, leading to higher surface site availability and higher catalytic activity.[11-13]

Many researchers have demonstrated that the activity of electrocatalyst is strongly dependent on many factors, such as particle size and its distribution, the electrocatalysts' morphology and composition, particularly it's surface composition, the oxidation state of Pt and the second metal atom, and the surface structure of the catalyst.[10] Bimetallic alloys offer a way of tuning the electronic structure and catalytic properties of a metal surface. The composition and structure of an alloy surface is crucial to its catalytic performance.[14-15] The bonding of adsorbates may induce changes in the local atomic composition and surface structure thereby modify, the activity and selectivity of the catalyst.

PtCo bimetallic catalysts have been studied exhaustively during the past decade. It was reported that Pt alloyed with Co with various Pt to Co ratios ranging from 1:1 to 1:3 on the carbon support yield better catalytic activity than pure Pt.[16-18] Few reasons for the high catalytic activity of these alloys are credited to the modification of the electronic structure of Pt upon alloying with Co and the resulting structural effect on Pt. A novel preparation procedure core shell structured nanoparticles using CO as an adsorbate-induced surface segregation effect has been demonstrated by Mayrhofer et al.[19] The composition of the surface of a bimetallic system can vary from the bulk; it depends on the heat of segregation and the surface mixing energy. Mayrhofer found that utilizing this strategy resulted in a highly active catalyst with a low amount of noble metal.

In this study, we focus on the use of a PtCo/C commercial electrocatalyst from PREMETEK in order to study the effect of the heat-treatment under CO atmosphere and corresponding origin of electrocatalytic activity towards ORR in H_2-fed PEMFC' single cell.

2. Experimental Section

2.1. Catalyst Preparation

A commercial PtCo supported on carbon Vulcan XC 72 (nominal atomic ratio 50:50) with 20 wt% metal loading from PREMETEK was used in this study. Heat-treatment was performed by treating the catalyst sample with CO as an adsorbate at a temperature of 200 ^{o}C for various times of 1, 3, 7 and 15 h using a U-tube reactor. Prior to the heat-treatment, the catalyst was treated by flowing with H_2 at 300 ^{o}C for 2 h in order to remove the impurities if present any and to make the catalyst in metallic state condition.

2.2.   XRD Measurements

X-ray diffractograms of the electrocatalysts were obtained in a universal diffractometer Rigaku, operating with Cu Kα radiation (λ = 0.15406 nm) generated at 40 kV and 100 mA. Scans were done at 10 degree for 2θ values between 20° and 90°. An average value of the lattice parameter was obtained from the Pt (111), (200), (220) and (311) peaks. The crystalline sizes were obtained from the Pt (220) reflection using Scherrer's equation.

2.3.   Electrode Preparation

Membrane electrode assemblies (MEA) were prepared via a coating technique. A PtCo/C either treated or untreated and Pt/C served as the catalyst material at the cathode and anode respectively. In contrast to our homemade standard single cell measurement, the platinum alloy loading of each MEA was set at 0.5 mg/cm^2 per electrode. The catalyst were mixed with 5wt% Nafion ionomer, water and 2-propanol to form a homogenous suspension in an ultrasonic bath and were coated on a carbon paper gas diffusion layer (GDL) which was supported by a micro porous layer (MPL) purchased from the Gas Hub. Coating was done on a hot plate at a temperature of 40 ^{o}C. Two carbon papers were pressed onto an NRE 212 ion exchange membrane purchased from DuPont to produce MEA. Hot press was done at a temperature of 120 ^{o}C and a pressure of 65 Bar for 1 min.

2.4.   Fuel Cell Performance

The obtained MEA was housed in a homemade standard single stack PEM fuel cell with parallel plates purchased from USA (www.fuelcellstore.com).

The single stack PEM fuel cell first passed a leak test before being used. The leak test involved flowing inert gas to the hydrogen inlet valve of a PEM fuel cell. The hydrogen outlet valve was closed, and bubbles monitored the oxygen inlet-outlet valves. A tube of hydrogen and oxygen was then set for measurement after no leak was measured.

Prior to the measurement of the fuel cell performance, the single stack PEM fuel cell was humidified. Conditioning was done by flowing hydrogen and oxygen to a single stack PEM fuel cell at a flow rate of 100 ml/min, at a temperature of 50 ^{o}C at ambient pressure for at least 3 h. Performance of the single stack was measured by an electronic discharge meter 3300 C Electronic Load Mainframe Prodigit 3311D 60V/60A, 300 V.

3. Result and Discussion

Figure 1 shows the comparison of the XRD patterns of a PtCo/C electrocatalyst with various treatment times. The first peak located at about 25° in all XRD patterns is attributed to the (002) plane of the hexagonal structure of the Vulcan

XC 72 carbon support.[6-7] The other four peaks of the electrocatalyst that exhibit diffraction from (111), (200) and (220) and (311) appeared at 2θ values of ca. 40°, 48°, 70° and 84° respectively, characteristic of a face centered cubic (fcc) crystalline Pt according to XRD standard JCPDS no. 04-0802.[7]

From figure 1, it can be clearly seen that the XRD pattern of PtCo1 (sample without heat-treatment in CO atmosphere) and PtCo2 (heat-treated in CO atmosphere at 200 °C for 3 h) indicates that the catalysts are single phase solid solutions. No characteristic peaks for pure Co or its oxides were detected. Further there no super lattice reflections were present. However, their presence can't be discarded because they may be present in trace amounts or even in amorphous form.

Contrarily PtCo3 (heat-treated in CO atmosphere at 200 °C for 7 h) and PtCo4 (heat-treated in CO atmosphere at 200 °C for 15 h) showed the presence of Co peaks. The presence of the characteristic peaks associated with the Co species exhibit diffraction from (400), (331) and (531) according to XRD standard JCPDS No. 01-1259 at 2θ values of ca. 45°, 52° and 75° respectively. The presence of the Co is believed to be due to the phase separation in the catalyst sample at prolonged hours of heat-treatment.
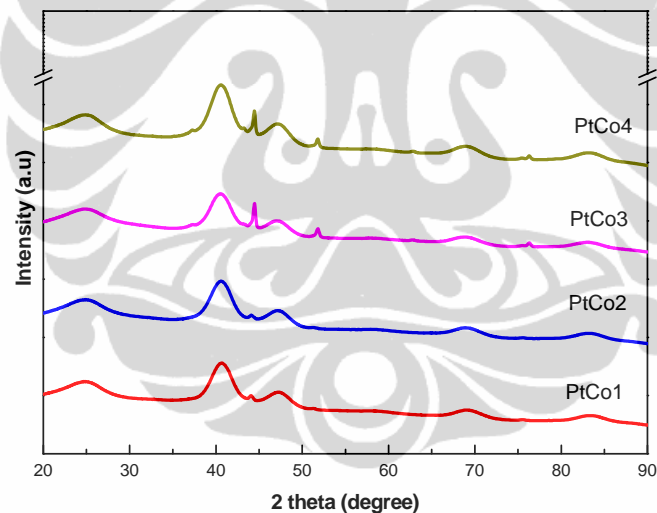
Figure 1. XRD Pattern of PtCo/C Catalyst with Various CO treatment Condition and Untreated Commercial PtCo/C Catalyst.

The XRD results showed that the catalyst consists of several phases or components that were probably have different catalytic activities. The activity of these phases depends on particle size, specific surface area and other factors. The average grain size associated with the catalyst is calculated by using Scherrer's equation and full-width at half maximum of peak (220). The calculations are listed in Table 1.

Table 1. Grain Size of the PtCo/C Commercial and PtCo/C Catalyst with Various CO Treatment Conditions.

Catalyst Code	Catalyst	Grain size, nm
PtCo1	PtCo/C – Commercial	3.052
PtCo2	PtCo/C – CO treatment 3 h	2.909
PtCo3	PtCo/C – CO treatment 7 h	3.073
PtCo4	PtCo/C – CO treatment 15 h	3.055

The average grain size is 3.004 nm. There is no any significant difference in observed grain sizes after heat-treatment in CO atmosphere when compared to the untreated catalyst. It is clear that the treatment does not change the size of the electrocatalyst and can compare the size-independent catalyst activity.

In order to study the effect of the treatment on the performance of the catalyst, the catalyst was applied to the single stack PEM fuel cell measurement. In this study, we compare the performance of untreated and treated PtCo/C catalyst and also Pt/Pt as comparison. Polarization was measured with PtCo/C treated with various CO treatment conditions as a catalyst on cathode side and of Pt/C as a catalyst on anode side.
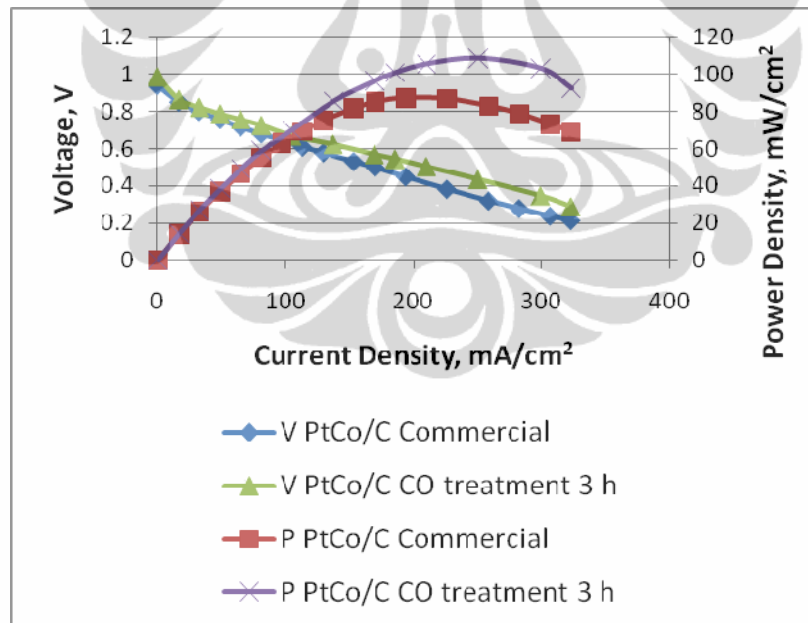
Figure 2. Polarization Curve on Single PEM Fuel Cell (only shown for untreated PtCo/C commercial and CO-treated PtCo/C for 3 h).

According to the polarization curve, the performance of the PEM fuel cell with a CO treated PtCo/C catalyst for 3 h as a cathode catalyst exhibit power density of about 108 mW/cm^2 which is significantly higher than that of an untreated PtCo/C commercial catalyst (87 mW/cm^2).

The performance data of all the PtCo/C catalyst studied here is shown in Table 2. The performance of the PtCo/C catalysts exposed to CO treatment for 7 and 15 h is decreased compared to the CO treated PtCo/C catalyst for 3 h as indicated from its variation in specific surface area (Table 3). Longer treatment will have strong effect on the stability and the unstable PtCo/C leads to decrease in the activity.

This indicates that CO treatment has strong effect on the surface composition of bimetal NPs and influences the NP activity, selectivity and stability.[20]

Table 2. Performance of Single Stack PEM Fuel Cell Using Various PtCo/C Catalysts.

Catalyst Code	Voltage (V)	Current (A)	Power (W)	Efficiency (%)
PtCo1	0.42	5.205	2.1861	65.35
PtCo2	0.434	6.206	2.6934	80.51
PtCo3	0.412	4.204	1.7320	67.03
PtCo4	0.427	3.8	1.6226	64.67
Pt/Pt	0.435	6.972	3.0328	72.53

The performance of the catalyst corresponds with the surface's specific area measurement. Calculating the surface area considering the area under Hupd curve, shows that the longer the treatment time, the smaller surface area.

The active surface area is calculated and estimated from two different mechanisms, CO stripping and hydrogen under deposition, Hupd. In this work, calculations are based on the Hupd mechanism, which is dominated by ionic (H$^+$) conduction. This ionic conduction is very much dependent on Nafion layer resistance.

Table 3. Specific Surface Area of Various PtCo/C Catalysts.

Catalyst Code	Specific Surface Area, m^2/g
PtCo1	33.4679
PtCo2	51.2452
PtCo3	36.4270
PtCo4	27.9214

The relationship between the efficiency of the fuel cell and the surface area is linear. The efficiency will be high if the surface area of the catalyst is also high. A high surface area will affect the activity of the catalyst. The more active the catalyst, the higher the efficiency of the fuel cell.

The efficiency of the fuel cell was not proportionate with the performance. This was caused by a mass transfer of hydrogen with different in each electrocatalyst in single cell stack. Nevertheless, modern PEM fuel cell have been designed for efficient delivery of reactive gases, thus mass transport effect are only of secondary importance, electrochemical kinetics are the primary cause of inefficiency.[21]

However, to our knowledge only a few reported studies have been carried out under operating conditions in a working fuel cell.[22-23] Similar information might be obtained more conveniently in an electrochemical, although, significant differences in the environment of the electrode surface can exist in these systems.

The decrease in the performance of the fuel cell was probably caused by the dissolution of Co. Leaching of Co from the cathode catalyst layer during the operation of the fuel cell can lead to the diffusion of Co into the electrolyte membrane and also to the anode side of MEA.[24]

4. Conclusion

CO treatment has been done successfully to the PtCo/C commercial electrocatalyst in order to study its effect on the performance when it is applied to the single stack of PEM fuel cells. CO treatment does not affect the particle size but it does changes the structure of the catalyst from an alloy to a core shell due to the surface segregation. However, prolonged CO treatment longer than 5 h leads to the separation of the catalyst as indicated from the XRD measurement. The best performance is shown from the PtCo/C exposed to CO treatment for 3 h with efficiency of about 80.51% indicating that there is improvement in the activity of the treated PtCo/C compared to the untreated PtCo/C.

Acknowledgment

References

[1] Steele, B. C. H., and Heinzel, A., 2001, "Materials for Fuel Cell Technologies," Nature., 414, pp. 345-352.
[2] Ghenciu, A. F., 2002, "Review of Fuel Processing Catalyst for Hydrogen Production in PEM Fuel Cell Systems," Current Opinion in Solid State and Material Science., 6, 389.
[3] Costamagna, P., and Srinivasan, S., 2001, "Quantum Jumps in the PEMFC Science and Technology from the 1960s to the Year 2000: Part I. Fundamental Scientific Aspects," J. Power Sources., 102, pp. 242-252.

[4] Costamagna, P., and Srinivasan, S., 2001, "Quantum Jumps in the PEMFC Science and Technology from the 1960s to the Year 2000: Part II. Engineering, Technology Development and Application Aspects," J. Power Sources., 102, pp. 253-269.

[5] Antolini, E., Salgado, J. R. C., and Gonzales, E. R., 2006, "The Stability of Pt-M (M = First Row Transition Metal) Alloy Catalysts and Its Effect on the Activity in Low Temperature Fuel Cells. A Literature Review and Tests on a Pt-Co Catalyst," J. Power Sources., 160, pp. 957-968.

[6] Zignani, S. C., Antolini, E., and Gonzalez, E. R., 2008, "Evaluation of The Stability and Durability of Pt and Pt-Co/C Catalysts for Polymer Electrolyte Membrane Fuel Cell," J. Power Sources., 182, pp. 83-90.

[7] Hwang, B. J., Kumar, S. M. S., Chen, C-H., Monalisa., Cheng, M-Y., Liu, D-G., and Lee, J-F., 2007, "An Investigation of Structure-Catalytic Activity Relationship for Pt-Co/C Bimetallic Nanoparticles the Oxygen Reduction Reaction," J. Phys. Chem. C., 111, pp. 15267-15276.

[8] Colon-Mercado, H. R., and Popov, B. N., 2006, "Stability of Platinum Based Alloy Cathode Catalysts in PEM Fuel Cells," J. Power Sources., 155, pp. 253-263.

[9] Yu, P., Pemberton, M., and Plasse, P., 2005, "PtCo/C Cathode Catalyst for Improved Durability in PEMFCs," J. Power Sources., 144, pp. 11-20.

[10] Lai, F-J., Sarma, L. S., Chou, H-L., Liu, D-G., Hsieh, C-A., Lee, J-F., and Hwang, B. J., 2009, "Architecture of Bimetallic Pt_xCo_{1-x} Electrocatalysts for Oxygen Reduction Reaction as Investigated by X-ray Absorption Spectroscopy," J. Phys. Chem. C., 113, pp. 12674-12681.

[11] Santos, L. G. R. A., Freitas, K. S., and Ticianelli, E. A., 2009, "Heat Treatment Effect of Pt-V/C and Pt/C on the Kinetics of the Oxygen Reduction Reaction in Acid Media," Electrochimica Acta., 54, pp. 5246-5251.

[12] Schulenburg, H., Muller, E., Khelashvili, G., Roser, T., Bonnemann, H., Wokaun, A., and Scherer, G. G., 2009, "Heat-Treated $PtCo_3$ Nanoparticles as Oxygen Reduction Catalysts," J. Phys. Chem. C., 113, pp. 4069-4077.

[13] Jayasayee, K., Dam, V. A. T., Verhoeven, T., Celebi, S., and de Bruijn, F. A., 2009, "Oxygen Reduction Kinetics on Electrodeposited PtCo as a Model Catalyst for Proton Exchange Membrane Fuel Cell Cathodes: Stability as a Function of PtCo Composition," J. Phys. Chem. C., 113, pp. 20371-20380.

[14] Soderberg, J. N., Sirk, A. H. C., Campbell, S. A., and Birss, V. I., 2005, "Oxygen Reductionby Sol-Derived Pt/Co-Based Alloys for PEM Fuel Cells," J. electroche. Soc., 152(10), pp. A2017-A2022.

[15] Andersson, K. J., Calle-Vallejo, F., Rossmeisl, J., and Chorkendorff, Ib., 2009, "Adsorption-Driven Surface Segregation of the Less Reactive Alloy Component," J. Am. Chem. Soc., 131, pp. 2404-2407.

[16] Paulus, U. A., Wokaun, A., Scherer, G. G., Schmidt, T. J., Stamenkovic, V., Radmilovic, V., Markovic, N. M., and Ross, P. N., 202, "Oxygen Reduction on Carbon Supported Pt-Ni and Pt-Co Alloy Catalysts," J. Phys. Chem. B., 106(16), pp. 4181-4191.

[17] Travitsky, N., Ripenbein, T., Golodnitsky, D., Rosenberg, Y., Burshtein, L and Peled, E., 2006. "Pt-, PtNi- and PtCo-Supported Catalysts for Oxygen Reduction in PEM Fuel Cells," J. Power Sources., 161, pp. 782-789.

[18] Gasteiger, H. A., Kocha, S. S., Sompalli, B., Wagner, F. T., 2005, "Activity Benchmarks and Requirements for Pt, Pt Alloy, and Non-Pt Oxygen Reduction Catalysts for PEMFCs," Appl. Catal. B., 56(1-2), pp. 9-35.

[19] Mayrhofer, K. J. J., Juhart, V., Hartl, K., Hanzlik, M., and Arenz, M., 2009, "Adsorbate-Induced Surface Segregation for Core-Shell Nanocatalysts," Angew. Chem. Int. Ed., 48, pp. 3529-3531

[20] Hwang, B. J., Sarma, L. S., Wang, G-R., Chen, C-H., Liu, D-G., Sheu, H-S., and Lee, J-F., 2007, "Heat-Induced Alterations in the Surface Population of Metal Sites in Bimetallic Nanoparticles," Chem. Eur. J., 13, pp. 6255-6264.

[21] Greeley, J., Stephens, I. E. L., Bondarenko, A. S., Johansson, T. P., Hansen, H. A., Jaramillo, T. F., Rossmeisl, J., Chorkendorff, I., and Norskov, J. K., 2009, "Alloys of Platinum and Early Transition Metals as Oxygen Reduction Electrocatalyst," Nature Chemistry., 1, pp. 552-556.

[22] Viswanathan, R., Hou, G., Liu, R., Bare, S. R., Modica, F., Mickelson, G., Segre, C. U., Leyarovska, N., and Smotkin, E. S., 2002, "In-Situ XANES of Carbon-Supported Pt-Ru Anode Electrocatalyst for Reformate-Air Polymer Electrolytr Fuel Cells," J. Phys. Chem. B., 106(13), pp. 3458-3465.

[23] Roth, C., Martz, N., Buhrmester, T., Scherer, J., and Fuess, H., 2002, "In-Situ XAFS Fuel Cell Measurements of a Carbon-Supported Pt-Ru Anode Electrocatalyst in Hydrogen and Direct Methanol Operation," Phys. Chem. Chem. Phys., 4, 3555

[24] Ball, S. C., Hudson, S. L., Theobald, B., and Thompsett, D., 2007, "PtCo, a Durable Catalyst for Automotive Proton Electrolyte Membrane Fuel Cells," ECS Trans., 11(1), pp. 1267-1278.

Paper 3 :
Atomic Distribution of PtCo/C Nanoparticles as Investigated by
X-ray Absorption Spectroscopy

Published at Indonesian Journal of Material Science,
Special Edition on Materials for Energy and Device,
2010, 35-39

Atomic Distribution of PtCo/C Nanoparticles as Investigated by X-ray Absorption Spectroscopy

Abdul Hamid Budiman[1], Eniya Listiani Dewi[2], Widodo Wahyu Purwanto[1], Rinaldy Dalimi[3], Bing Joe Hwang[4]

1   Chemical Engineering Department, University of Indonesia, New Campus UI, Depok 16424 Indonesia
2   Centre of Material Technology, Agency for the Assessment and Application of Technology, MH. Thamrin No. 8 BPPT II Bld, 22 Fl Jakarta 10340
3   Electrical Engineering Department, University of Indonesia, New Campus UI, Depok 16424 Indonesia
4   Nanoelectrochemistry Laboratory, Department of Chemical Engineering, National Taiwan University of Science and Technology, 43 Keelung Road section 4 Taipei, Taiwan

Abstract

X-ray absorption spectroscopy (XAS) was utilized to deduce the structural parameters that can provide information on atomic distribution and extent of alloying as well as the surface population of bimetallic nanoparticles (NPs). In this study, we focused on PtCo/C NPs treated by CO with various of time. XAS measurement showed that this experiment is related to the Case 3, which is $J_{Pt} < 100\%$ and $J_{Co} < 100\%$, then both Pt and Co atoms are not preferred to be alloyed, and it indicates that a higher extent of Pt/Co atoms prefer only to a lesser extent alloying between Pt and Co atoms. If $J_{Co} > J_{Pt}$, it appears that the core is rich in Pt atoms and shell is rich in Co atoms. On the contrary if $J_{Pt} > J_{Co}$ resulting in Co atoms are rich in the core and Pt atoms are rich in the shell. The XAS results reveal that the time of treatment influences the surface population hence the structure of the catalyst. Catalyst treated CO for 0, 3 and 5 h leads to higher population of Pt on the core and Co was moved to the surface resulting to Pt rich in core – Co rich in shell, while treated for 7 and 15 h leads to higher population of Pt on the shell and Co on the core resulting to Pt rich in shell – Co rich in core.

Keywords :   atomic distribution, X-ray Absorption Spectroscopy, coordination number, alloy extent

1. Introduction

Bimetallic nanoparticles (NPs) are of great interest[1-2] from both a scientific and technological perspective because of the modification of physical and chemical properties not only due to quantum size effects but also as a result of the combination of different metals. Bimetallic NPs display fascinating electronic and optical

properties different from those of the bulk metal.[2] In order to understand the nanostructure-property relationships, it is really necessary to investigate both the chemical states and the atomic distribution in bimetallic NPs.

In the field of heterogeneous catalysis, study of the surface composition of bimetallic NPs is being fundamental. The interaction of surface atoms of the catalyst with reactants will play a significant role in catalysis. In many cases, the surface composition of bimetallic NPs differ from that of the bulk and has a significant influence on NP activity, selectivity and stability.[3]

In the last two decades X-ray absorption spectroscopy (XAS) has increasingly been applied to study the structure of metal cluster. This is may be attributed to its unique potential to provide information regarding the oxidation state and local coordination, number and identity of neighbors of absorbing atom.[1,4-6] XAS techniques also can provide information on the morphology of the considered species, as well as the distribution of the two metals inside the species.

XAS studies can be distinguished into two parts : XANES and EXAFS. X-ray absorption near edge structure (XANES) provides critical information about the oxidation state and fractional d-electron density and electronic environment of the absorbing atoms. While extended X-ray absorption fine structure (EXAFS) provides details about the number, type and distance of backscattering atom surrounding the central absorbing atom, investigation on the short range ordering and provide geometric information. The XAS techniques has been proved as a powerful technique for the characterization of bimetallic catalysts, since it is difficult to obtain structural information on such system by means of conventional material analysis method at the early stages.[7-8]

PtCo bimetallic catalyst have been studied exhaustively during the past decade. It was reported that Pt alloyed with Co on the carbon support yield better catalytic activity than pure Pt, where the most study were PtCo with ratio of 1:1 to 1:3.[9-11] Few reasons for the high catalytic activity for these alloy are ascribed to the modification of the electronic structure of Pt on alloying with Co and structural effect on Pt. A novel preparation procedure of such core shell nanoparticle using an adsorbate- induced surface segregation effect has been demonstrated by Mayrhofer et al.[12] The composition of the surface of a bimetallic system can be very different from the bulk, it depends on the heat of segregation and the surface mixing energy. He found that utilizing this strategy resulting in a highly active catalyst with a low amount of noble metal.

In this study, we focused on PtCo/C NPs treated by CO with various of time. The XAS techniques is used to extract the structural parameters required for understanding the atomic distribution and alloying extent and the corresponding structure is revealed.

2. Experimental

2.1. Catalyst preparation

A commercial Carbon supported PtCo supported at Carbon Vulcan XC 72 (nominal atomic ratio 50 : 50) with 20 wt% metal loading electrocatalyst from PREMETEK was prepared by treated with CO as adsorbate at the temperature of 200 ^{o}C for different time 0, 3, 5, 7, and 15 h by using U tube reactor. Prior to CO treatment, the catalyst was treated with flowing H_2 at 300 ^{o}C for 2 h to clean the impurities and to eliminate the oxide contribution.

2.2. XAS Measurement

The X-ray absorption spectra were recorded at the beamline 17C1, National Synchrotron Radiation Research Centre, Hsinchu, Taiwan. The electron storage ring was operated at 1.5 GeV with a current of 300 mA. A Si (111) double crystal monochromator was employed for the energy selection with a resolution $\Delta E/E$ better than 2×10^{-4} at both the Pt L_{III}-edge (11564 eV) and the Co K-edge (7709 eV). All of the experiments on bimetallic nanoparticles were conducted on a homemade cells fabricated with stainless steel for an XAS powder study. Prior to the XAS measurements, sample were reduced with 10% H_2 for 1 h at 300 ^{o}C to remove the oxidized species if any remained on the surface during catalyst preparation. The total amount of the sample was adjusted to reach the optimum absorption thickness ($\Delta \mu x$ = 1.0, $\Delta \mu$ is the absorption edge, x is the thickness of the sample) so that the proper edge jump step could be achieved during measurements. All of the spectra were recorded at room temperature in a transmission mode. Higher harmonics were eliminated by detuning the double crystal Si(111) monochromator. Three gas filled ionization chambers were used in series to measure the intensities of the incident beam (I_0), the beam transmitted by the sample (I_t) and the beam subsequently transmitted by the reference foil (I_r). The third ion chamber was used in conjunction with the reference sample, which was a Pt foil for Pt L_{III}-edge measurements and a Co foil for the Co K-edge measurements. The control of parameters for EXAFS measurements, data collection modes, and calculation of errors were all carried out according to the guidelines set by the International XAFS Society Standards and Criteria Committee.[13]

EXAFS Data Analysis. The XAS experimental data were treated by utilizing the standard procedures. The EXAFS function, χ , was obtained by subtracting the post edge background from the overall absorption and then normalized with respect to the edge jump step. The normalized $\chi(E)$ was transformed from energy space to k-space, were "k" is the photoelectron wave vector. The $\chi(k)$ data were multiplied by k^2 to compensate for the damping of EXAFS oscillations in the high k-region. Subsequently, k^2 weighted $\chi(k)$ data in k-space ranging from 3.53 to 13.95 Å^{-1} for the Pt L_{III}-edge and from 3.53 to 10.36 Å^{-1} for the Co K-edge were Fourier transformed (FT) into r-space to separate the EXAFS contribution from the different coordination

shells. A non linear least squares algorithm was applied to the curve fitting of an EXAFS in the r-space between 1.8 and 3.2 Å for both Pt and Co depending on the bond to be fitted. The PtCo reference file was determined by a theoretical calculation. Reference phase and amplitude for the Pt-Pt absorber scatter pairs were obtained from a Pt foil. For the Co-Co and Co-O absorber scatter pairs, the phase and amplitude were obtained from the reference Co foil and CoO, respectively. All of the computer programs were implemented in the UWXAFS 3.0 package, with the backscattering amplitude and the phase shift for the specific atom pairs being theoretically calculated by using the Feff7 code. From these analysis, structural parameters such as coordination numbers (N), bond distance (R), Debye-Waller factor ($\Delta\sigma_j^2$) and inner potential shift (ΔE_0) have been calculated. For the amplitude reduction factor, S_0^2, values for the Pt and Co were obtained by analyzing the Pt and Co foil reference sample respectively, and by fixing the coordination number in the FEFFIT input file.

3. Result and Discussion

The structure of bimetallic NPs which contains two kinds of metal elements, may posses the crystal structure similar either to the bulk alloy or another type that is the distribution of each metal elements is different from the bulk.

Many reports have appeared describe the applicability of XAS to figure the structural models for bimetallic NPs, but researchers have proposed only qualitatively the structural models of bimetallic NPs such as random alloy, cluster and core shell structure.

It is of interest to estimate the alloy extent or atomic distribution of element in bimetallic NPs to get more detail about the structure and the composition. In this direction, we have analyzed the bimetallic NPs of type A-B by XAS. Firstly we estimate the ratio of the coordination number of Pt around Co and also coordination number of Co around Pt to the total coordination number, then we deduced the qualitative parameter, J_{Pt} and J_{Co} for the alloying extent in PtCo bimetallic NPs. These structural parameter are not only helpful to distinguish random and non random alloying Pt and Co in a PtCo cluster but also give information about the extent Pt and Co atomic distribution in nanoparticle.[3-5]

The calculation of J_{Pt} and J_{Co} of PtCo bimetallic NPs involves, obtaining the ratio of scattering atom Co coordination number around absorbing Pt atom (N_{Pt-Co}) to the total coordination number of absorbing platinum atom ($\sum N_{Pt-i} = N_{Pt-Co} + N_{Pt-Pt}$) denoted as $P_{observed}$ ($P_{observed} = N_{Pt-Co}/\sum N_{Pt-i}$). The $P_{observed}$ provides information on the probability of Pt bonds with a Co atom and serves as an index to Pt atomic distribution in a PtCo cluster. Similarly, the ratio of the scattering atom Pt coordination number around absorbing Co atom to the total coordination number of absorbing cobalt atom ($\sum N_{Co-i} = N_{Co-Pt} + N_{Co-Co}$) denoted as $R_{observed}$. ($R_{observed} = N_{Co-}$

$_{Pt}/\sum N_{Co-i}$). $R_{observed}$ provides information on the Co atomic distribution in a PtCo cluster.

Once $P_{observed}$ and $R_{observed}$ values are determined from XAS coordination number parameter, the J_{Pt} dan J_{Co} of values can be estimated by using the equation 1 and 2 respectively

$$J_{Pt} = \frac{P_{observed}}{P_{random}} x100 \qquad (1)$$

$$J_{Co} = \frac{R_{observed}}{R_{random}} x100 \qquad (2)$$

Where P_{random} dan R_{random} can be calculated from the atomic ratio of Pt and Co in PtCo NPs.

Table 1. Coordination Number and Alloying Extent PtCo/C

No.	Time of CO treatmet	$\sum N_{Pt-i}$	$\sum N_{Co-i}$	J_{Pt}	J_{Co}
1.	0 h	8.65	7.28	70.51	78.40
2.	3 h	8.93	6.78	64.88	80.12
3.	5 h	8.78	7.37	65.99	73.70
4.	7 h	8.56	8.63	69.59	64.77
5.	15 h	8.56	8.69	61.04	56.39

From Table 1, we can see that for PtCo treated CO for 0, 3 and 5 h, the total coordination number parameter relationship of $\sum N_{Pt-i} > \sum N_{Co-i}$ and the alloying extent $J_{Pt} < J_{Co}$ indicate that Co atom are segregate to the surface of the nanoparticle and Pt atom to the core resulting Pt-rich$_{core}$-Co-rich$_{shell}$ structure. Meanwhile for PtCo treated CO for 7 and 15 h, the total coordination number parameter relationship of $\sum N_{Pt-i} < \sum N_{Co-I}$ and alloying extent $J_{Pt} > J_{Co}$ indicate that Pt atom are segregate to the surface of the nanoparticle and Co atom to the core resulting Pt-rich$_{shell}$-Co-rich$_{core}$ structure.

The atomic structure of PtCo/C nanoparticle are derived form experimentally obtained XAS structural parameter and the alloying extent of Platinum (J_{Pt}) as well as Cobalt (J_{Co}). These structural parameter are not only helpful to distinguish random and non random alloying Pt and Co in a PtCo cluster but also give information about the extent Pt and Co atomic distribution in nanoparticle as shown in Figure 1.
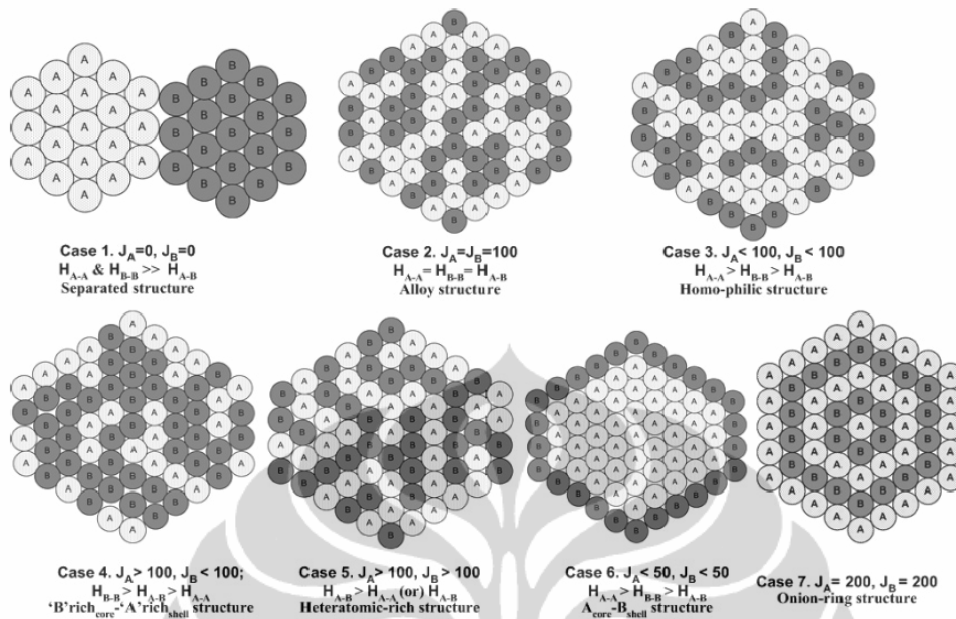
Figure 1. Schematic of bimetallic nanoparticles at various degree of alloying[1]

The surface of a bimetallic system can be very different from the bulk, it depends on the heat of segregation and the surface mixing surface. The chemical potential of the gas phase is also influence the system since the strong bonding of adsorbates will result in a gain in energy of the system.[12] An adsorbate induce to the system will control the surface segregation as shown in the Figure 2.
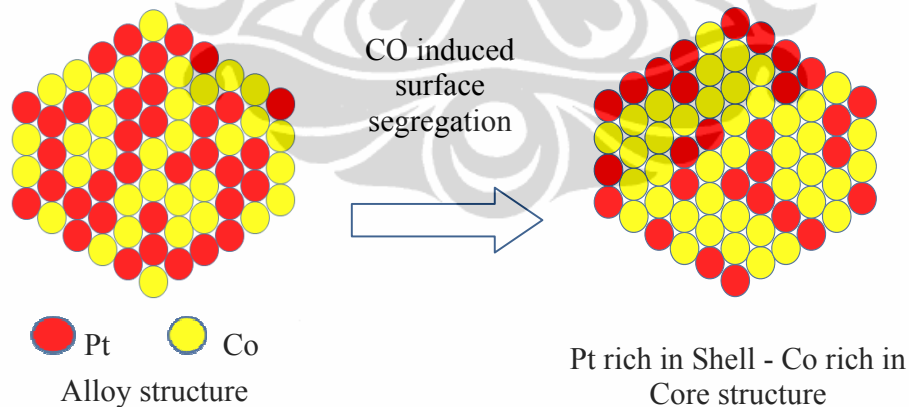
Figure 2. Structure Catalyst was changed by induced surface segregation.

From the XAS measurement it can be concluded that this experiment is related to the Case 3, which is $J_{Pt} < 100\%$ and $J_{Co} < 100\%$, then both Pt and Co atoms are not preferred to be alloyed, and it indicates that a higher extent of Pt/Co atoms prefer only to a lesser extent alloying between Pt and Co atoms. If $J_{Co} > J_{Pt}$, it

appears that the core is rich in Pt atoms and shell is rich in Co atoms. On the contrary if $J_{Pt} > J_{Co}$ resulting in Co atoms are rich in the core and Pt atoms are rich in the shell.

4. Conclusion

The relationship between alloying extent and Pt d-band vacancies in PtCo/C electrocatalyst has been established, which is tunable with Pt and Co composition and strongly impact on the catalytic activity for ORR. It is found that the catalytic activity of PtCo/C treated CO for 3 h, the ORR is the highest due to its higher alloying extent. The XAS results reveal that the time of treatment influences the surface population hence the structure of the catalyst. Catalyst treated for 0, 3 and 5 h leads to higher population of Pt on the core and Co was moved to the surface resulting to Pt rich in core – Co rich in shell, while treated for 7 and 15 h leads to higher population of Pt on the shell and Co on the core resulting to Pt rich in shell – Co rich in core.

Acknowledgements

References

(1) B.J. Hwang, L.S. Sarma, J.M. Chen, C.H. Chen, S.C. Shih, G.R. Wang, D.G. Liu, J.F. Lee, M.T. Tang, J.Am.Chem.Soc, **127**, (2005) 11140-11145

(2) C.H. Chen, B.J. Hwang, G.R. Wang, L.S. Sarma, M.T. Tang, D.G. Liu, J.F. Lee,   J. Phys. Chem. B, **109**, (2005) 21566-21575

(3) B.J. Hwang, L.S. Sarma, G.R. Wang, C.H. Chen, D.G. Liu, H.S. Sheu, J.F. Lee, J.; Chem . Eur. J, **13**, (2007) 6255-6264

(4) B.J. Hwang, L.S. Sarma, C.H. Chen, M.T. Tang, D.G. Liu, J.F. Lee, Applied Physics Letter, **91**, (2007) 023108

(5) F.J. Lai, L.S. Sarma, H.L. Chou, D.G. Liu, C.A. Hsich, J.F. Lee, B.J. Hwang, J.Phys. Chem. C, **113**, (2009) 12674-12681

(6) B.J. Hwang, L.S. Sarma, C.H. Chen, C. Bock, F.J. Lai, S.H. Chang, S.C. Yen, D.G. Liu, H.S. Sheu, J.F. Lee, J. Phys. Chem C, **112**, (2008) 19922-19929

(7) B.J. Hwang, C.H. Chen, L.S. Sarma, J.M. Chen, G.R. Wang, M.T. Tang, D.G. Liu, J.F. Lee, J. Phys. Chem. B, **110**, (2006) 6475-6482

(8) L.S. Sarma, C.H. Chen, S.M.S. Kumar, G.R. Wang, S.C. Yen, D.G. Liu, H.S. Sheu, K.L. Yu, M.T. Tang, J.F. Lee, C. Bock, K.H. Chen, B.J. Hwang, Langmuir, **23**, (2007) 5802-5809

(9) U.A. Paulus, A. Wokaun, G.G. Scherer, T.J. Schmidt, V. Stamenkovic, V. Radmilovic, N.M. Markovic, P.N. Ross, J. Phys. Chem. B, **106**, (2002) 4181

(10)   N. Travitsky, T. Ripenbein, D. Golodnitsky, Y. Rosenberg, L. Burshtein, E. Peled, J. Power Sources, **161**, (2006) 782-789

(11)   H.A. Gasteiger, S.S. Kocha, B. Sompalli, F.T. Wagner, Appl. Catal, B, **56** (2005) 9-35

(12)   K.J.J. Mayrhofer, V. Juhart, K. Hartl, M. Hanzlik, M. Arenz, Angew. Chem. Int. Ed, **48**, (2009) 3529-3531.

(13)   (a) See for example the guidelines for data collection modes for EXAFS measurements and user controlled parameter: http://ixs.iit.edu/subcommittee_reports/sc/sc00report.pdf. (b) See for example the guidlines for errors reporting: http://ixs.iit.edu/subcommitte_reports/sc/err-rep.pdf.

Paper 4 :
Effect of PtCo/C Treatment on Performance of Single Cell PEM
Fuel Cell

Published at Indonesian Journal of Materials Science,
Volume 11, No. 3, 2010, 145-149

Effect of PtCo/C Treatment on Performance of Single Cell PEM Fuel Cell

Abdul Hamid Budiman[1], Eniya Listiani Dewi[2], Widodo Wahyu Purwanto[1], Rinaldy Dalimi[3], Bing Joe Hwang[4]

1. Chemical Engineering Department , University of Indonesia
2. Centre for Material Technology, Agency for the Assessment and Application of Technology (BPPT)
3. Electrical Engineering Department, University of Indonesia
4. Chemical Engineering Department, National Taiwan University of Science and Technology

Abstract

PtCo/C electrocatalyst for oxygen reduction were prepared from commercial PREMETEK and treated with carbon monoxide (CO) at 200 ^{o}C for various time: (1) no treatment, (2) 3 hours, (3) 7 hours and (4) 15 hours. The XRD measurement showed that the particle size of the catalyst remained constant (3 nm). The sintering leads to the changing catalyst structure from alloy to core shell. It is recognize that catalyst treated on 7 and 15 hours leads to the phase separation. The fuel cell performance was done with single cell measurement and showed that PtCo2 is the best performance. The treatment has successfully improved the catalytic activity toward ORR as indicated from its surface specific activity.

Keyword : core shell, phase separation, catalytic activity

1. Introduction

Platinum is popular as the best catalytic activity for the oxygen reduction and when supported on a conductive carbon served as state of the art electrocatalyst in low temperature fuel cell air cathode.[1-5] However, due to kinetic limitations of oxygen reduction reaction (ORR) the cathodic overpotential losses amount to 0.3-0.4 V under typical PEMFC operating conditions. In addition, Pt is expensive and the world's supply is limited. Therefore, the development of more active and less expensive oxygen reduction electrocatalyst than pure Pt has been the subject of extensive research for a number of decades and has favored the use of suitable Pt alloys.[3-5]

Platinum alloys as cathode catalyst have attracted wide attention as a candidate to achieve high performance, to increase in power density as well as to reduce a component cost of PEMFCs.[5] Numerous studies have highlighted the alloying of Pt with transition metals such as Co, Ni, Fe, Mn, Cr and V as promising approach toward improving ORR electrocatalysis in order to increase the activity.[3,6]

Alloying Pt with Fe, Ni or Co can facilitate desorption of oxygen species, leading to higher surface site availability and higher catalytic activity[7-8] and it has proved to be a better alternative for supported Pt catalyst in terms of electrocatalytic activity and cost.[9] Furthermore, the stability of Pt bimetal nanoparticle (NPs) is often suggested to be superior to that of plain Pt NPs.

A number of explanations for the improvement in activity of Pt alloy with the addition of less noble metals have been given, including the lowering of the Pt oxidation state, the suppression of Pt oxide formation, the formation of a new electronic structure with higher Pt 5d orbital vacancies, a decrease in Pt-Pt distance and therefore a more favorable adsorption of O_2 and the formation of a catalytic and thin Pt skin on the surface of the alloy.[3,10]

Many researchers have demonstrated that activity of electrocatalyst is strongly dependent on many factors such as particle size and its distribution, its morphology, composition and particularly its surface composition, oxidation state of Pt and second metal atom and also surface structure of the catalyst.[6] Bimetallic alloys offer a way of tuning electronic structure and catalytic properties of metal surface. The composition and structure of an alloy surface is crucial to its catalytic performance.[11] The bonding of adsorbates may induce changes in local atomic composition and surface structure, changing the activity and selectivity of the catalyst.

PtCo bimetallic catalyst have been studied exhaustively during the past decade. It was reported that Pt alloyed with Co on the carbon support yield better catalytic activity than pure Pt, where the most study were PtCo with ratio of 1:1 to 3:1.[12-14] Few reasons for the high catalytic activity for these alloy are ascribed to the modification of the electronic structure of Pt on alloying with Co and structural effect on Pt. A novel preparation procedure of such core shell nanoparticle using CO as an adsorbate- induced surface segregation effect has been demonstrated by Mayrhofer et al.[15] The composition of the surface of a bimetallic system can be vary different from the bulk, it depends on the heat of segregation and the surface mixing energy. He found that utilizing this strategy resulting in a highly active catalyst with a low amount of noble metal.

In this study, we are focusing the used of PtCo/C commercial electrocatalyst from PREMETEK in order to study the effect of the carbon monoxide (CO) heat treatment to its performance on PEMFC single stack, including mass transfer reaction and their efficiencies.

2. Experimental Section
2.1. Catalyst Preparation

A commercial PtCo supported on carbon Vulcan XC 72 (nominal atomic ratio 50 : 50) with 20 wt% metal loading from PREMETEK was used in this study and were prepared by treated with CO as an adsorbate at the temperature of 200 $^{\circ}$C for various time of 1, 3, 7 and 15 hours using U-tube reactor. Previously, the catalyst was flowed with H_2 at 300 $^{\circ}$C for 2 hours in order to clean the impurities and to make metal state condition.

2.2. XRD Measurement

Xray diffractograms of the electrocatalyst were obtained in a universal diffractometer Rigaku, operating with Cu Kα radiation (λ = 0.15406 nm) generated at 40 kV and 100 mA. Scan were done at 10 degree for 2θ values between 20 and 90°. An average value of the lattice parameter was obtained from the Pt (111), (200), (220) and (311) peaks. The crystalline sizes were obtained from the Pt (220) reflection using Scherrer's equation.

2.3. Electrode Preparation

Membrane electrode assembly (MEA) were prepared by a coating technique using doctor blade. A PtCo, Pt served as catalyst material at the cathode and anode with a variation both on Vulcan XC 72. In contrast to our home made standard single cell measurement, the platinum alloy loading of each MEA were conducted at 0.5mg/cm^2 per electrode. The catalyst were mixed with 5wt% Nafion ionomer and water : 2-propanol to form a homogent ink in an ultrasonic bath and were coated in carbon paper as gas diffusion layer (GDL) with supported by micro porous layer (MPL) that were purchased from Gas Hub. Coating was done above hot plate at temperature of 40 °C. Two carbon paper were pressed onto a NRE 212 ion exchange membrane from DuPont membrane to produced MEA. Hot press was done at temperature of 120 °C and pressure of 65 Bar for 1 minute.

2.4. Fuel Cell Performance

The obtained MEA were stacked to a homemade standard single stack PEM fuel cell with parallel plate that purchased from fuel cell store, USA.

Single stack PEM fuel cell was firstly pass cross leak test before ready to use. The leak test was done by flowing inert gas to hydrogen inlet valve of PEM fuel cell then hydrogen outlet valve was closed, and oxygen inlet-outlet valve were monitored by soap bubbles. Tube of hydrogen and oxygen can be set for measurement after no leak was measured.

Prior to measurement of fuel cell performance, single stack PEM fuel cell was humidified. Conditioning was done by flowing hydrogen and oxygen to single stack PEM fuel cell at flow rate of 100 ml/min, temperature of 50 °C at ambient pressure for at least 3 hours. Performance of single stack was measured by electronic discharge meter 3300 C Electronic Load Mainframe Prodigit 3311D 60V/60A, 300 V.

3. Result and Discussion

The composition of the PtCo/C electrocatalyst was determined from X-ray absorption near edge spectra (XANES) and it was found that the atomic composition is very close to the nominal value (1:1) which is X Pt : 0.4919 and X Co : 0.5081.

Figure 1 shows the comparison of XRD patterns of PtCo/C electrocatalyst with various treatment time. The first peak located at about 25° in all XRD patterns

is attributed to the (002) plane of the hexagonal structure of the Vulcan XC 72 carbon support.[2,3] The other four peaks of electrocatalyst that exhibit diffraction from (111), (200) and (220) and (311) appeared at 2θ values of ca. 40°, 48°, 70° and 84° respectively, characteristic of a face centered cubic (fcc) crystalline Pt according to XRD standard JCPDS no. 04-0802.[3]

From Figure 1, it can be clearly seen that the XRD pattern of PtCo1 and PtCo2 indicates that the catalysts are single phase solid solutions. No characteristic of peaks for pure Co or its oxides were detected. No superlattice reflection were present. Their presence can not be discarded because they may be present in small amount or even in amorphous form.

In other side, on PtCo3 and PtCo4 showed the presence of Co peaks. The presence of characteristic peaks associated with the Co species exhibit diffraction from (400), (331) and (531) according to XRD standard JCPDS No. 01-1259 at 2θ values of ca. 45°, 52° and 75° respectively. The presence of the Co is due to the phase separation.
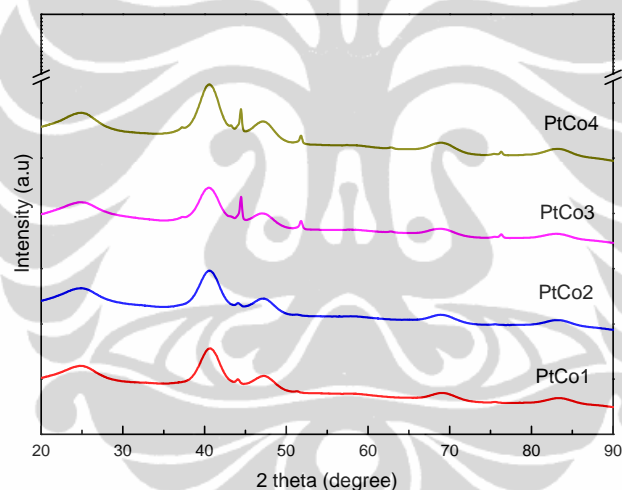
Figure 1. XRD pattern of PtCo/C with CO treatment.

The XRD results showed that the catalyst consists of several phases or components which were probably have different catalytic activities. The activity of these phases depends on particle size, specific surface area or other factor.

The average grain size associated with the catalyst is calculated by using Scherrer's equation and full-width at half maximum of peak (220) and listed in Table 1.

Table 1. Grain size of the PtCo/C commercial with CO treatment with various time

Sample	Catalyst	Grain size, nm
PtCo1	PtCo/C – Commercial	3.052
PtCo2	PtCo/C – CO treatment 3 hr	2.909
PtCo3	PtCo/C – CO treatment 7 hr	3.073
PtCo4	PtCo/C – CO treatment 15 hr	3.055

The average grain size is 3.004 nm. It can be said that there is no any significant different, thus the grain size remains constant. It is clearly that the treatment does not change the size of the electrocatalyst.

The surface of a bimetallic system can be very different from the bulk, it depends on the heat of segregation and the surface mixing surface. The chemical potential of the gas phase is also influence the system since the strong bonding of adsorbates will result in a gain in energy of the system. An adosrbate induce to the system will control the surface segregation as shown in the Figure 2.
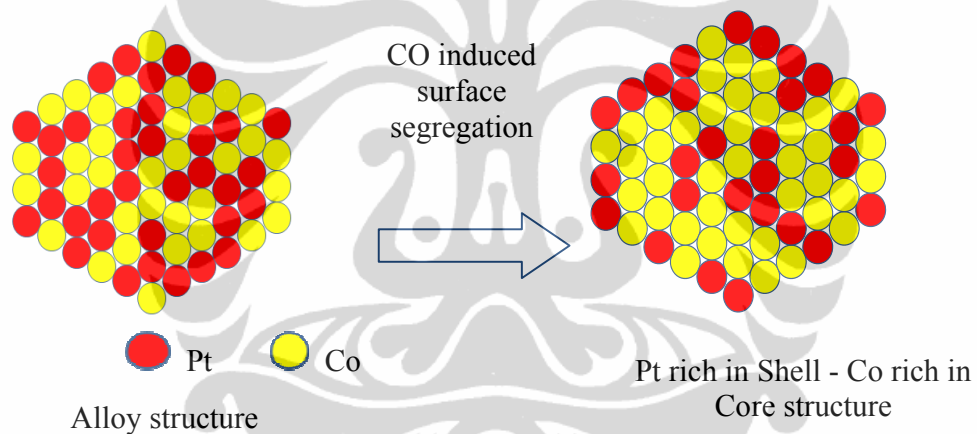
Figure 2. Structure Catalyst was changed by induced surface segregation.

In order to study the effect of the treatment on the performance of catalyst, catalyst was applied to the single cell PEM fuel cell measurement. The test was done with flowing inert gas such as nitrogen to hydrogen inlet valve of PEM fuel cell, then hydrogen outlet valve was closed. The oxygen inlet-outlet valve were monitored by bubbles to check whether there is leak or not. The schematic of experiment are shown in Figure 3.
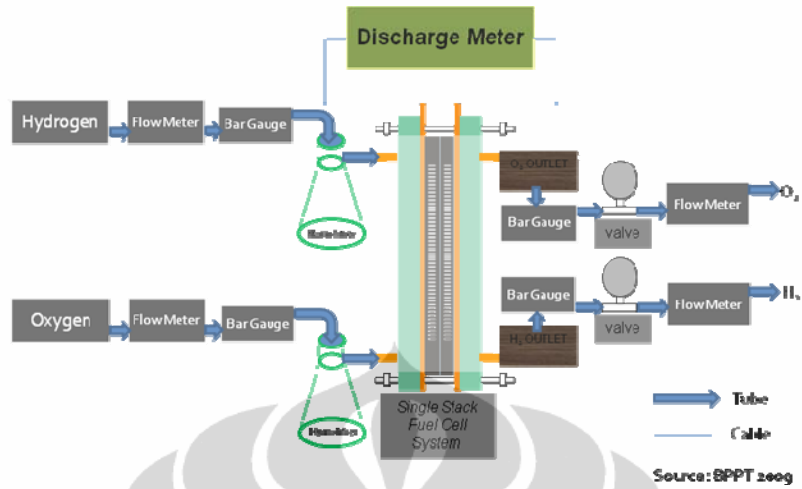
Figure 3. Schematic of system operation for measurement of single cell PEM fuel cell

In this study, we compare the performance of untreated and treated PtCo/C commercial and also Pt/Pt as comparison. Polarization was measured with variation of PtCo/C as catalyst on cathode and Pt/C as catalyst on anode.
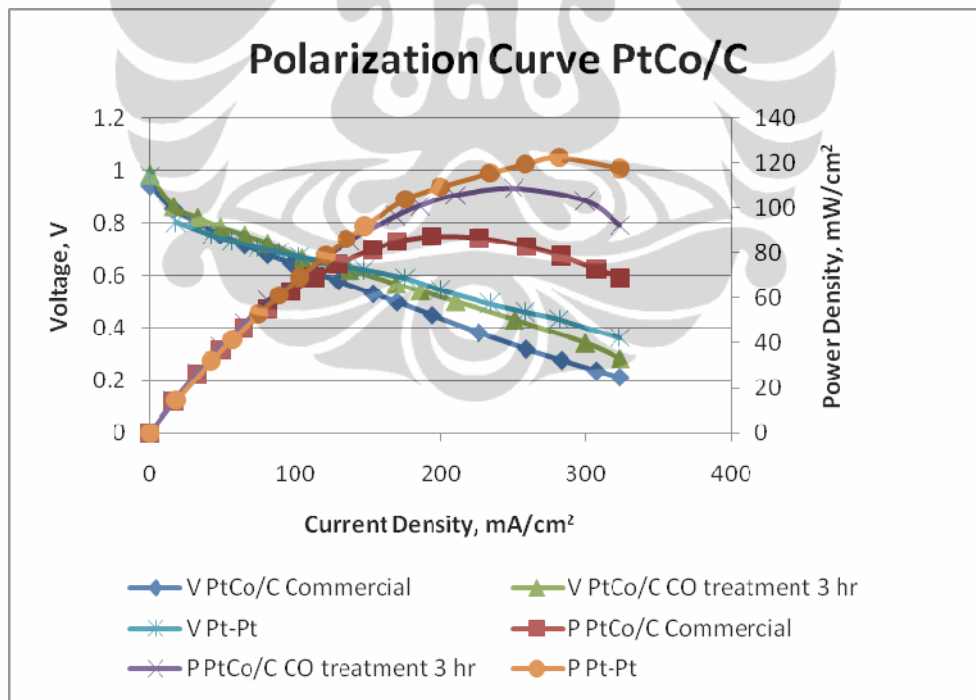

Figure 4. Polarization curve on single PEM fuel cell

According to the polarization curve, it showed that performance of PEM fuel cell with PtCo/C–CO treatment (108 mW/cm^2) have power density higher than that of PtCo/C Commercial (87 mW/cm^2).

The performance of PtCo/C-CO treatment 7 and 15 hours has decreased comparing to PtCo/C-CO treatment 3 hours as indicate from its specific surface area. The longer treatment will effect to the unstable PtCo/C and leads to decrease the activity.

PtCo/C-CO treatment 3 hour showed the highest activity due to the stable condition of the catalyst and had a largest specific surface area as presented in Table 2. This is considered that CO treatment on surface composition of bimetal NPs have significant influence on NP activity, selectivity and stability.[16]

Table 2. Specific surface area of PtCo/C

Sample	Specific Surface Area, m^2/g
PtCo1	33.4679
PtCo2	51.2452
PtCo3	36.4270
PtCo4	27.9214

The performance of the catalyst is in a good agreement with the surface specific area measurement. By calculating the surface area under H$_{upd}$, shows that the longer treatment time the smaller surface area.

Active surface area could be calculated and estimated from two different mechanism, the first one is CO stripping and the second is hydrogen under deposition, H$_{upd}$. In this work, we calculated based from H$_{upd}$ mechanism which is dominated by ionic (H$^+$) conduction. This ionic conduction is very much depend on Nafion layer resistance. The integrated area for H$_{upd}$ is calculated by taking a end point of H$_{upd}$. Usually the lowest current in the double layer region (around 0.4-0.5 V). After that, find the point in the beginning of H$_{upd}$ which correspond to the same current with the end point. All the current data between was minus the current of beginning and end point of H$_{upd}$, after that, integrate the area.

The relationship between efficiency of fuel cell and the surface area is linear. The efficiency will be high if the surface area of the catalyst is also high. High surface area will effect on the activity of the catalyst. The more active catalyst the higher efficiency of the fuel cell.

However, to our knowledge only a few reported studies have been carried out under operating conditions in a working fuel cell.[17-18] Similar information perhaps could be obtained more conveniently in an electrochemical, although, significant differences in the environment of the electrode surface can exist in these systems.

Decreasing the performance probably caused by dissolution of Co. Leaching of Co from the cathode catalyst layer during the operation of the fuel cell can lead to

the diffusion of Co into the electrolyte membrane and also to anode side of MEA.[19-20]

4. Conclusion

CO treatment has been done successfully to the PtCo/C commercial electrocatalyst in order to study its effect on the performance when it is applied to the single stack of PEM fuel cells. CO treatment does not effect on the particle size but it changes the structure of the catalyst from alloy to core shell due to the surface segregation. However, treatment longer than 5 hours leads to the separation of the catalyst as indicate from the XRD measurement. The best performance is shown from the PtCo2 which has the highest specific surface area indicate that there is improvement in an activity of the treated PtCo/C compare to the untreated PtCo/C.
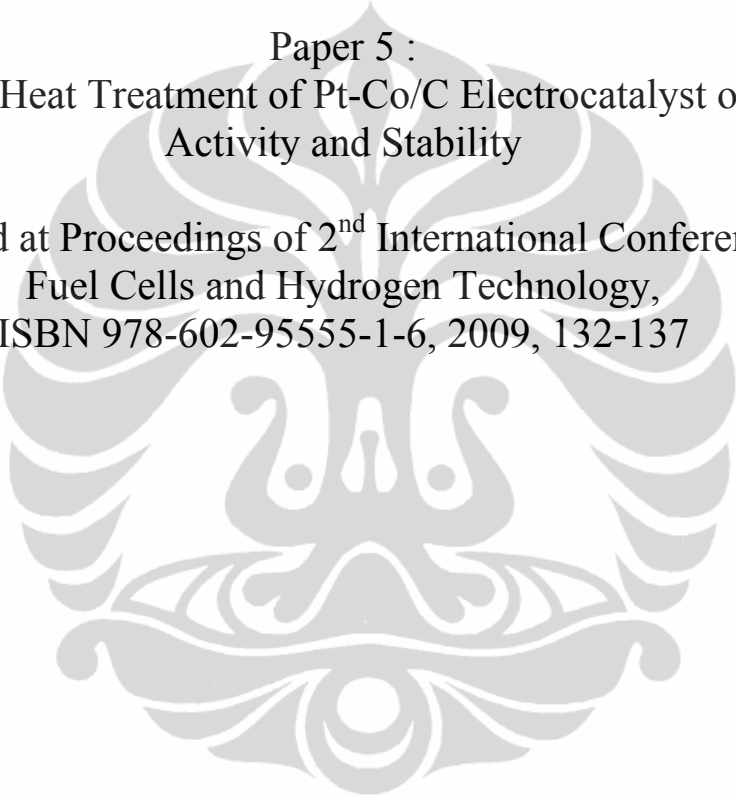
Acknowledgment

References

1. E. Antolini., J.R.C. Salgado., E.R. Gonzalez., J. Power Sources 160 (2006) 957
2. S.C. Zignani., E. Antolini., E.R. Gonzalez., J. Power Sources 182 (2008) 83
3. B.J. Hwang., S.M.S. Kumar., C.H. Chen., Monalisa., M.Y. Cheng., D.G. Liu., J.F. Lee., J. Phys. Chem. C 111 (2007) 15267
4. H.R.C. Mercado., B.N. Popov., J. Power Sources 155 (2006) 253
5. P. Yu., M. Pamberton., P. Plasse., J. Power Sources 144 (2005) 11
6. F.J. Lai., L.S. Sarma., H.L. Chou., D.G. Liu., C.A. Hsieh., J.F. Lee., B.J. Hwang.,   J. Phys. Chem. C 113 (2009) 12674
7. L.G.R.A. Santos., K.S. Freitas., E.A. Ticianelli., Electrochimica Acta 54 (2009) 5246
8. H. Schulenburg., E. Muller., G. Khelashvili., T. Roser., H. Bonnemann., A. Wokaun., G.G. Scherer., J. Phys. Chem. C 113 (2009) 4069
9. K. Jayasayee., V.A.T. Dam., T. Verhoeven., S. Celebi., F.A. de Bruijn., J. Phys. Chem. C 113 (2009) 20371
10. J.N. Soderberg., A.H.C. Sirk., S.A. Campbell., V.I. Birss., J. the Electrochemical Society, 10 152 (2005) A2017
11. Andersson, K.J., Calle-Vallejo, F., Rossmeis, J., Chorkendorff, Ib., J. Am. Chem. Soc. Vol. 131. No. 6, 2009
12. Paulus, U.A., Wokaun, A., Scherer, G.G., Schmidt, T.J., Stamenkovic, V., Radmilovic, V., Markovic, N.M., Ross, P.N., J. Phys. Chem. B 106 (2002) 4181

13. Travitsky, N., Ripenbein, T., Golodnitsky, D., Rosenberg, Y., Burshtein, L., Peled, E., J. Power Sources 161 (2006), 782-789
14. Gasteiger, H.A.; Kocha, S.S.; Sompalli, B.; Wagner, F.T.;Appl. Catal, B 56 (2005), 9-35
15. Mayrhofer, Karl, J.J., Juhart, V., Hartl, K., Hanzlik, M., Arenz, M., Angew. Chem. Int. Ed. 2009, 48, 3529-3531
16. B.J. Hwang., L.S. Sarma., G.R. Wang., C.H. Chen., D.G. Liu., H.S. Sheu., J.F. Lee., Chem Eur J. 2007, 13, 6255
17. R. Viswanathan., G. Hou., R. Liu., S.R. Bare., F. Modica., G. Mickelson., C.U. Segre., N. Leyarovska., E.S. Smotkin., J. Phys. Chem B 106 (2002) 3458
18. C. Roth., N. Martz., Th. Buhrmester., H. Fuess., Phs. Chem 2002, 4, 3555
19. H.A. Gasteiger., S.S. Kocha., B. Sompalli., F.t. Wagner., Appl. Catal. B 2005, 56 (1-2), 9
20. S.C. Ball., S.L. Hudson., B. Theobald., D. Thompsett., ECS Trans, 2007, 11 (1), 1267
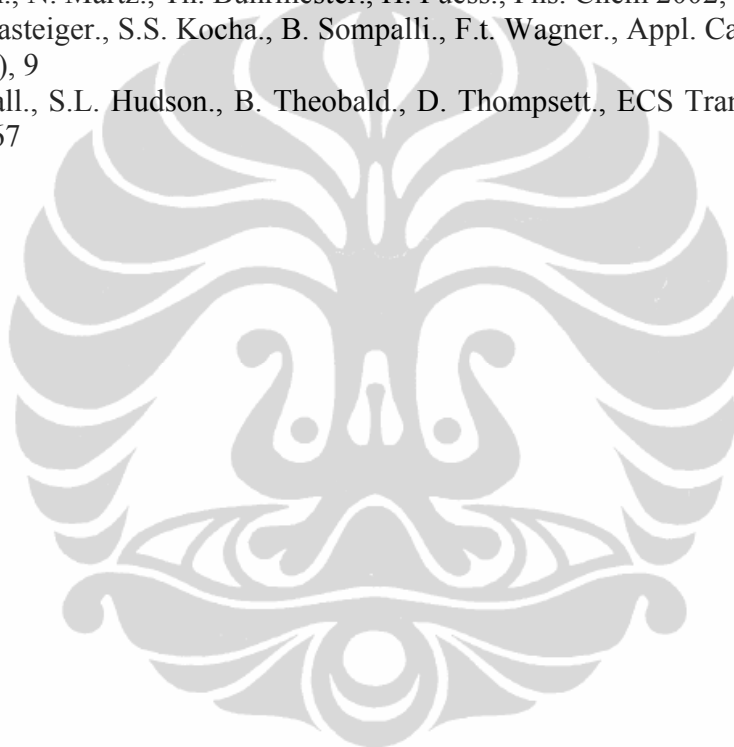
Paper 5 :
Effect of Heat Treatment of Pt-Co/C Electrocatalyst on their
Activity and Stability

Published at Proceedings of 2nd International Conference on
Fuel Cells and Hydrogen Technology,
ISBN 978-602-95555-1-6, 2009, 132-137

Effect of Heat Treatment of Pt-Co/C Electrocatalyst on their Activity and Stability

Abdul Hamid Budiman[1], Widodo Wahyu Purwanto[2], Eniya Listiani Dewi[3]

1) Chemical Engineering Department, University of Indonesia
Center for Energy Conversion and Conservation Technology
Agency for the Assessment and Application of Technology
BPPT II Building, 20th Floor
MH. Thamrin No. 8 Jakarta
Email : hamidbudiman@yahoo.com
2) Chemical Engineering Department, University of Indonesia, Depok-West Java
3) Centre of Material Technology, Agency for the Assessment and Application of Technology

Abstract

PtCo/C commercial was used for the study to determined the effect of heat treatment on their activity and stability. The treatment was carried out under Nitrogen atmosphere at different temperature, namely, 300, 400, 500, 600 and 700 ^{o}C for 2 hours. The catalyst was previously pretreated under Hydrogen atmosphere at 300 ^{o}C also for 2 hours. Form XRD pattern, it could be seen that the particle size is bigger as the temperature of treatment is increased due to the agglomeration. This is in agreement with TEM result, that the particle size is become bigger. The electrochemical analysis showed that the activity of the catalyst was decreased when the particle size is bigger and it is contradiction that the stability of the catalyst was increased when the particle size was also increased

Keyword :heat treatment, agglomeration, activity, stability

1. Introduction

Proton Exchange Membrane Fuel Cells (PEMFCs) have been widely proposed as potentially inexpensive, efficient and clean energy source for automotive portable as well as for stationary applications.[1] There are several problems that should be solved, in order to make PEMFC economically viable. The main one is to find more efficient catalyst than Pt for oxygen reduction reaction (ORR). Pt is the most common electrode catalyst used in PEMFC. However, the sluggish oxygen reduction kinetics on the cathode inhibit the energy conversion efficiency of fuel cells.

Over the past years, many efforts to develop alternative catalyst to Pt focused primarily on Pt based bimetallic alloys, in which platinum is partially replaced by other less expensive metals such as Fe, Co and Ni. Recent studies showed that the activity enhancement of Pt based alloys varies from 2-4[2-4] to 10-25 times.[5,6]

The origin of enhanced oxygen reduction activity remain unclear, since the detailed reaction mechanism have not been fully understood. A number of explanations for the improvement in activity by the addition of less noble metals to Pt have been given, including the lowering of the Pt oxidation state[7], the suppression of Pt oxide formation,[7,8] the formation of new electronic structure with higher Pt 5d orbital vacancies,[9] a decrease in Pt-Pt distance and an adsorption of oxygen,[9] the formation of a catalytic and thin Pt skin on the surface of the alloy.[10-12]

Carbon supported Pt and Pt-M electrocatalysts are generally used in low temperature fuel cells to enhance the rates of the hydrogen oxidation and oxygen reduction reactions. In such catalyst, the high surface to volume ratio of the metal particles maximizes the area of the surface available for reaction.[13] A loss of electrochemical activity will occur if the morphology of the catalyst layer change from the initial state.

The benefit of alloying Pt with other d block metals was initiated by Jalan in 1983.[14]. In the following years, the Pt-Co alloys attracted the highest interest, due to their high catalytic activity. Commercial Pt-Co/C catalyst has already showed mass activities are about twice as high as Pt/C. In addition, Pt-Co/C catalyst also seem to be more stable toward sintering than Pt/C, especially under varying load conditions.[15]

Indeed, one of the major problems of this catalyst is their stability in the acid environment of PAFC and PEMFC. The loss of activity in PAFC during testing has been explained by the loss of active surface area due in part to agglomeration of particle and the leaching of the alloying metal into electrolyte.[16] The acid environment in the PEMFC is different from that of PAFCs because the anions of the perfluorinated sulfonic acid polymer are only weakly adsorbed to the Pt surface. Beside that, the operating temperature of the PEMFC is more than half that of PAFCs. Based on that, a better stability is expected for the catalyst in the PEMFC.

The objective of this work was to study the effect of temperature treatment to the stability of the Pt-Co/C commercial electrocatalyst.

2. Experimental

In this work, we used commercial catalyst Pt-Co supported on Vulcan XC 72 from ETEK, with 30 wt % metal loading.

2.1. Catalyst preparation

Catalyst was prepared by treated the commercial PtCo/C in the U tube heater with different temperature, namely, 300, 400, 500, 600 and 700 $^{\circ}$C in the N_2 atmosphere for 2 hours. Before treating with the N_2, catalyst was pretreated in H_2

atmosphere at 300 ^{o}C also for 2 hours. The treatment was finished after letting the temperature treatment cool down to 25 ^{o}C .

2.2. XRD measurement

X ray diffractograms of the electrocatalysts were obtained in a universal diffractometer Rigaku. Scans were done at 5° per minute for 2θ values between 20 and 90°.

2.3. TEM measurement

Transmission electron microscopy (TEM) and electron diffraction measurements were carried out on Phillips TEM. High angle annular dark field scanning transmission electron microscopy images were obtained with Tecnai G2 F20 operated at 300 kV. Particle size distributions were determined using image tool by measuring the particle sizes of several hundred particles for each catalyst.

2.4. Electrode preparation

The commercial catalyst Pt-Co/C supported on Vulcan XC 72 (30wt % metal loading) was purchased from ETEK. The electrodes were prepared by ultrasonically blending of catalyst, nafion solution for 2 hours. The catalyst solution was dropped using pipette on the surface of working electrode

2.5. Electrochemical measurement

For cyclic voltammetry (CV) and rotating disk electrode (RDE) measurements, a three compartment cell was used. This electrode was used for the determination of the active surface area and evaluation of the electrocatalytic activity. The experiments were performed in 0.5 M H_2SO_4 solution at room temperature, where saturated calomel electrode was used as reference electrode. The catalyst ink was prepared by ultrasonically blending the catalyst with nafion 0.5%. The ink was then dropped on the glassy carbon surface of the RDE. Initially, in order to clean the surface of the catalyst, the system was purged with N_2 and cycled between 0.856 and -0.194 V versus normalized hydrogen electrode (NHE) at a scan rate of 100 mV/s. For this pretreatment, the system was performed to 10 cycles.

Cyclic voltammetry was performed with two different scan rate, namely, 10mV/s and 25 mV/s, and was carried out to 2 cycles.

Linear Sweep Voltammetry (LSV) was conducted at rotation rate 1600 rpm with O_2 for ORR, and it were recorded between 0.856 and -0.244 V versus NHE with scan rate of 1 mV/s

2.6. Stability study

To know the stability of the catalyst, the system was performed to 2000 cycles, and every 500 cycles the solution was changed. With the scan rate of 100 mV/s, the system was cycled between 0.856 and 0.355 V. The stability was measured under O_2 atmosphere and was recorded every 500 cycles.

3. Result and Discussion

3.1. Physical properties of the Pt-Co/C electrocatalyst

The powder X ray diffraction pattern of the PtCo/C commercial and treated electrocatalyst are given in fig 1. The diffraction peak at 2θ of 25 ^{o} shown for all catalysts are associated to the (002) plane of hexagonal structure of the Vulcan XC 72 carbon.
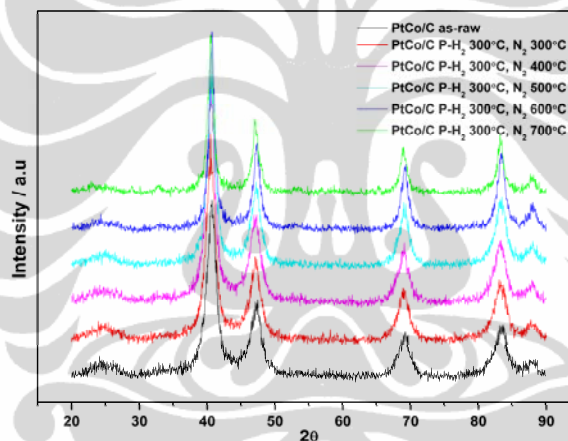
Fig 1. XRD pattern of PtCo/C in different temperature treatment

The increase in magnitude observed in the carbon peak intensity of the sample can be explained by the contribution of the carbon on the microporous layer on GDL.

As indicated in fig 1. the XRD pattern showed the five main characteristic peaks of the face centered cubic (fcc) crystalline Pt, namely, the planes (111), (200), ((220), (311) and (222). In the PtCo/C electrocatalyst the peaks are slightly shifted to higher angles with respect to those in the Pt/C electrocatalyst, indicating a contraction of the lattice and alloy formation.

In this PtCo/C XRD pattern showed there is no superlattice reflection, which indicates the formation of only disordered solid solution. Also there is no peaks for pure Co or its oxides was found. This presence can not be discarded because may be they present in a small amount or even in amorphous form.[17]

The lattice parameter, particle size of the catalyst are reported in Table 1 and was calculated by using Bragg law.

Table 1. XRD calculation

Sample	2θ	FWHM	D, nm	Lattice parameter, Å
PtCo/C commercial	40.646	1.599	5.532	3.838
PtCo/C - 300 °C	40.536	1.598	5.534	3.848
PtCo/C - 400 °C	40.506	1.438	6.146	3.851
PtCo/C - 500 °C	40.571	1.351	6.543	3.845
PtCo/C - 600 °C	40.694	0.945	9.361	3.834
PtC0/C - 700 °C	40.501	0.921	9.594	3.852

As we can see in the fig 2, the morphology and the size distribution of the catalyst is well with the higher particle size with the higher temperature treatment due to the agglomeration of the catalyst.
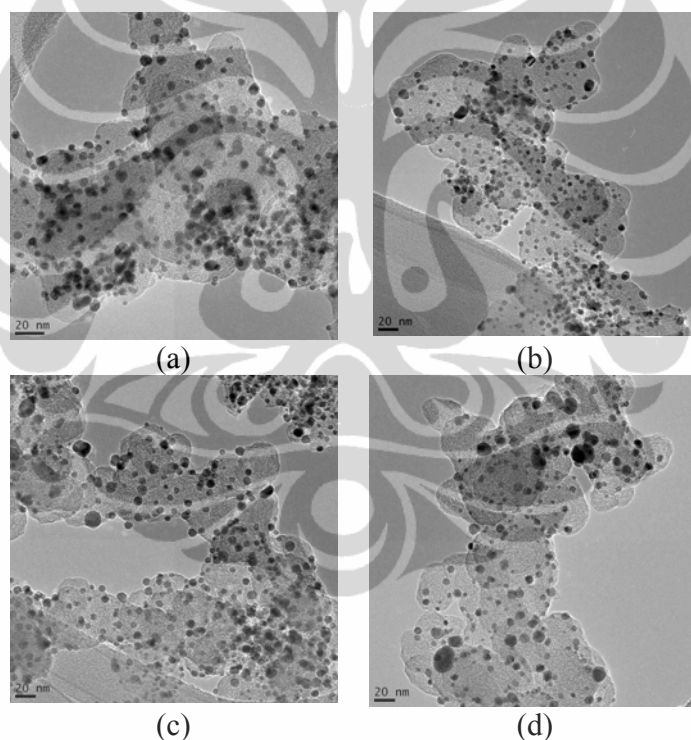
Fig 2. TEM images of the catalyst with different temperature treatment (a) pretreatment H_2 300 °C, (b) N_2 treatment 300 °C, (c) N_2 treatment 400 °C (d) N_2 treatment 600 °C

Compared to the commercial catalyst (fig 3) the size distribution of this catalyst is more uniform, and from the X ray absorption, it was obtained the composition was 0.72 and 0.28 for Pt and Co respectively.
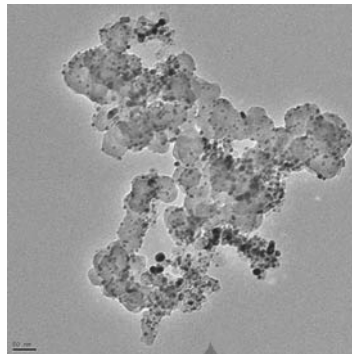
Fig 3. TEM images of PtCo/C commercial

Fig 4. shows a typical CV obtained for PtCo/C commercial catalyst. It can be seen, there are two peaks observed correspond to the oxidation-reduction of Pt and desorption-adsorption of hydrogen on the Pt surface. In the case of PtCo/C alloy indicates the creation of a weakly adsorbed oxide layer on the Pt surface, which is easier to reduce, consequently increase the ORR activity. This is in agreement with Paulus et al.[18]
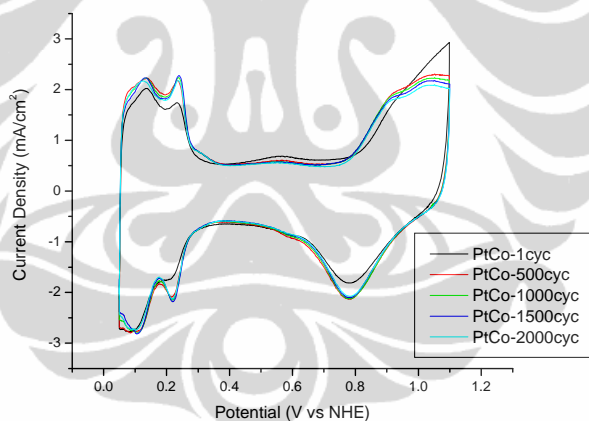

Fig.4. CV for PtCo/C commercial (1 cycle – 2000 cycle)

It is clearly observed that the base voltammogram becomes more Pt like, which is probably indicative of leaching of Co from the surface. This is due to the dissolution of Co component from the alloy, so that the structure becomes Pt skin.

According to Gasteiger et al[13] there are at least three possible causes for the leaching of base metal from a Pt alloy/C catalyst in PEMFCs : (i) excess base metal deposited onto the carbon support during preparation, (ii) incomplete alloying of these base element to Pt due to a low alloying temperature applied during formation of the alloy, (iii) even a well alloyed base metal may leach out of the surface under PEMFC operating conditions and leave a Pt enriched surface or skin since

thermodynamically base metal are unstable under PEMFC potentials in acidic electrolytes.

Toda et al[5] on his experiment by XPS measurement found that most of the Ni, Co and Fe easily disappeared from all the Pt alloy surface layer, probably by dissolution, by submitting the surface to an anodic potential or even in diluted acid solution at room temperature.
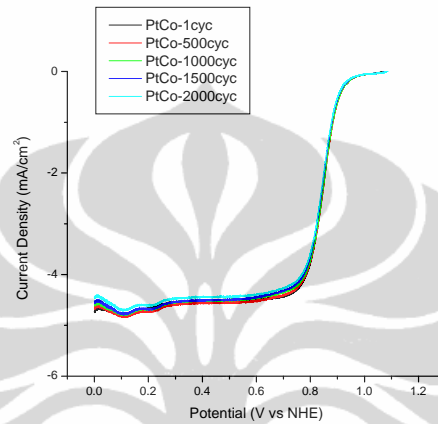

Fig. 5. LSV for the PtCo/C commercial

Fig 5. show the LSV for the PtCo/C commercial catalyst. It is clearly observed that the performance of the system remain constant, there are no changes of the ORR even after several cycles, since there is no treatment on this commercial catalyst.

Unlike the untreated catalyst, the PtCo/Cc treated in the different temperature showed the CV and LSV performance that indicate the activity of the catalyst is decreased, as we can see in the figure 6 and 7 respectively.
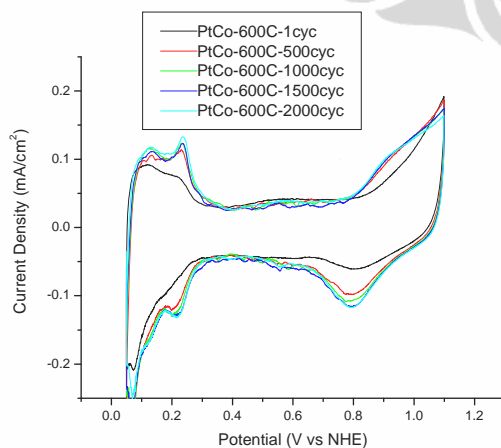
Fig 6. CV for the PtCo/C treated at 600 ^{o}C 600 ^{o}C
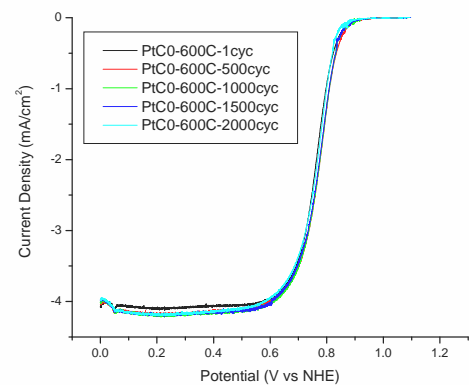
Fig 7. LSV for the PtCo/C treated at

This phenomena is in agreement with Antolini et al[13] that metal particle size of the Pt alloy influences the dissolution of the base metal in acid environment. The higher temperature treatment will effect on the particle agglomeration, consequently it will loss the active surface area. However, higher stability of PtCo/C alloy with large particle sizes than that of catalyst with small particle sizes was observed .

4. Conclusion

The influence of the treatment on the activity and stability of PtCo/C commercial catalyst was studied. The particle size of the catalyst is bigger as the temperature of treatment is increased.

The increased of the particle size will effect to the catalytic activity, the more big particle size, the more decrease the activity.

Due to the Co dissolution, the structure of PtCo/C become a Pt skin. In this structure, the activity of ORR is increased compare to Pt/C. However, the increased of particle size will effect to the stability of the catalyst.

The metal particle size of the Pt alloy influences the dissolution of the base metal in acid environment. Higher stability of PtCo/C alloy with large particle sizes than that of catalyst with small particle sizes

The base metal dissolution can effect the characteristics of the catalyst in two opposite ways. The one is increase the ORR and the other one is decrease the ORR activity. The non precious metal loss increase the ORR activity by surface roughening, so that increased Pt surface area, or by modification of the electronic structure of the Pt skin layer. The other hand, the loss of alloyed non noble metal decrease the ORR activity due to loss of the structural modification of Pt metal by alloying

Acknowledgements

References

(1) Hwang, B.J., Kumar, S.M.S.; Chen, C.; Monalisa.; Cheng, M.; Liu, D.; Lee, J.; J. Phys. Chem. C 2007, 111, 15267-15276
(2) Mukerjee, S.; Srinivasan, S.; Soriaga, M.P.; J. Electrochem. Soc. 1995, 142, 1409-1422

(3) Paulus, U.A.; Wokaun, A.; Scherer, G.G.; Schmidt, T.J.; Stamenkovic, V.; Radmilovic, V.; Markovic, N.M.; Ross, P.N.; J. Phys. Chem. B 2002, 106, 4181-4191

(4) Stamenkovic, V.; Schmidt, T.J.; Ross, P.N.; Markovic, N.M.; J. Phys. Chem B 2002, 106, 11970-11979

(5) Toda, T.; Igarashi, H.; Uchida, H.; Watanabe, M.; J. Electrochem. Soc. 1999, 146, 3750-3756

(6) Toda, T.; Igarashi, H.; Watanabe, M.; J. Electroanal. Chem. 1999, 460, 258-262

(7) Arico, A.S.; Shukla, A.K.; Kim, H.; Park, S.; Min, M.; Antonucci, V.; Appl. Surf. Sci. 2001, 172, 33

(8) Shukla, A.K.; Neergat, M.; Bera, P.; Jayaram, V.; Hedge, M.S.; J. Electroanal. Chem. 2001, 504, 111

(9) Min, M.; Cho, J.; Cho, K.; Kim, H.; Electrochim. Acta 2000, 45, 4211

(10) Toda, T.; Igarashi, H.; Watanabe, M.; J. Electrochem. Soc. 1998, 145, 4185

(11) Toda, T.; Igarashi, H.; Uchida, H.; Watanabe, M.; J. Electrochem. Soc. 1999, 146, 3750

(12) Stamenkovic, V.; Schmidt, T.J.; Ross, P.N.; Markovic, N.M.; J. Phys. Chem B 2002, 106, 11970.

(13) Antolini, E.; Salgado, J.R.C.; Gonzalez, E.R.; J. Power Sources 160, 2006, 957-968

(14) Jalan, V.; Taylor, E.J.; J. Electrochem. Soc. 1983, 11, 2299

(15) Schulenburg, H.; Muller, E.; Khelashvili, G.; Roser, T.; Bonnemann, H.; Wokaun, A.; Scherer, G.G.; J. Phys. Chem. C 2009, 113, 4069-4077

(16) Colon Mercado, H.R.; Popov, B.N.; J. Power Sources 155, 2006, 253-263

(17) Zignani, S.C.; Antolini, E.; Gonzalez, E.R.; J. Power Sources 182, 2008, 83-90

(18) Paulus, U.A.; Wokaun, A.; Scherer, G.G.; Schmidt, T.J.; Stamenkovic, V.; Markovic, N.M.; Ross, P.N.; Electrochim. Acta 47, 2002, 3787-3798

Paper 6 :
Material Combination for Cathode PEMFC Electrocatalyst
Development : A Review

Accepted at International Conference on Advance and
Sustainable Polymer, 2008

Material Combinations for Cathode PEMFC Electrocatalyst Development : A Review

Abdul Hamid Budiman[1], Widodo W Purwanto[1], Rinaldy Dalimi[2], Eniya L Dewi[3]

1) Chemical Engineering Department University of Indonesia
2) Electrical Engineering DepartmentUniversity of Indonesia
3) Centre of Material Technology
Agency for the Assessment and Application of Technology

Abstract

The cost of Proton Exchange Membrane Fuel Cell (PEMFC) can be drastically reduced by using little or no platinum (Pt) electrocatalyst in the electrodes. However, Pt is the only catalyst proven to date to withstand thousands of hours of operation in the highly corrosive and acidic conditions at PEMFC electrodes. Material combinations can be used to develop electrocatalyst for cathode PEMFC performance. This method is selected on their acid stability and their electronic state. Metal support interaction which is the support affects the electronic state of the metal. The oxygen reduction reaction (ORR) at cathode PEMFC with slow kinetic reaction is a main barrier for better performance PEMFC. This slow kinetic reaction will cause over potential in excess of 300 mV from the thermodynamic potential for ORR. Designing new catalyst is necessary to overcome the slow kinetic reaction. New catalyst is designed by combining Pt with electron withdrawing compounds. Combining Pt with Ti, Zr, Nb, Ta, W which is supported with acidic phosphate and also Au with Al, Si, Ge and Sn which is supported with tin oxide showed that the activity of this new catalyst was increased. Here in we describe a review of those catalysts and also Pt alloy with transition metal electrocatalyst.

Keywords : electrocatalyst, cathode PEMFC, electronic state, material combination

Introduction

One of the technical barriers to the commercialization of PEMFC is that cost. A significant cost component is platinum catalyst used in the fuel cell to increase the rate of reaction. Platinum that is the only catalyst proven to date in the highly corrosive and acidic conditions at PEMFC electrodes, is an expensive and low abundant.

Using little or no platinum in the electrode can drastically reduce the cost of PEMFC.[1] A significant performance loss in the PEMFC is related to the oxygen reduction reaction (ORR) at the cathode.
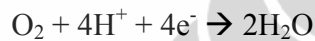
The drive to reduce metal loadings and cost and also to improve activity means that new materials such as Pt alloys has become an alternative catalyst, are constantly being sought.

The activity of noble metal catalysts can be improved or modified by metal support interaction, whereby the support affects the electronic state of metal.
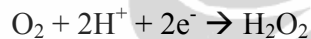
Oxygen reduction reaction (ORR)

This reaction proceeds either via direct reduction to water or via an indirect reduction to hydrogen peroxide as intermediate or side product as follow :
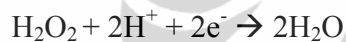
Direct reduction :

$$O_2 + 4H^+ + 4e^- \rightarrow 2H_2O$$

Indirect reduction :

$$O_2 + 2H^+ + 2e^- \rightarrow H_2O_2$$

Followed by a further reduction via :

$$H_2O_2 + 2H^+ + 2e^- \rightarrow 2H_2O$$

Several different models were developed to describe the two competing reaction. Wroblowa and Bagotskii et al [2] have introduced the reaction scheme for the ORR
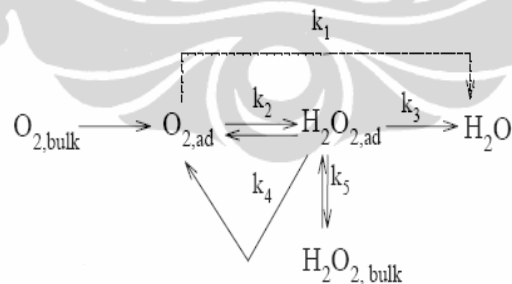

Fig.1. Scheme for ORR

The scheme distinguishes between a direct four electron reduction resulting to water (k_1) or through a series pathway forming H_2O_2 as an intermediate (k_2) that followed reduced to water (k_3). In addition, H_2O_2 can either decompose to water and O_2 (k_4) or be desorbed into the solution (k_5)
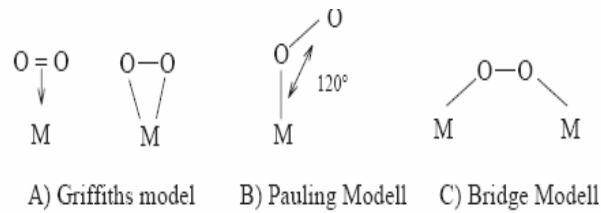
Fig 2. Oxygen adsorption model at catalyst surface

Figure below presents the assumed adsorption possibilities for oxygen and the resulting possible reaction pathways :

Once oxygen is adsorbed one sided (ie. Pauling model) the O-O binding will remain almost unchanged. Therefore pathway II is preferred and thus the formation of peroxide is favored. Meanwhile, adsorption on both side (Griffiths model and Bridge model) streches the O-O binding and then prepares the decomposition of O_2 molecule. Consequently pathway I or III is favored.
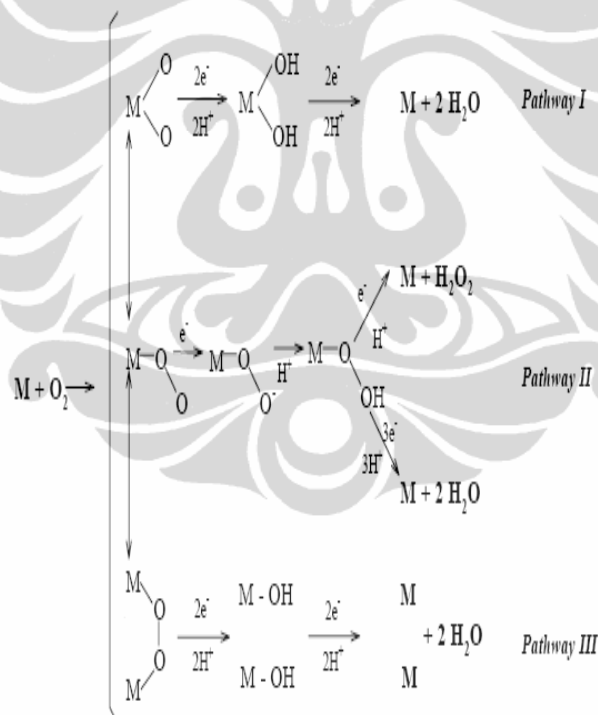

Fig. 3. ORR mechanism at acidic condition

When dealing with fuel cells, the ORR is preferred to take place via four electron transfer either in a direct or series patrhway. The two electron reduction with H_2O_2 as side product leads to a decreased utilization of the cathode feed gas and degradation of membrane

Material Combinatory

Material combinations are selected by their acid stability and their electronic state. To design new catalysts, platinum is combined with the electron withdrawing or proton donating compounds. Through Pourbaix diagram, these elements are non toxic and predicted to withstand the highly corrosive conditions at PEMFC cathode. These include Ti, Zr, Nb, Ta, W, Al, Si, Ge, Sn, Ir, Pt and Au as shown at picture below.
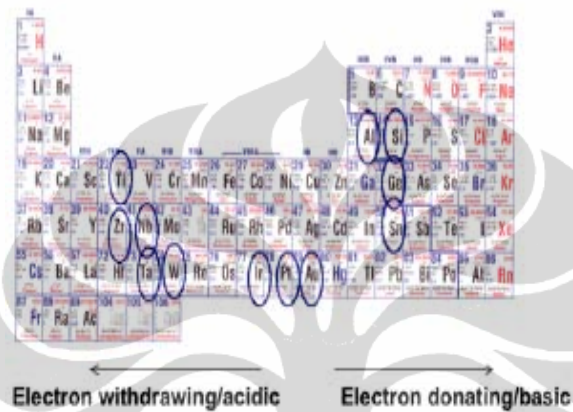

Fig. 4. Pourbaix diagram

New catalyst is design by combining Pt with the electron withdrawing compound to the left (e.g Ta) and Au is supported on basic supports to the right (e.g Sn). The supports are either metal hydrous phosphates or hydrous oxide. This support is selected due to the key component of the ORR that is high stability to corrosion and ability to transport water and proton

Once Pt is supported on acidic phosphate such as hydrous tantalum phosphate (TaPO), it shifts the electronic state of the platinum and serve as a proton conducting medium for the transport of water. Beside that Au when supported on hydrous tin oxide (SnO), it becomes active as an oxygen reduction catalyst.[1]
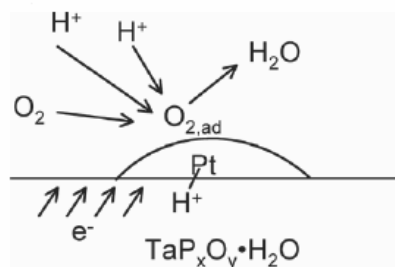

Fig. 5. Oxygen activation mechanism on Pt supported hydrous tantalum phosphate

It can be concluded that there are significant opportunities for improving Pt catalyst by metal support interactions. This is an alternative to taken with alloying because oxide based supports are highly stable in acid. The improves mass activity of Pt-TaPO catalyst is attributed to the MSI between the Pt and TaPO. TaPO is electron deficient compared to Pt therefore is electron withdrawing or acidic. The contact of these two material leads to lower density and therefore increase activity of the Pt.

The method chosen to determine whether a new catalyst composition is better is a complex issue. Many variable effect the fuel cell performance, those are composition, fabrication method, particle size distribution, loading catalyst, support material etc.

One way to improve cathode performance is to use supported Pt catalyst that have higher surface area and lower platinum loading. It can be achieved by using Pt based alloys with transition metal. In order to develop new material for electrocatalyst for oxygen reduction, it is better to consider on these criteria :

- high oxygen adsorption capacity
- structural stability during oxygen adsorption and reduction
- stability in electrolyte medium
- ability to decompose H_2O_2
- high conductivity
- low cost

Several research has been conducted in order to create new ORR materials for the PEMFC cathode. It has been reported that Pt alloyed with Ni, Co, Cr, Fe and Mn enhances the electrocatalytic activity for the oxygen reduction reaction (ORR) by up to several orders of magnitude.

Here, we describe the new ORR material based on Pt X alloys. (X = Ni, Co and Fe). N Wakabayashi et al showed that their Pt alloys has a higher onset oxidation potential for the ORR. V Stamenkovic et al also observed the formation of a Pt skin. It showed that activity for the ORR was increased for Pt_3Fe and Pt_3Co due to reduced numbers of blocking species at the surface.[3]

He at al[4] studied on Pt binary alloys and reported that $Pt_{78}Co_{22}$ was the optimum oxygen reducing. It was stable, had the highest mass fraction specific activity and a half wave potential 110 mV higher than Pt.

Mukerjee and Srinivasan[5] studied $Pt_{75}Co_{25}$ in single cell test and found that the alloy had a better ORR activity. They reported that the ORR onset potential for the Pt Co alloy was 52 mV higher than pure Pt at 40 ^{0}C and 28 mV higher at 80 ^{0}C. Beside that, Mukerjee et al also found that PtCo cathode catalyst and found it performed better than Pt.

Markovic and Ross [6] performed RDE work on Pt, $Pt_{75}Co_{25}$ and $Pt_{75}Ni_{25}$ alloys and reported that the pt Co alloy in perchloric acid electrolyte was better than the pure Pt and Pt-Ni.

Ross and Markovic compared $Pt_{75}Co_{25}$ that had an enriched Pt skin against a $Pt_{75}Co_{25}$ catalyst that had been sputtered. It is reported tahat both catalysts outperformed Pt but the skin catalyst was more active than the sputtered catalyst

Mukerjee et al and Tamizhmani et al found activity enhancement of 2-3 when studying Pt-Co, Pt-Ni and Pt-Cr versus Pt. Toda et al[7] reported enhancement factor of as much as 10, when using sputtered films of Pt-Ni, Pt-Co and Pt-Fe compared to pure Pt film in 0.1 M $HClO_4$ at room temperature.

Recently, Adzic et al[8] developed a new class of electrocatalyst for ORR consisting of a monolayer of Pt deposited on a metal or alloy carbon supported nanoparticles. These electrocatalyst showed up to a 20 fold increase in Pt mass activity compared with conventional Pt electrocatalyst.

Conclusion

From the it can be conclude that development of cathode PEMFC can be done by material combinatory through alloying Pt electrocatalyst. Development of Pt alloy electrocatalyst will give advantages on improving performance, improving durability and reducing the cost.

From the research done by several researcher, it showed that improvement of catalyst has performed significantly increase activity of ORR. Nevertheless, understanding of ORR mechanism has to be studied clearly.

Pt alloys electrocatalyst improve significantly the catalytic activity toward oxygen reduction and also inhibits the catalyst particle agglomeration, since the transition metal (such Co) acts as an anchor on the carbon surface, resulting on impeding the migration of Pt.

Reference

1. Lyons, Karen Swider et al., DOE Hydrogen Program., FY 2005 Progress Report
2. Wroblowa, H S et al., Journal of the Electroanalytical Chemistry, 69 (1976)
3. Ball, Sarah C ., Electrochemistry of Proton Conducting Membrane Fuel Cells., Paltinum Metal Review, 2005, 49 (1), 27-32
4. T. He et al., Journal Electrochem Soc., 153 (2006) A 1637 -1643
5. S. Mukerjee and Srinivasan., J. Electroanal Chem, 357 (1993) 201 – 224
6. N.M. Markovic and P.N Ross., Surf. Sci. Rep., 45 (2002) 121-229
7. Antoline et al., Journal of Power Sources 160 (2006) 957-968
8. Adzic et al., DOE Hydrogren Program FY 2007 Annual Progress Report